Schweizerische Eidgenossenschaft
Confédération suisse
Confederazione Svizzera
Confederaziun svizra

Department of the Environment, Transport, Energy and Communication DETEC

Swiss Federal Office of Energy SFOE
Energy Research

Final Report 21.12.2018

NextICE

Next Generation of Alternative Fuel Converters in the Transportation Sector

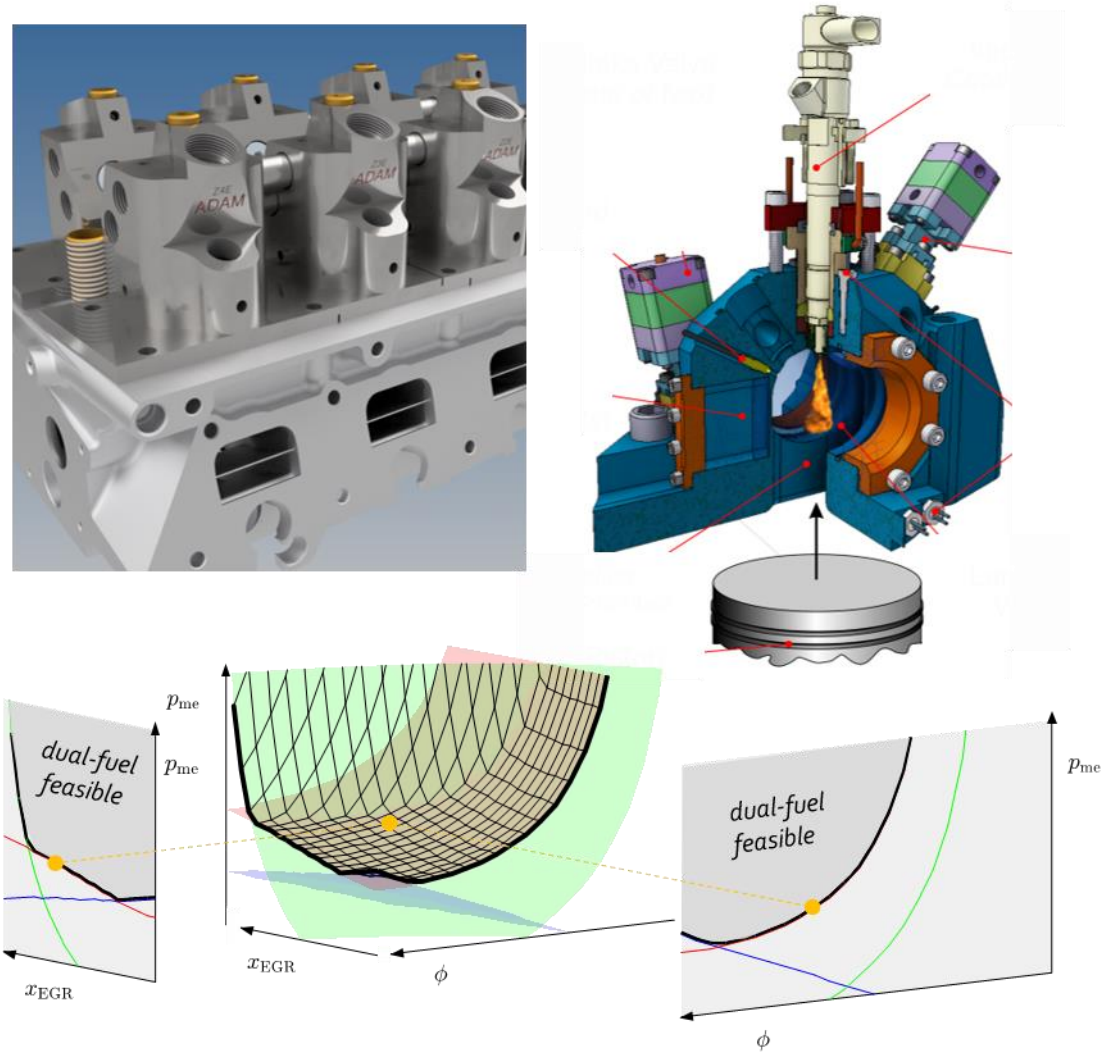

Date: 21. December 2018
Town: Zürich and Dübendorf

Publisher:
Swiss Federal Office of Energy SFOE
Research Programme Mobility
CH-3003 Bern
www.bfe.admin.ch

Project Partners:
ETH Zürich, Institut für dynamische Systeme und Regelungstechnik, IDSC
Prof. Christopher Onder
Sonneggstrasse 3
CH-8092 Zürich
www.idsc.ethz.ch

ETH Zürich, Institut für Energietechnik, LAV
Prof. Konstantinos Boulouchos
Sonneggstrasse 3
CH-8092 Zürich
www.lav.ethz.ch

Empa, Aumotovie Powertrain Technologies Laboratory
Dr. Patrik Soltic
Überlandstrasse 129
CH-8600 Dübendorf
www.empa.ch

Authors:
Christopher Onder, IDSC, onder@idsc.mavt.ethz.ch
Richard Hutter, IDSC, rihutter@idsc.mavt.ethz.ch
Konstantinos Boulouchos, LAV, boulouchos@lav.mavt.ethz.ch
Christophe Barro, LAV, barro@lav.mavt.ethz.ch
Patrik Soltic, Automotive Powertrain Technologies Laboratory, patrik.Soltic@empa.ch

SFOE head of domain: Rolf Schmitz
SFOE programme manager: Martin Pulfer, martin.pulfer@bfe.admin.ch
SFOE contract number: SI/501020-01 / 8100079

Swiss Federal Office of Energy SFOE
Mühlestrasse 4, CH-3063 Ittigen; postal address: CH-3003 Bern
Phone +41 58 462 56 11 · Fax +41 58 463 25 00 · contact@bfe.admin.ch · www.bfe.admin.ch

Contents

List of abbreviations

OME	Poly(oxymethylene) dimethyl ethers
WLTC	Worldwide Harmonized Light-Duty Vehicles Test Cycle
EGR	Exhaust Gas Recirculation
HC	Unburnt Hydrocarbons
NOx	Nitrogen Oxide (NO and NO2)
DOI	Duration of Injection
SOI	Start of Injection

Project goals

The latest generation of renewable fuels has a good ecological balance, does not compete with food production and is suitable for use in combustion engines. Today, in the field of combustion engine drives for vehicles and mobile machines, almost exclusively petrol and diesel engines are used. These are technically very sophisticated, can be used in all types of vehicles, have long ranges and long service lives and can be used in all possible environmental conditions. The disadvantage is that they cannot simply be converted to renewable fuels. By contrast, alternative propulsion systems (e.g. natural gas engines) have significant restrictions, but they can often be operated relatively simply with renewable fuels. However, little is known what can be achieved in the best case by exploiting the properties of a specific renewable fuel. This project contributes to the efficient use of renewable fuels in transportation systems by persueing the following objectives in three distinct work packages (WP).

WP1 *Combustion processes*

On the one hand, the combustion of oxymethylene ether (OME) under stoichiometric conditions and, on the other hand, the dual-fuel process, in which natural gas is ignited by a diesel-like fuel, are being investigated. In both cases, combustion is to be diffusion-controlled. For this purpose, a single-stroke engine will be designed.

WP2 *Thermomanagement*

Highly efficient drive systems are characterized by low exhaust gas temperatures which lead to problems in exhaust gas aftertreatment, especially when operating with natural gas. Using the example of the Diesel-ignited natural gas full engine, it will be investigated which measures can lead to efficient and cost-effective exhaust aftertreatment.

WP3 *Fully variable valve train for Otto-engines*

A new concept for an energy-efficient, fully variable, electrohydraulic valve train is developed and implemented in a functional model.

Summary

The studies carried out within the NextICE project cover a wide range of methods. Starting with the fundamental research on the combustion process of oxygenated fuels and blends, the creation of mathematical models for the the purpose of emission control, up to the commissioning of a new valve drive. All of these sub-projects have contributed to possibility of using renewable fuels in an efficient and cost-effective way. With the experimental work in the WP1 that was conducted on both a constant volume cell as well as a single cylinder heavy-duty Diesel engine, several highly oxygenated fuels belonging to the poly(oxymethylene)dimethilethers family were investigated. It could be demonstrated that pure oxygenated fuels are characterized by a nearly smokeless combustion and when used in a blend with Diesel, a massive reduction in soot formation is achieved by adding a relatively little amount of oxygenated fuel. In addition, the particulate matter in oxygenated fuels is characterized by far smaller dimensions with respect to those from commercial Diesel combustion probably because of an oxidation effect on nucleation cores. In the second work package, WP2, we examined the conditions under which methane can be used efficiently in a dual-fuel engine within the legal pollution limits. Based on mathematical models we were able to point out reasons behind the limitations in the aftertreatment system and further to introduce a methodology for finding optimal operation strategies. In WP3 an electrohydraulic valvetrain could be invented and build that allows a fully flexible actuation of the intake and exhaust valves in an internal combustion engine. The prototype shows excellent performance, e.g. it outperforms a classical camshaft in terms of the required energy.

Work undertaken and findings obtained

WP 1 (LAV)

1.1. Investigation of OME

1.1.1. Management Summary

The use of oxygenated fuels in diesel engines is of particular interest because of the low environmental impact that can be achieved. Oxygenated fuels produced from methane-based products (poly oxymethylene dimethyl ethers OME also POMDME and PODE) have been investigated in three different parts: in a first part, the combustion behaviour of different OME compositions, OME-Diesel blends and reference Diesel has been investigated in a opticalli well accesible constant volume chamber. In a second part, OME-Diesel blends have been compared with reference Diesel in a single cylinder heavy duty engine and third, neat OME has been fired in the prevoiusly mentioned engine under extreem EGR rates to achieve globally stoichiometric conditions.

In the constant volume chamber with large optical access, the combustion evolution and soot formation and oxidation processes has been studied using optical techniques such as OH chemiluminescense and two dimensional two colour pyrometry (2D2CP). Moreover a fast particle spectrometer has been used at the chamber exhaust in order to analyze the soot emissions from the different investigated fuels. The investigation included the calculation of the kL factor, demonstrating a reduction of the soot formation dominated phase when increasing the oxygenated fraction in the blend. Furthermore, fuel jet images show a reduction of the soot formation area when increasing the oxygen content in the blend. The activity even focused on the analysis of soot emissions acquired by means of the fast particle spectrometer and results highlighted nearly smokeless combustion for pure oxygenated fuels and a non-linear soot emission reduction with increasing O_2 content in the blend. In order to achieve a complete overview of the impact of the oxygenated fuels on engine performance and exhaust emissions, an investigation on a single cylinder heavy duty direct injection diesel engine has been performed during in the second and third part of this WP.

In the second part, two OME in diesel blends, namely 5 and 10% in volume OME in commercial diesel, have been tested in order to compare emission and performance results with the ones from the reference diesel fuel. The activity focused not only on soot and NO_X but on CO_2 as well in order to achieve an in depth analysis of combustion efficiency from the different fuels. Two different BMEP values have been explored, namely 8 and 10.5 bar while a single injection strategy has been selected, exploring the effect of the specific fuel and oxygen concentration at intake on engine out emissions and performance. The comparison between the POMDME diesel blends and commercial diesel has shown a significant reduction in soot emissions, up to almost 35%. Moreover no significant increase in NO_X emissions has been found, highlighting as molecular oxygen can be not crucial (at least up to the percentages considered in the present work) for this pollutant in a premixed plus diffusive combustion mode. Moreover the activity provided results highlighting no significant decrease in combustion efficiency when fuelling the engine with the oxygenated blends and an increase in break specific fuel consumption for the 5 and 10% POMDME in diesel blends of around 2 and 4% respectively.

In the third part, the combustion behaviour of neat OME in a composition of approximately 80% OME3 and 20% OME4 has been investigated using again the single cylinder heavy duty engine. For the operation with OME, the eight injector nozzle holes were increased from 0.24 mm to 0.29 mm to compensate the lower heating value of OME. The operating conditions included variations in fuel, nozzle size, EGR, boost pressure and load. A significant number of operating conditions with OME have been investigated under stoichiometric global air/fuel ratio conditions. It was observed that the ignition delay of OME is shorter than the one of Diesel, due to the higher cetane number of the

oxygenated fuel. Moreover OME showed a faster combustion. The reason for this fast combustion behaviour has not been found in the lower demand on air directly, but mainly in the higher turbulence level for mixing due to combustion closer to the injector nozzle tip as a result of the lower oxygen demand. A computationally fast description for steady state sprays has been used to express a characteristic time scale which is required for the fuel to mix with surrounding air up to stoichiometric conditions. The resulting characteristic number τspray correlates well with the characteristic mixing rate τmix, calculated from the measurement data. This description offers the possibility to predict the diffusion combustion rate in a very wide range of engine operation parameter variations, including changes in nozzle size, fuel injection pressure or fuel composition with strongly air demand. It was observed that CO and HC show an extreme spike in globally stoichiometric operation. Furthermore, the total HC emissions contain a substantial amount of methane. NOx emissions within the recorded operating conditions have shown a strong dependence on the applied EGR rate. The particle emissions using OME show high number in a size range mainly below 20 nm. TEM imaging combined with an energy dispersive X-Ray system revealed that these particles are soot mostly with a few nanometers large metal inclusions.

1.1.2. Introduction

Several studies on the use of oxygenated fuels have shown a reduction of particulate matter and recommend the use of oxygenates to suppress the C-C bonds and therefore the soot precursor species. However, some of them, e.g. Dimethyl ether (DME), are not appropriate for diesel engines because of their properties (e.g. vapour pressure, low viscosity, low lubricating capability and being in a gaseous state under atmospheric) requiring significant modifications to the fuel injection system. Therefore, oxygenates with higher viscosity and boiling point are definitely more attractive. Poly(oxymethylene) dimethyl ethers (POMDME or OME in abbreviated form) are characterized by a CH_3-O-$(CH_2$-O$)_n$-CH_3 general structure, with a mass fraction of oxygen within the molecule up to almost 50%. The first fuel of the OME family is dimethoxymethane (DMM or OME1: one –O–CH_2– group) which is still more volatile than diesel, having its boiling point at 42°C. Therefore problems related to vapour lock may occur. Because of the low cetane number (CN), high volatility and weak viscosity and lubricity of OME1, higher OMEs (n=3,4,5) are considered to be more suitable for application in a diesel engine allowing no modifications to the injection system. Table 1 reports the main properties of the OME family fuels.

Table 1: Physical properties of conventional diesel (CDF), DME, DMM and OMEs

	CDF	DME	DMM	OME		
				n=2	n=3	n=4
Melting point (°C)	-	-141	-105	-70	-43	-10
Boiling point (°C)	170 – 390	-25	42	105	156	201
Viscosity (25°C) (mPa*s)	2.71	-	0.58	0.64	1.05	1.75
Density liquid (25°C) (kg/l)	0.83	-	0.860	0.960	1.024	1.067
Cetane number	55	55	29	63	70	90
Oxygen content (wt%)	-	34.7	42.1	45.3	47.1	48.2

1.1.3. Objective of the project

The present activity had, as main objective, the investigation of oxygenated fuels properties on combustion evolution, engine performance and exhaust emissions. Poly(oxymethylene) dimethyl ethers (OME) with a CH_3-O-$(CH_2$-O$)_n$-CH_3 general molecular structure have been studied focusing, with respect to combustion evolution, both on the fuels properties and oxygen at intake. In order to study the combustion evolution and soot formation and oxidation processes, optical techniques such as OH chemiluminescense and two dimensional two color pyrometry (2D2CP) have been applied. Moreover soot emissions from the different investigated fuels have been analyzed by means of a fast particle spectrometer. The deeper knowledge of the oxygenated fuel effect on soot formation/oxidation processes provided by this first activity is currently being applied, in a second phase of the project, to an investigation on a single cylinder “heavy duty” direct injection diesel engine. The aim of this part of the project is to achieve a complete overview of the impact of OME1 on engine performance and exhaust emissions. Great attention is reserved to the analysis of the different engine out emission: soot as well as nitrogen oxides, unburned hydrocarbons, carbon monoxide and carbon dioxide are considered.

The investigation of the second and third part has been conducted on a single cylinder heavy duty direct injection diesel engine and mixtures of different OMEs blended into commercial diesel in diverse percentages have been investigated. With respect to exhaust emissions, not only particulate matter but even nitrogen oxides, and carbon dioxide have been taken into account. The attention to the investigated particular OME mixture is due to the fact that it is characterized by similar physical properties to diesel thus not requiring substantial modifications to the engine infrastructure. Therefore it could be of particular interest for the market. A production on industrial scale of OME to be blended with commercial diesel would be of interest in order to obtain blends characterized by diesel high energy content and OME strong capability of reducing soot formation.

The goal of this work is the operation and characterisation of neat OME in a composition of approximately of 80% OME3 and 20% OME4 with a lower heating value of 19.4 MJ/kg. The experiments are carried out in a single cylinder research engine. The work is divided in two parts, presented in two distinct publications. The focus of this first part is the combustion behaviour. Therefore, the differences in combustion between Diesel reference cases and OME at high air-to-fuel ratio are discussed to introduce useful tools to describe the injection spray behaviour of the two fuels and its influence on the reaction rate. On the other hand, also the behaviour of OME at stoichiometric conditions is investigated, in particular observing the heat release rate and the EGR tolerance. The second focus is the behaviour of the gaseous and particle exhaust emissions under wide range of EGR rates and globally lean as well as stoichiometric equivalence ratios to evaluate the range of operating strategies using OME.

1.1.4. Experimental Set-up

Cylindrical constant volume chamber set-up

The first phase of the project has been carried on a cylindrical constant volume chamber (CCVC) with large optical accesses. Its air path contains an autoclave, a connecting inlet tube, the chamber itself (Figure 1) and an exhaust tube while an external compressor is used to achieve suitable in-cell pressures before combustion. This is connected to an autoclave via a pressure control valve to reduce the pressure to a set point value. The autoclave is characterized by a considerably larger volume compared to the cell body and feeds it via the connecting inlet tube as soon as a cycle is initiated. This pressure reservoir, the inlet tube and the chamber are equipped with pressure and temperature sensors as well as heating elements which allow, for the chamber, temperatures up to 800 K. Moreover, in order to emulate engine-like conditions at start of main injection combustion, a pilot injection can be applied to further increase, through its combustion, pressure and temperature values prior to the main injection event.

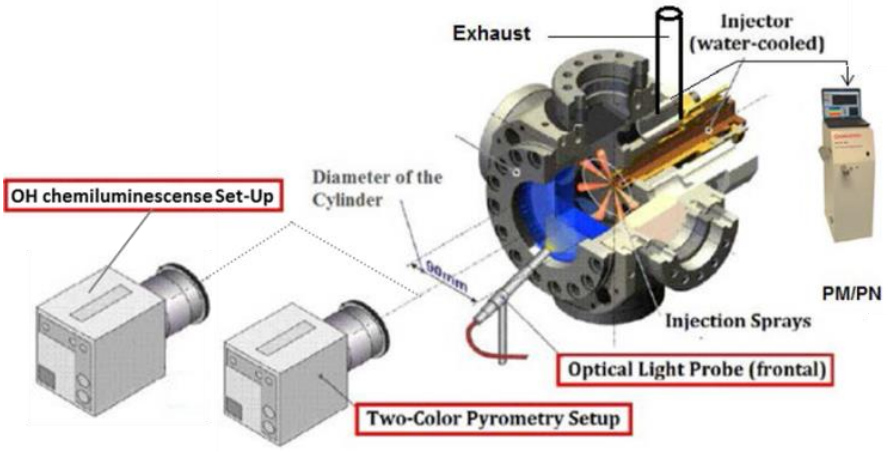

Figure 1: Experimental apparatus (cell, optical set-up and particle spectrometer)

The fuel pressure is achieved by a pneumatic high pressure pump, which is able to generate fuel pressures up to 1600 bar, connected to a rail and a passenger car Bosch piezo injector (8 holes, 0.108 mm nozzle diameter). In order to have optical access to the complete combustion volume, the originally cubic-formed vessel has been retrofitted with steel cylindrical walls, concentric to the axis of the injector. Due to the insertion of these cylindrical walls, the optical access is limited to the front window but allows a complete view of the combustion chamber. Because of heat losses (figure 2), the in-cell pressure trace presents a decreasing trend after the combustion event meaning that a variation of exhaust valve opening timing determines different values of gas pressure being released in the exhaust. Part of the exhaust volume is sampled and analyzed using a Cambustion DMS 500 fast particle spectrometer.

Investigated fuels

The investigated fuels have been:

- Commercial diesel as the reference fuel;
- Dimethoxymethane (OME1or DMM);
- OME2 (POMDME with n=2) pure and blended in diesel in different percentages (5, 30 and 50% in volume, identified in the following with the abbreviations OME2-5%, OME2-30% and OME2-50% respectively);
- A mixture of POMDME mainly comprising n=2,3,4 (abbreviated form: OME2/3/4, characterized by the following composition: 33.1 wt-% OME2, 37.9 wt-% OME3, 27.4 wt-% OME4, 0.3 wt-% OME1, 1.2 wt-% Trioxane).

Operating conditions

In order to operate in engine-like conditions, the cell has been preheated during the experiments by means of several electrical resistances which assured, before start of combustion, a constant temperature of around 713K for the cell walls. In addition, for any investigated condition and fuel, two injections have been activated, the first of them (pilot injection) with the only purpose of further increasing the cell temperature prior to start of main combustion. Moreover a modification of the dwell time has been performed in order to determine different temperatures at start of main combustion. In fact, as shown in Figure 2, the cell pressure, due to heat losses, is characterized by a decreasing trend (after the combustion process) over time.

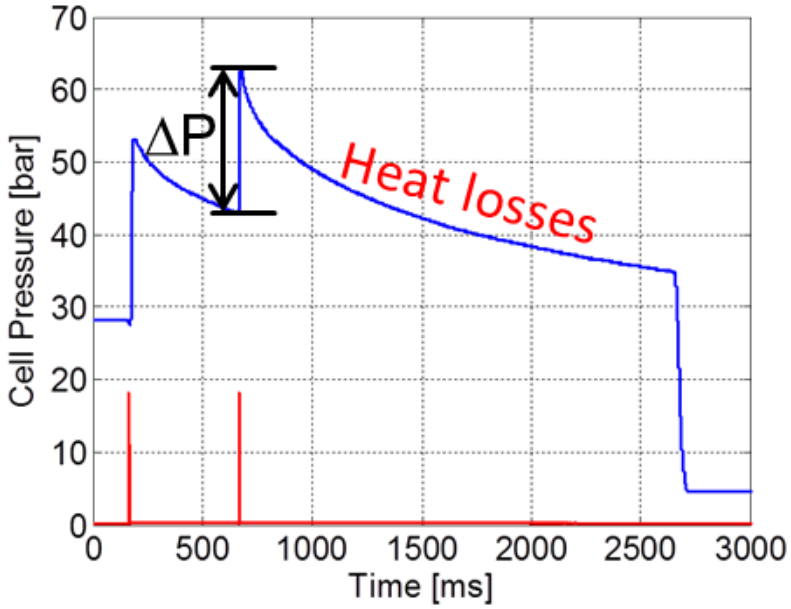

Figure 2: In cell pressure and energizing signal to the injector

Different temperatures at start of main combustion (SOC), which lead to a modification in ignition delay and therefore premixed combustion fraction variation, are investigated in order to evaluate, for the different fuels, their influence on soot formation. Considering the different fuels energy and oxygen content, a calibration of injection duration has been performed for each fuel to achieve the same injected energy (4.1 kJ per injection) and thus the same ΔP=20 bar (figure 2).

Engine set-up

The second and the third part of the project is conducted on an experimental single-cylinder DI diesel engine (Figure 3). It is based on a MTU 396 series engine and is equipped with a common rail injector system capable of injection pressures up to 1600 bar and an 8 hole Ganser 218 solenoid injector. The engine is connected to a Zöller – Kiel AG B-300 AC dynamometer characterized by a maximum absorbable power of 260 kW and a maximum speed of 7500 rpm. An external compressor able to supply pressurized air up to 5 bar is connected to the engine intake while a heating/cooling system allows conditioning the intake air in a 17 – 100°C temperature range.

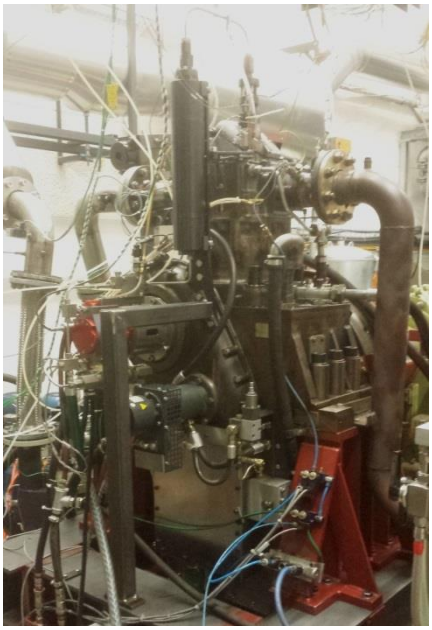

Figure 3: MTU-396 Single Cylinder Diesel Engine

Moreover, the experimental engine, which main characteristics are reported in Table 2, is provided with an exhaust gas throttle allowing the exhaust gas back pressure management.

Table 2: MTU – 396 single cylinder engine specifications

Parameter	Unit	Value
Bore	mm	165
Stroke	mm	185
Compression Ratio		13.7
Speed Range	rpm	800 – 2100
Number of valves		4 (3 with extra access)
Maximum in-cylinder pressure	bar	155

A piezo-quartz pressure transducer (±0.1% accuracy) to detect the in-cylinder pressure signal, several pressure and temperature sensors in different parts of the engine and a current probe to acquire the energizing current to the injector are installed. The engine management (e.g. load, injection pressure and injection timing) has been achieved using d-Space. For the acquisition of the in-cylinder pressure signal, intake and exhaust pressures and the energizing current to the injector a Trans AS data recording system has been used while the data post – processing has been carried on with Matlab. In order to investigate the OME1 fuel and have the possibility of switching from conventional diesel to it with the engine in operation, aa additional injection system is being realized and described in the following (sketch of the whole injection system in Figure 4).

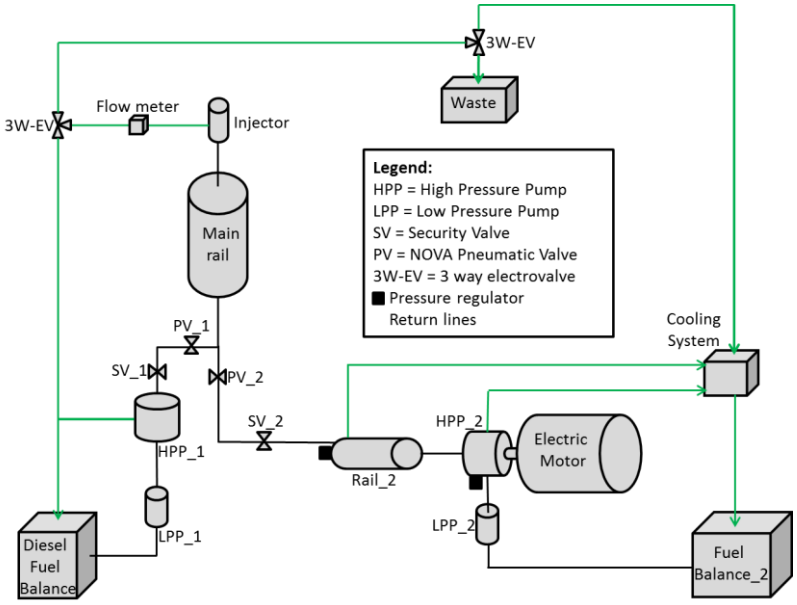

Figure 4: Sketch of the MTU engine injection system

The additional system consists of a fuel balance, a low pressure pump (LPP_2), an electric motor driving a high pressure pump (HPP_2) and a rail. Two pneumatic valves, PV_1, normally opened, and PV_2, normally closed, allow the main rail to be filled either by fuel coming from the engine fuel line (Diesel balance, LPP_1 and HPP_1) or from the auxiliary fuel line. On both fuel lines, before the pneumatic valves, two security valves have been inserted in order to ensure that, in case of a system failure, pressure is never exceeding 2000 bar. The management of the pressure in Rail_2 is done controlling, through a PWM digital modulation, the pressure regulators mounted on HPP_2 and Rail_2. In addition, on the return line from the injector, a flow meter (used to control the correct injector behavior especially when the OME fuel is adopted) and two electronically controlled 3 way valves are mounted. The two valves are used to connect the injector return line to the diesel fuel balance (when commercial diesel is used), to a waste tank (during transients) or to the Fuel balance_2. Transients are verified as soon as PV_2 opens (and PV_1 simultaneously closes) connecting the OME fuel line with the main rail. In fact, as soon as OME starts to enter in the Main rail, a diesel-OME blend, with increasing OME percentage, will be formed. During the transient period, fuel consumption measurements are not significant thus the return line from the injector is sent to a waste tank. The remaining diesel in the main rail is consumed in about 5 minutes (depending on the injected quantity); once only OME will be filling the rail, the second 3W-EV switches the circuit connecting the line to Fuel Balance_2 and allowing measurements with OME. The whole system is controlled through d-Space in order to manage the injection pressure (an additional pressure sensor is mounted on Rail_2) ensuring, in the auxiliary system, the same pressure of that in the main system. This avoids the formation of pressure waves once PV_2 is opened. Moreover, since OME (with low chain length, OME1 and OME2) is characterized by a low boiling point at atmospheric pressure, the return fuel line is cooled before reaching Fuel Balance_2 in order to avoid evaporation.

Exhaust emissions have been measured by means of the following analyzers:

An ECO PHYSICS CLD 82 for NO_X emissions,

An ABB Uras 26 for CO_2 emissions.

An ABB Magnos 206 for O_2

An AVL 415 Smoke Meter for soot measurements.

Investigated fuels

In part two, the investigation focused on the comparison between the reference diesel fuel and two blends composed of 90% baseline diesel – 10% POMDME by volume and 95 % baseline diesel – 5% POMDME by volume respectively. The POMDME fuel (characterized by the following composition: 0.55 wt-% Methylal, 0.07 wt-% Methanol, 0.05 wt-% Ethanol, 41.51 wt% OME2, 15.5 wt-% OME3, 27.52 wt-% OME4, 8.74 wt-% OME5, 4.58 wt-% OME6, 2.15 wt-% OME7 and 0.33 wt-% Trioxane) presented an oxygen overall mass fraction of 0.46 g/g, an energy content below 22 MJ/kg and a density of 1012.96 kg/m3 at 25°C. At the same temperature of 25°C, instead, the commercial diesel density is 840 kg/m^3. Therefore the two investigated blends, denoted in the following as 5% POMDME and 10% POMDME, are characterized by an oxygen mass fraction of 2.74 and 5.44 wt-% respectively.

In part three, neat OME in a composition of approximately of 80% OME_3 and 20% OME_4 with a lower heating value of 19.4 *MJ/kg* is used.

Operating conditions

In the second part, the experimental investigation focused on exploring the effect of fuel and oxygen concentration at intake on engine out emissions and performance. Tests have been performed at 1050 rpm and two BMEP values, 8 and 10.5 bar. Table 3 reports the investigated operating conditions.

Table 3: Operating conditions

SOI [cad atdc]	O_2 at intake [%]	BMEP [bar]	Intake Pressure [bar]	Exhaust Pressure [bar]	Injection pressure [bar]
-12, -9, -6	15, 18 and 21	8	1.5	1	800
-12, -9, -6	15, 18 and 21	10.5	2	1.5	1000

A single injection strategy has been chosen for the tests and, in order to fix the BMEP at the constant values of 8 and 10.5 bar for fuels characterized by different energy content, the duration of injection has been tuned for each fuel. The tuning has been conducted for the conditions without EGR and the same injection duration has then been kept for conditions with EGR.

In the third part, This section provides detailed results of distinct reference operating conditions and characteristic values, calculated for all recorded operating conditions, including variations in fuel, nozzle size (diesel: small and big nozzle, OME only big nozzle), EGR, boost pressure and load. A significant number of operating conditions with OME have been measured under global stoichiometric conditions. Figure 5 provides an overview concerning the operating conditions recorded, showing the ranges of BMEP and global lambda for all points. The third part can be derived into 3 sub-parts:

Diesel standard operating conditions.

Reference operation conditions using the bigger nozzle holes for operation with Diesel and OME without EGR.

Engine parameter variation using OME, approaching stoichiometric conditions.

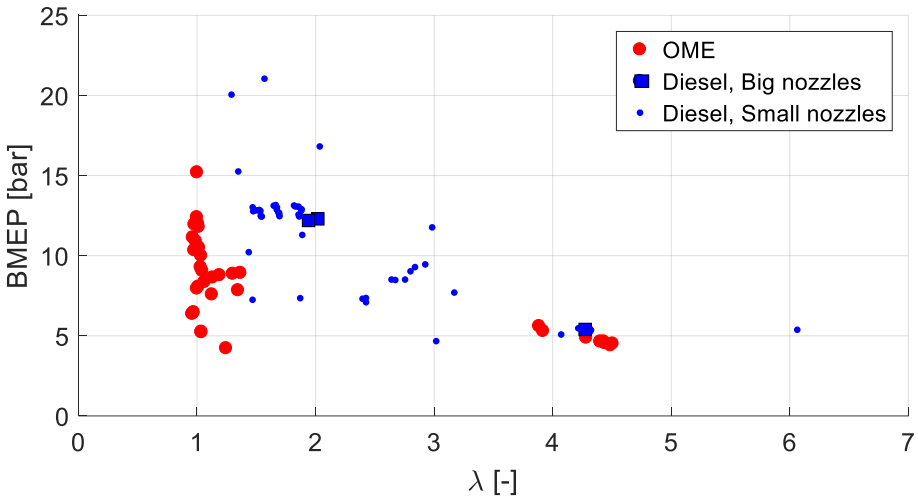

Figure 5: operating conditions overview. Red: OME, blue: Diesel, small circle: 0.24 mm nozzle, big square: 0.29 mm nozzle.

1.1.5. Experimental Results

Part one: Constant Volume Chamber
The results are discussed in two sections: a first section for the main optical results and a second section for exhaust measurements comparing the different oxygen content effect on soot emissions.

Optical results
The investigation focuses on the impact of different oxygen content on flame temperature and soot formation/oxidation processes through the 2D2CP technique with the calculation of the kL factor. The four investigated fuels, for this specific comparison, are OME2 pure (oxygen content: 45.3% in mass), OME2-50%, OME2-30% and OME2-5%. The three blends present an oxygen content of about 24.4, 14.8 and 2.6% in mass respectively. Results from pure OME2 are not shown because no soot was optically detected for any investigated operating condition, meaning that the particulate matter from pure OME2, if any, is below the detection threshold of the technique. For each fuel a temperatures at SOC of 1150K has been considered and results are reported in Figure 6 (kL factor and energizing signal to piezo injector).

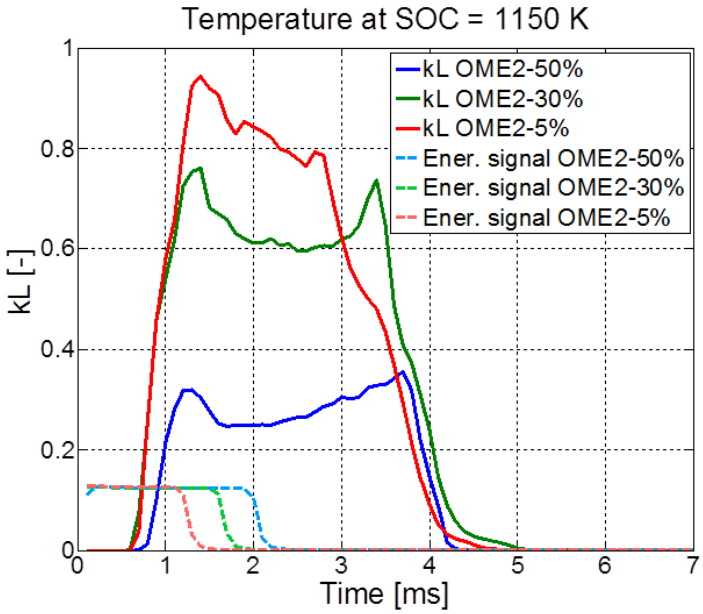

Figure 6: kL factor and energizing signal to piezo injector (start at time 0) for OME2-50%, OME2-30% and OME2-5% at 1150K@SOC

The energizing curves reported in the Figure 6 show longer injection duration for higher oxygen content of the blend to keep the total injected energy constant. A first evidence coming from Figure 6 is that increasing the oxygenated fraction in the blend, a massive reduction of the peak at end of the soot formation dominated phase is achieved. This first phase is followed by a second formation/oxidation phase in which soot formation and oxidation processes roughly cancel each other out. OME2-5% shows the shortest duration of this process because it is characterized by the shortest injection duration. Finally, during the third, oxidation dominated phase, temperatures rapidly decrease and flame luminosity falls below the minimum detectable value. The second peak, corresponding to the end of the balanced soot formation/oxidation phase, particularly showed by the OME2-30% blend, is correlated to a decrease in lift-off length which brings the flame luminosity backwards towards the injector tip with an increase of the soot formation area. The lift off length is affected by temperature and fuel oxygen content. In a constant volume chamber, with the lack of expansion, shorter lift off lengths with increasing injection durations are expected. This explains the presence of the peak corresponding to the end of the balanced soot formation/oxidation phase particularly for the blends, characterized by longer injection duration because of their lower energy content.

For OME2-5% and OME2-50%, at 1150K @ SOC, Figure 7shows the evolution of one of the eight jets from the piezo injector. The evolution is seen in the image of the jet at 1.4 ms, 2.2 ms and 3.5 ms after start of injection (SOI). These three timings represent an early phase of combustion, an instant around the maximum soot formation timing and a relatively late phase of combustion respectively. The images from the two blends are overlapped, subtracted from each other and contoured by a red line for the OME2-5% blend and a blue line for the OME2-50% one. This means that white areas within both the red and blue contours state an equal intensity from the two blends. At any timing after SOI, the OME2-50% blend shows a far smaller area of soot formation, perfectly overlapped only for the first two timings. In fact at 3.5 ms after SOI, the combustion process relative to the OME2-5% blend has spread at annulus shape giving no more chance to detect the fuel jet while for the OME2-50% blend it is still visible. This inequality is due to the different injection duration characterizing the two fuels.

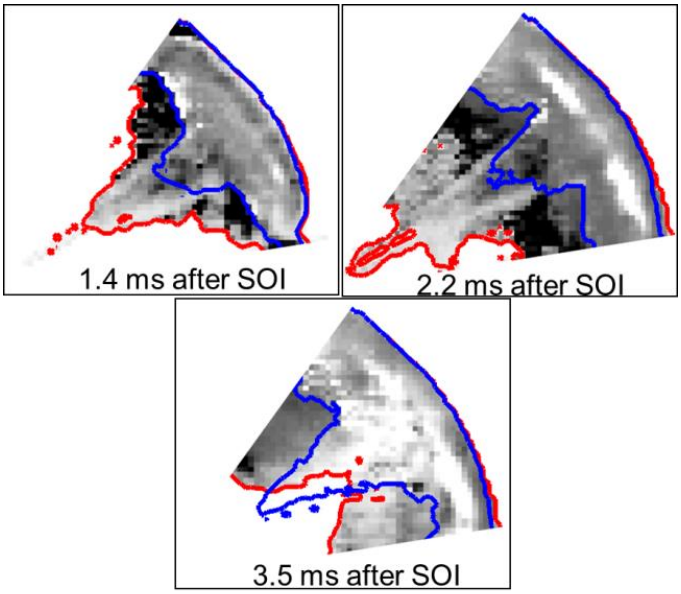

Figure 7: Overlapping of fuel jet for OME2-5% (contoured in red) and OME2-50% (contoured in blue) at 1150K@SOC and 1.4, 2.2 and 3.5 ms after SOI

The Figure 8, instead, shows luminosity at 309±5 nm wavelength (OH-peak in the emission spectrum) results for pure OME2 and OME2 in diesel blends with the aim of following the evolution of combustion precursors. Figure 8 displays 4 images (representing only one quarter of the cell), one for each investigated fuel, at a specific temperature at SOC. Images are shown in clockwise layout from highest to lowest fuel oxygen content. The images from the three blends (increasing brightness with lower percentage of oxygenated fuel) are characterized by a higher luminosity with respect to pure OME2. This effect is probably coming from soot (emitting all over the spectra) which emits even at 309 nm, covering, in this way, the OH signal. This means that the only fuel from which information on combustion precursors can be considered is the OME2 pure. This fuel in fact has shown a soot level below the 2D2CP detection sensitivity threshold.

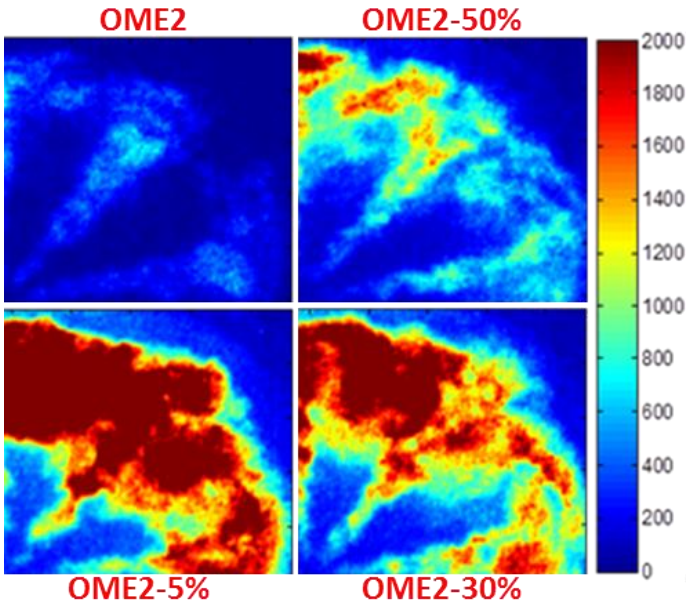

Figure 8: Luminosity at 309±5 nm – 1150K@SOC

Exhaust results

In order to compare exhaust emissions results from the different investigated fuels, a Cambustion DMS 500 fast particle spectrometer has been used. For each fuel the exhaust emission values presented in the following are normalized to the one of commercial diesel at 1010K@SOC. Figure 8 reports normalized soot values vs fuel oxygen content of the investigated fuels at the operative condition of 1010K@SOC. Error bars have been inserted in the figure in order to take into account the relatively high values of cycle to cycle variation provided by the measurements. The Figure 9 shows as an increase in fuel oxygen content determines always a decrease in soot emissions. It is worth to underline as the soot emissions reduction is not linear with the oxygen content increase. In fact since the different investigated fuels are characterized by a different adiabatic flame temperature, number of C-C bonds and local air fuel ratio (parameters correlated to soot formation), a linear correlation soot reduction – oxygen content may not be expected. Pure OME2 and OME2/3/4 basically show an almost smokeless combustion while still some soot mass is detected with OME1. A remarkable result, though, is related to OME2-5%: a 2.6 % oxygen content in the blend already leads to a reduction of about 30% in soot mass.

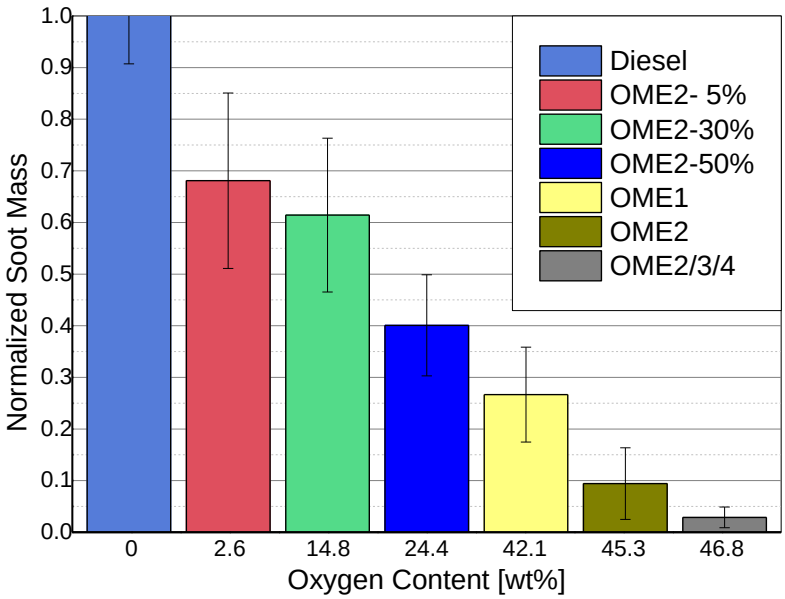

Figure 9: Normalized Soot Mass for the investigated fuels at 1010K @ SOC

Figure 10 reports the comparison of OME2, OME2/3/4 and the OME2 blends at different temperatures at SOC. The yellow arrows indicate the direction of soot reduction with respect to temperature at SOC. OME2 and OME2/3/4 lead to a reduction of more than 85% with respect to the reference diesel for any operating condition. The effect of temperature at start of combustion has to be analyzed in two different ranges: a slight trend (within the repeatability, error bar, of the measurements) towards higher exhaust soot with lower temperature is visible down to 960K.

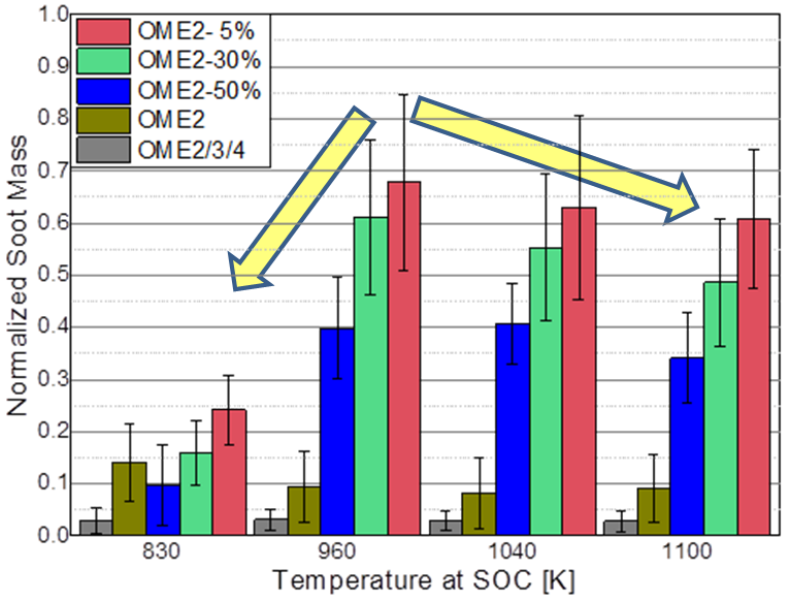

Figure 10 Normalized Soot Mass: OME2/3/4, OME2 pure and OME2 in diesel blends at different temperatures @ SOC

In fact, a decrease in temperature determines a decrease in soot formation on one hand but a slower oxidation process on the other hand. As a result, an overall slight increase of soot detected at the exhaust is observed. A further decrease in temperature (960K to 830K), instead, determines, for all

the investigated fuels, the transition towards a partially premixed combustion mode which permits a massive reduction in soot emissions due to reduced mass fraction burnt during diffusive combustion, as shown in the figure.

Finally, a comparison of particle concentration with respect to particle diameter for OME2-5% and OME2 pure is reported in logarithmic scale in Figure 11. In order to show the particle concentration of the two fuels on a single scale, a break on the y-axis has been introduced. The main difference which clearly appears comparing the two fuels is that the pure oxygenated fuel produces no particles bigger than 50 nm (diameter) while the combustion of OME2-5% shows a minor number of presumably volatile particles up to 20 nm (since no volatile particle remover was used) and larger particle agglomerations, up to 500 nm. This means that even for pure oxygenated fuels the first nucleation phase of the soot formation process takes place but the following agglomeration phase is strongly reduced. This effect is most probably due to the molecule oxygen content which could then oxidize the "new born" nucleation cores. In addition, the larger particles from OME2-5% (bigger than 50 nm diameter) act as a sponge during the agglomeration phase thus reducing the total number of particles, even though the total mass is increased with respect to OME2 pure. Instead OME2 is characterized by volatile particles up to 20 nm and solid particles, in the range 20-50 nm, which determine most of the contribution to mass from it. It is worth to underline that no volatile particle remover has been used since their contribution to the total mass is very low.

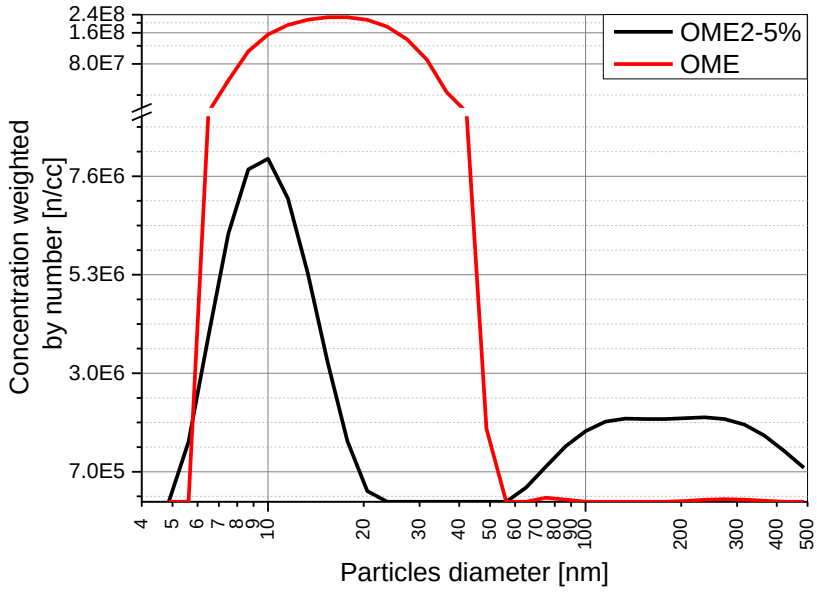

Figure 11: OME2-5% and OME2 pure at 1150K @ SOC: particle concentration

Part two: Engine with OME Diesel Blend

Since fuels from the POMDME family (with n>2) are characterized by similar physical properties with respect to commercial diesel, thus not requiring substantial modifications to the engine infrastructure, an industrial scale production could be desirable to obtain blends with diesel. In this way they could take the advantage of diesel high energy content and POMDME capability of reducing soot formation. The experimental work conducted on the MTU single cylinder "heavy duty" direct injection diesel engine aimed at examining achievable engine performance and exhaust emissions. Results for the 8 bar BMEP condition are presented in a first section, while the 10.5 bar BMEP one is discussed in a second section.

Figure 12 shows smoke results for the investigated fuels at BMEP=8 bar for the different O_2 contents at intake and start of injection. As expected, for any operating condition, a decrease in smoke emissions is noticed with decreasing EGR and increasing oxygen content of the blend. In addition, the

figure reports the average soot reduction values (with respect to commercial diesel) obtained with 5% POMDME and 10% POMDME over the whole experimental campaign at BMEP=8 bar, 19.7 and 31.4% respectively. No significant difference in smoke emissions is detected, instead, for the different starts of injection, probably because of the comparable premixed - diffusive combustion mode ratio achieved over the selected SOIs.

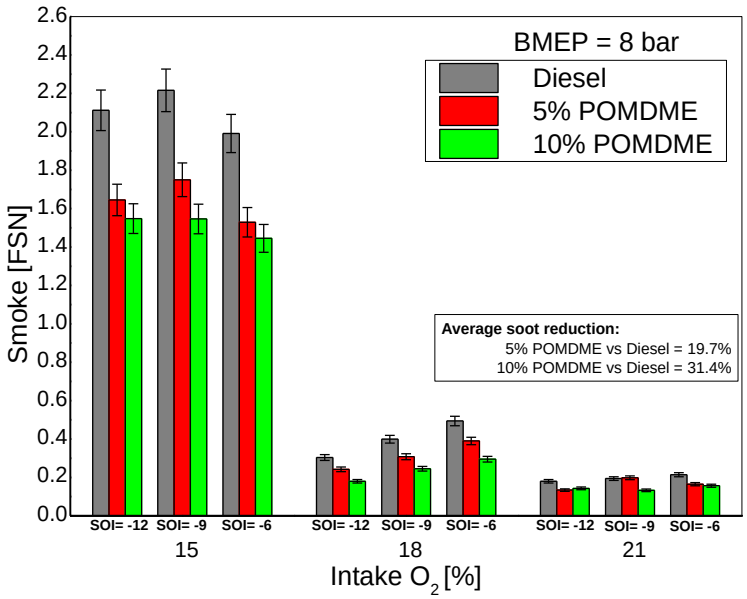

Figure 12: Diesel, 5% POMDME and 10% POMDME - Smoke emissions @ BMEP=8bar

With respect to NO_X emissions (Figure 13), a similar behavior of the different fuels in operating conditions with EGR has been observed. This allows stating that the recirculation of exhaust gases determines the major variation of this pollutant while low NO_X values have been achieved even with fuels containing molecular oxygen. An increase in NO_X emissions, especially with the 10% POMDME, has been though detected under zero EGR operating conditions.

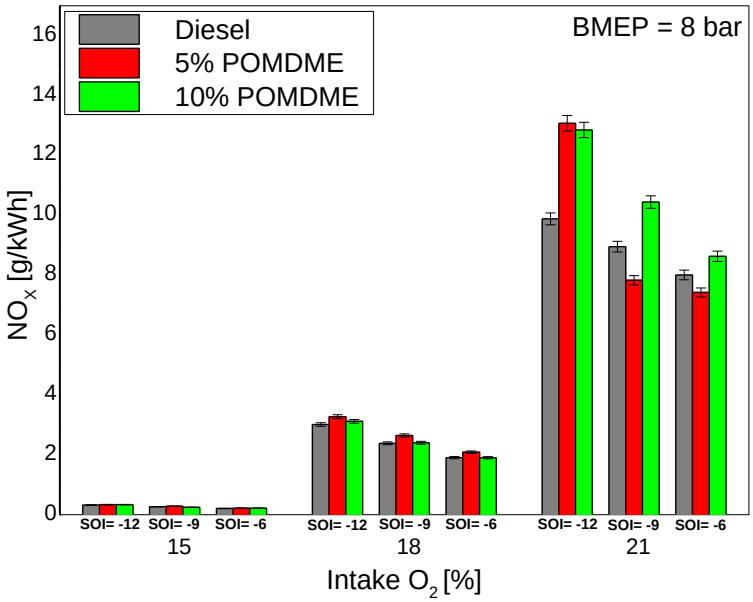

Figure 13: Diesel, 5% POMDME and 10% POMDME - NO_X emissions @ BMEP=8bar

In order to analyze the trade-off Soot NO_X for the different investigated fuels, results are reported in Figure 14. The condition allowing the best compromise between the two pollutant species is the intake O_2=18% one. Within this condition, the figure clearly shows as the adoption of the oxygenated blends allows a reduction in soot associated with no significant increase in NO_X, thus achieving a better trade-off. Trend curves have been inserted in the figure in order to show how the green scatters associated to the 10%POMDME lay constantly below the grey ones (commercial diesel). The figure even shows a countered blue line area representing the minimum emission area. It has been selected so that the NO_X fulfils the IMO TIER III regulation for an engine with rpm_{max}=2000 and the smoke limit is below 0.5 FSN. The only operating point included in the mentioned area is the one corresponding to the 10% POMDME blend.

In order to further understand the behavior of the different investigated fuels for the intake O_2=18% condition (being the most interesting one), heat release curves are shown in figure 5 for the SOI=-12 cad atdc case. The same considerations, though, are still valid for the other SOIs. The curves show a similar profile both in the premixed and diffusive combustion phase allowing to consider that the addition of the oxygenated fraction does not introduce deep modifications in the ignition delay, combustion behavior and combustion efficiency, as will be further discussed in the following. This explains the similar NO_X emissions, shown in figure 4 even though, the presence of molecular oxygen allows, for the blends, a reduction in smoke emissions. In addition, it is worth to observe from Figure 15, as the final part of diffusive combustion (from 370 cad atdc) seems to be slightly faster for the blends. This fact has to be connected with the higher oxygen fraction which enhances the oxidation process.

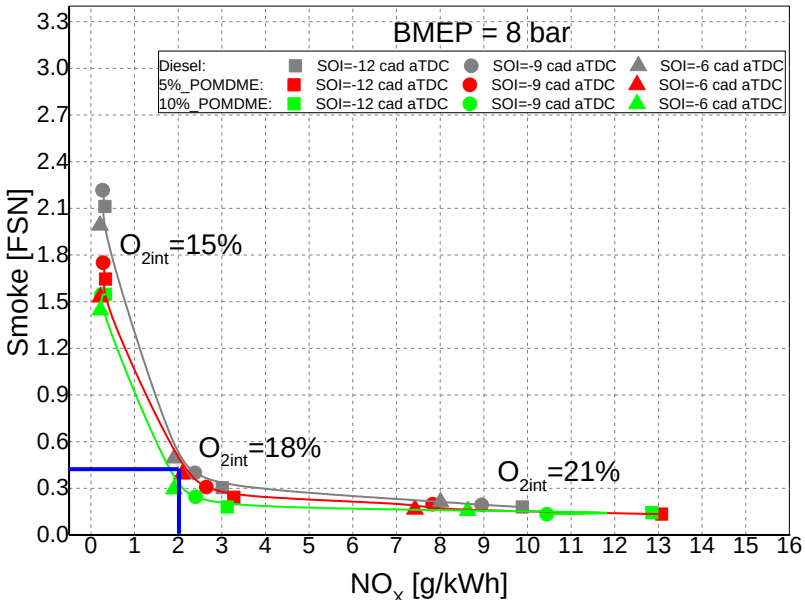

Figure 14: Diesel, 5% POMDME and 10% POMDME – Smoke NO_X trade off @ BMEP=8bar

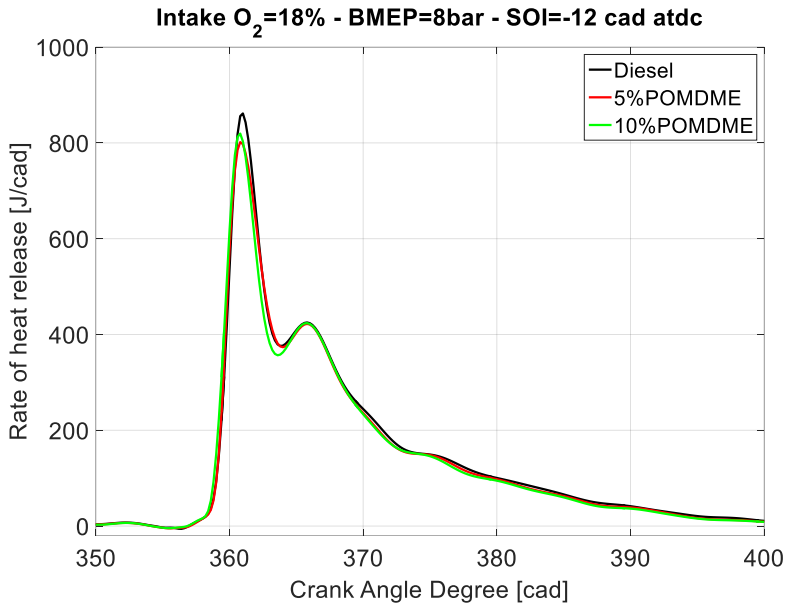

Figure 15: Diesel, 5% POMDME and 10% POMDME – Rate of heat release curves @BMEP=8bar, intake O_2=18% and SOI=-12 cad atdc

Results of break specific fuel consumption for the different investigated fuels are discussed in Figure 16. The low energy content of the oxygenated fuels (less than 22 MJ/kg) determine, for the two investigated blends, a higher amount of fuel that has to be introduced in the system in order to achieve the same power output. Therefore, fuel economy could be the main reason for considering, in a hypothetical industrial scale production, 10% POMDME as a maximum percentage to be blended in commercial diesel. Figure 17 reports BSFC trends with respect to the different fuels and operating conditions as well as the average increment (with respect to commercial diesel) detected with 5% POMDME and 10% POMDME, 2.2 and 4 wt-% respectively (considering the whole experimental

campaign at 8bar BMEP). In addition, an increase in BSFC is shown for any investigated fuel when retarding the start of injection from -12 to -6 cad atdc because of a lower efficiency due to a higher fraction of the combustion process taking place during the expansion stroke. Finally, an increase in BSFC, as expected, is even noticed with increased EGR rates.

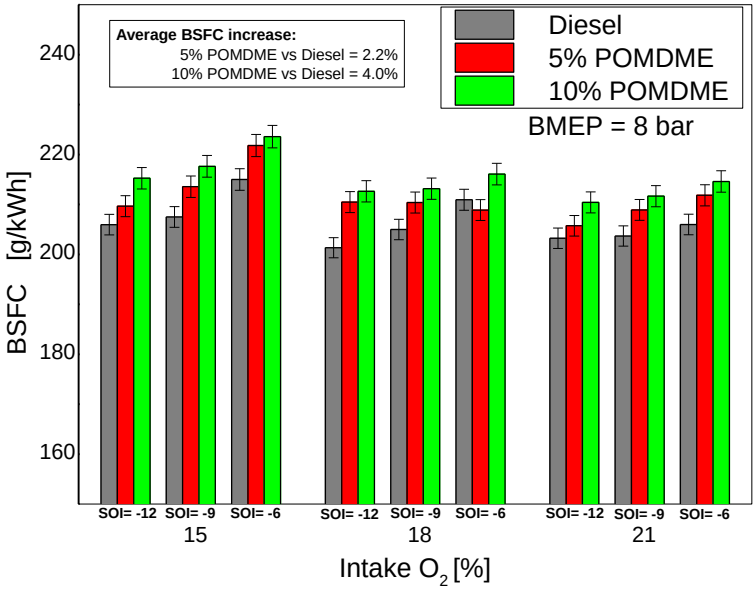

Figure 16 Diesel, 5% POMDME and 10% POMDME – BSFC @ BMEP=8bar

Moreover, in order to further discuss the behavior of the different fuels towards combustion efficiency, Figure 17 reports values of CO_2 measured at the exhaust. CO_2 emissions, which give indications on the efficiency of the combustion process, range on similar values for the different fuels and SOIs. This confirms that no decrease in combustion efficiency is introduced with the oxygenated blends while an increase in EGR leads to more CO_2 detected at the engine exhaust.

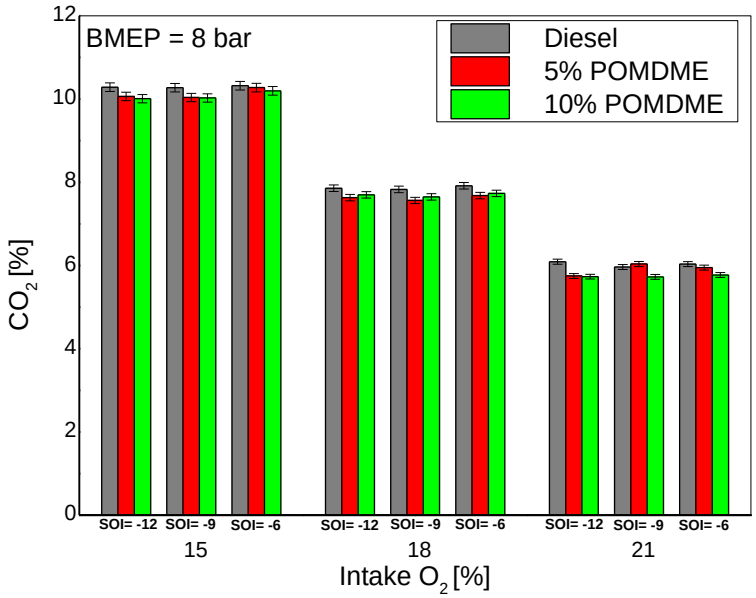

Figure 17: Diesel, 5% POMDME and 10% POMDME – CO_2 emissions @ BMEP=8bar

The second part of this section discusses the main results achieved at the higher investigated load condition, 10.5 bar BMEP. As shown in Figure 18, a reduction in soot emissions has been achieved, even at this higher load, for any operative condition when adopting the 5% POMDME and 10% POMDME blends. An average soot reduction (with respect to commercial diesel) over the whole experimental campaign at BMEP = 10.5 bar has been calculated for the two blends and the result shows that almost 35% of soot reduction is achieved with the 10% POMDME blend while more than 10% reduction is obtained with the 5% POMDME one. In addition, as discussed for the 8 bar BMEP load, still no significant difference in smoke emissions is detected for the different starts of injection. At 10.5 bar BMEP though, just a minor decrease in soot is noticed when moving from the 18% O_2 at intake condition to the zero EGR one probably because of the effect of higher temperatures favorable for soot oxidation. A further increase in EGR, though determines a massive increase in soot for any investigated fuel. In fact, the 15% O_2 at intake condition determines a substantial reduction of combustion temperatures because of the high amount of inert gas introduced in the cylinder. As a consequence NO_X emissions are almost completely removed, as shown in Figure 19 but the soot oxidation phase is strongly affected with unacceptable soot values detected at the exhaust. Figure 19 demonstrates as, even at 10.5 bar BMEP, the investigated oxygenated fuels did not lead to significant increase in NO_X emissions.

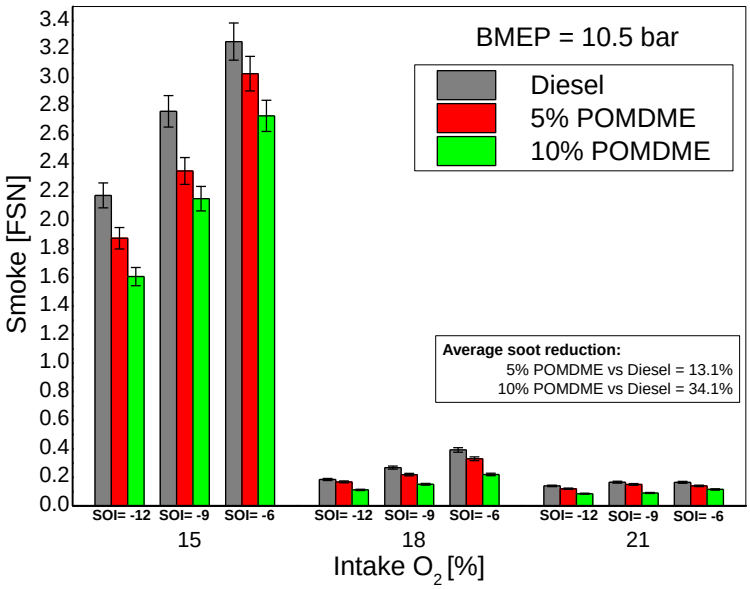

Figure 18: Diesel, 5% POMDME and 10% POMDME - Smoke emissions @ BMEP=10.5bar

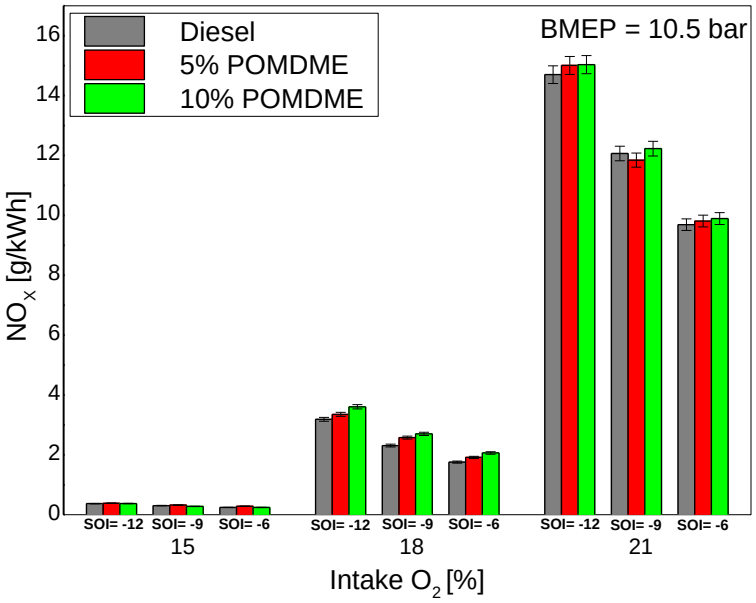

Figure 19:Diesel, 5% POMDME and 10% POMDME - NO_X emissions @ BMEP=10.5bar

A trade-off Soot NO_X plot is shown, even for the 10.5 bar BMEP (Figure 20), in order to clearly highlight the operating conditions providing the best results. Within the 18% O_2 at intake condition, which clearly appears to be the best compromise for a reduction in both soot and NO_X, the most retarded start of injection (-6 cad atdc) allows, for any investigated fuels, a further reduction in NO_X probably because of the decrease in combustion temperature due to a higher fraction of the combustion process taking place during the expansion stroke. Even for this BMEP condition, the trend curves demonstrate the possibility to reduce smoke in the whole range of NO_X emissions. Furthermore, within the 18% O_2 at intake and SOI = -6 cad atdc condition, the 10%POMDME still allows to fulfil the IMO TIER III NO_X regulation showing, in addition, a strong reduction in smoke with respect to commercial diesel.

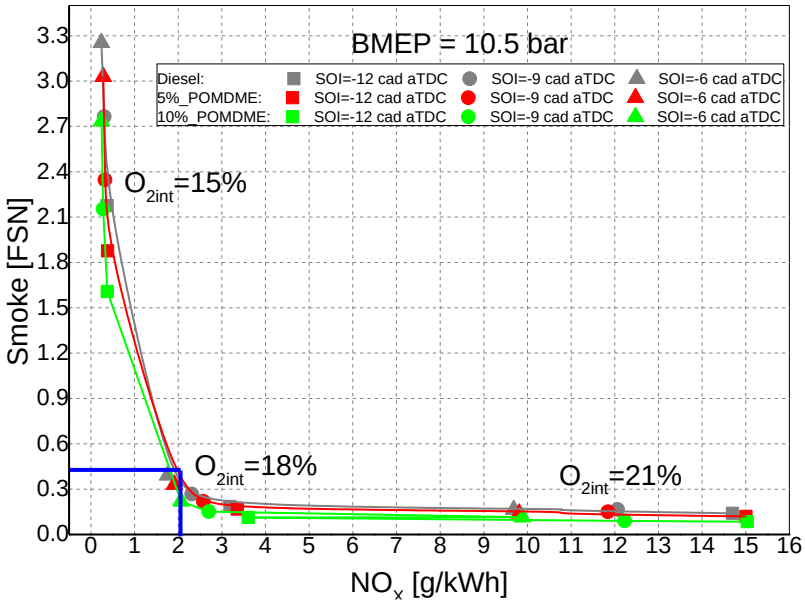

Figure 20: Diesel, 5% POMDME and 10% POMDME - Smoke NO_X trade-off @BMEP=10.5bar

Finally results of break specific fuel consumption for the different investigated fuels are discussed in Figure 21. Once more the lower energy content of the oxygenated fuels forces to increase the injected fuel amount in order to achieve a fixed power output value. An average increase of 2.3% and 4.3% has been calculated over the whole experimental investigation at 10.5 bar BMEP for the 5% POMDME and 10% POMDME blends respectively. Despite the observed increase in break specific fuel consumption, no significant variation in CO_2 at exhaust for the different fuels is found (Figure 22), underlining, once more, as the use of the oxygenated blends is not negatively affecting combustion efficiency.

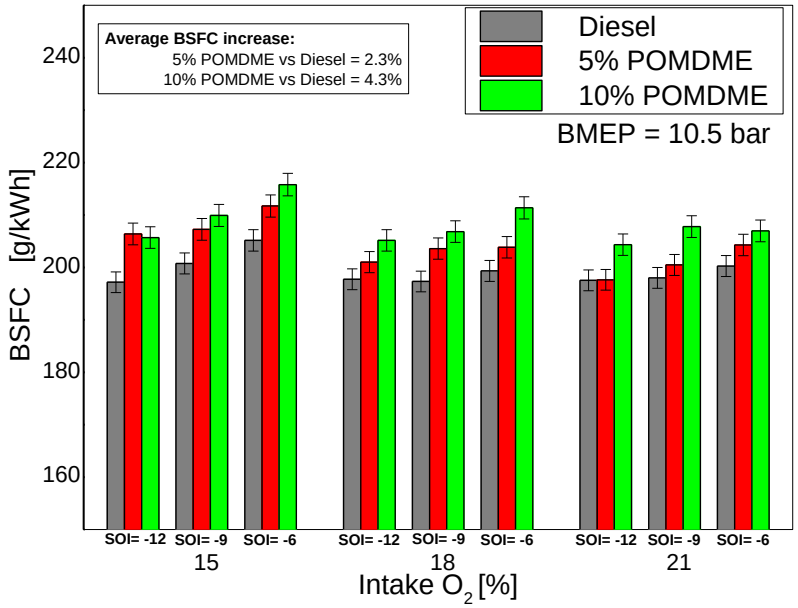

Figure 21: Diesel, 5% POMDME and 10% POMDME – BSFC @ BMEP=10.5bar

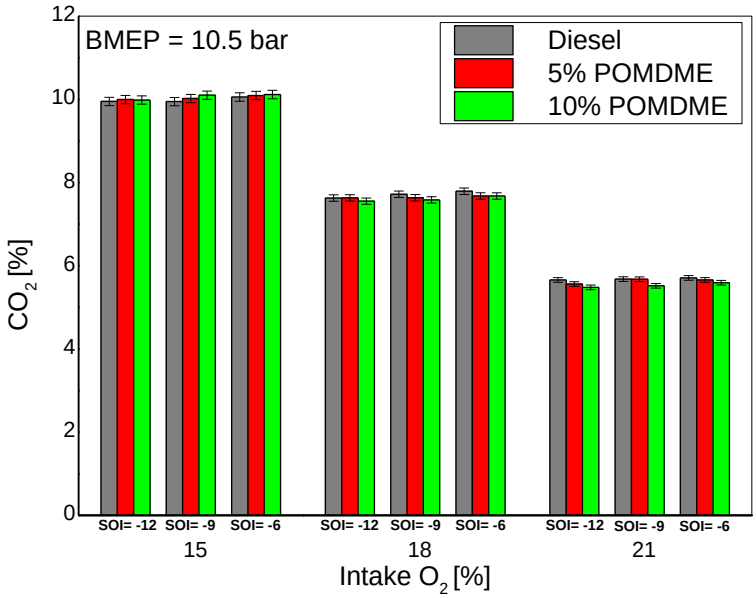

Figure 22:Diesel, 5% POMDME and 10% POMDME – CO_2 emissions @ BMEP=10.5bar

Part three: Neat OME under Stoichiometric Operation

Methodology

Modelling of the Fuel Injection

In the present work the information available about the injection process is used to determine where the fuel-air mixture reaches a flammable composition. This is then used to evaluate the influence of turbulence originating from the injection on the mixing of fuel and oxidant and therefore on the heat release rate.

Approach

Considering the requirements presented above, the approach adopted to simulate the injection process uses two, mutually redundant, models. The first is a 1-D model by Musculus and Kattke and relies on momentum and mass conservation. The corresponding conservation equations for the spray cross section averaged quantities are solved in the axial direction of the jet. The spray is discretized in "slices" perpendicular to its axis. This means that there is one single control volume per (discrete) axial position. The cone angle of the spray is an input parameter and remains constant.

The model provides local speed and fuel volume fraction for any time at any (discretized) location in the spray. The second model, developed by Naber and Siebers to describe the injection of a fluid into another one can be used to predict the behaviour of isothermal and incompressible sprays with rectangular injection profiles. It is assumed that the velocity profile is uniform, the velocity of the fuel and of the entrained air is the equal and the spray cone angle is constant. The model provides the spray penetration and the equivalence ratio over spray distance and time during the injection process. The Naber-Siebers model is computationally less expensive. The Muskulus-Kattke model is used as reference model. For similar quantities, the Naber-Siebers model is preferred due to its simplicity.

Tools for the Analysis of the HRR

This section provides an overview about the tools used to analyse and characterize the heat release rates of the diesel and OME combustion processes.

Characteristic mixing time τ_{mix}

A typical heat release in a Diesel engine is divided into two parts: the first premixed phase where the limiting factor of the reaction speed is the chemical kinetics, and the diffusion phase, where the rate with which fuel and oxidant mix is decisive for the rate of heat release. In this second phase, the temperature for fast chemistry is sufficiently high and the rate limiting mechanism is the diffusion respectively the supply of fuel. In order to characterize the diffusion mechanism the concept of *mixing time* is introduced. To quantify this mixing ability the characteristic mixing time τ_{mix} is used. This describes the time the fuel takes to find the necessary oxygen to burn.

It is assumed that during the diffusion phase of combustion the heat release rate is limited to the available fuel energy input:

$$HRR_{diff} \cdot C = Q_{avail} \tag{1}$$

The proportionality constant C is a characteristic time, resulting from the analysis of the units.

$$C = \frac{Q_{avail}[J]}{HRR_{diff}[J/s]} =: \tau_{mix}[s] \tag{2}$$

The available fuel Q_{avail} can be defined in various manners. First, all the fuel injected is available; second, all the evaporated fuel is available or third, only fuel, which has already mixed to the lower flammability limit is available.

If the first definition is used, the available fuel is the difference between the injected energy in form of fuel and the released heat through combustion:

$$Q_{avail}(t) = \int_{SOI}^{t} \dot{m}_{inj} \cdot dt - \int_{SOI}^{t} HRR \cdot dt \tag{3}$$

Assuming fast evaporation and a significant diffusion combustion portion, the approach is sufficient. However, in the early phase of diffusion combustion, also the available respectively entrained oxygen can be rate limiting and need to be considered as in the third approach. Therefore, the mechanics of the spray injecting fuel into the combustion chamber have to be considered. In order to estimate the local air-to-fuel ratio and to determine the amount which is above the flammability limit, the previously described Musculus-Kattke model for air entrainment was used. The lower flammability limit was arbitrary set to λ=0.3. In this case the available energy as a function of the time is computed as

$$Q_{avail}(t) = Q_{ready} - \int_{SOI}^{t} HRR \cdot dt \tag{4}$$

where Q_{ready} is that energy given by the amount of fuel which is flammable (above λ=0.3), multiplied with its lower heating value.

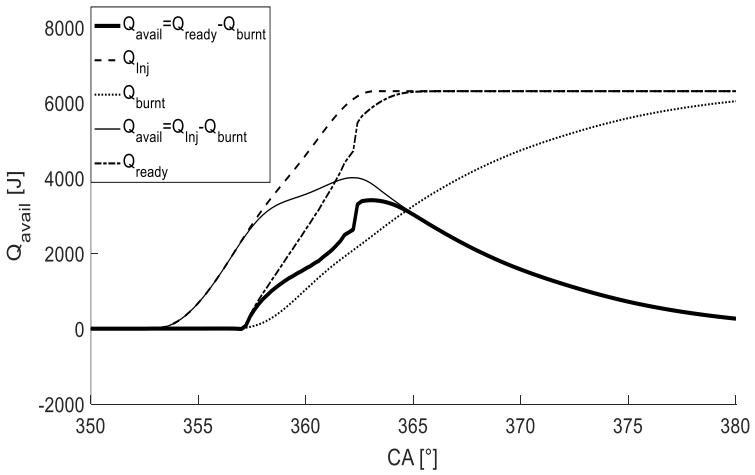

Figure 23: Available energy for a sample operating condition using different approaches

The dotted line in Figure 23 represents the integral of the heat released, the dashed line is the integral of the injection rate in form fuel energy. The thin solid line is the available energy Q_{avail} computed by subtracting the heat released from the energy injected. The dashed dotted line is the available flammable fuel and the thick solid is the resulting available energy obtained with it. The characteristic mixing time obtained with the first interpretation of Q_{avail} is referred to as *conventional* τ_{mix} while if the

third definition of the available energy is used, the characteristic mixing time obtained, is defined as $\tau_{mix,air}$.

In order to isolate the heat released in the diffusion combustion regime from the total heat released, a separation algorithm was developed. This procedure finds the first peak of the total heat release rate by finding the minimum of its second derivative. A Vibe function (also known as Wiebe) is then fitted to this first peak and is subtracted from the total heat release rate in order to get the diffusion heat release rate. Then, the rates obtained are smoothed with a moving average algorithm and the final premixed heat release rate is calculated by subtracting the diffusion heat release rate from the total one. Figure 24 shows a heat release rate of a sample operating condition with the corresponding premixed and diffusion phases. In addition, the injection profile in form of fuel energy is depicted.

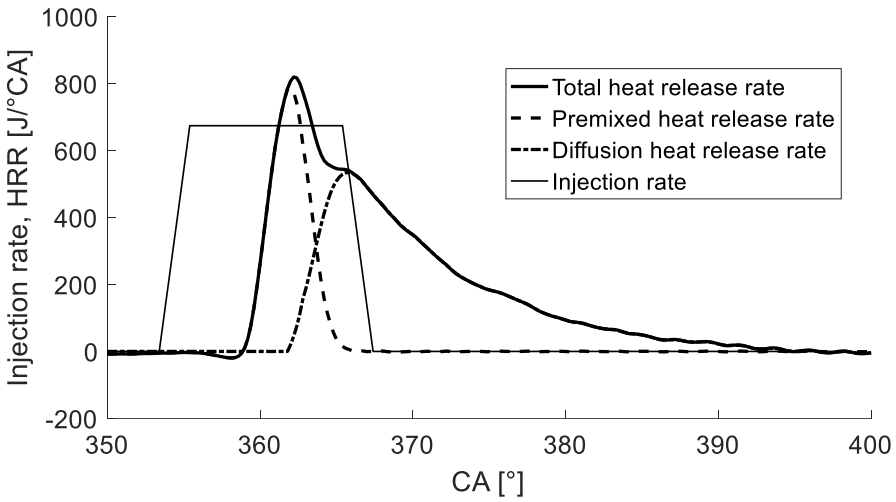

Figure 24: Sample heat release rate and injection profile, electrical SOI=10°BTDC

Influence of turbulence on air fuel mixing

In order to understand the difference in diffusion (ie. mixing) controlled combustion between diesel and OME, a comparison of the turbulence level is of high importance, as this is one of driving mechanisms for mixing. The level of turbulence cannot be described in an absolute manner with the modelling approaches used, but the rate of dissipation of kinetic energy, which can be obtained by the Musculus-Kattke approach, can be used.

The Musculus-Kattke model returns the cross sectional averaged velocity of the jet ū and the cross sectional averaged fuel volume $\bar{X}_f$ that is defined as

$$\bar{\bar{X}}_f = \frac{\Delta V_{fuel}}{V_{tot}} = \frac{m_{fuel}/\rho_{fuel}}{\Delta V} \tag{5}$$

Therefore, the kinetic energy of the spray at any given point is calculated as

$$E_{kin,s} = \frac{1}{2} m v^2 = \frac{1}{2} m_{fuel} \bar{\bar{u}}^2 = \frac{1}{2} \bar{\bar{X}}_f \Delta V \rho_f \bar{\bar{u}}^2 \tag{6}$$

In order to understand the diffusion combustion of OME and its differences compared to Diesel, it is more important to know *where* the mixing takes place and with which (relative) magnitude instead of *when*. For this reason the loss of spray kinetic energy along the spray axis is computed:

$$E_{Kin}diss = \frac{\partial E_{kin,s}}{\partial x} \quad (7)$$

The dissipation of kinetic energy is used as a quantity of turbulence, since it is the major source of turbulence generation form the spray.

Heat Release Rate

OME combustion behaviour

Figure 25 shows a comparison of the OME combustion and the diesel reference case (both with the large nozzle diameter). A lower volumetric heating value with the same injector nozzle either needs longer injection duration or higher rail pressures to achieve an equivalent power output using OME. The reference comparison uses prolonged injection duration with similar fuel rail pressure. The figure shows a comparison of the heat release rate (thick solid lines, blue for diesel, red for OME) with the corresponding premixed (dashed) and diffusion (dashed-dotted) combustion phase. In addition, a simplified fuel injection rate (thin solid) is shown in the plot. The heat release rate reveals already strong differences in the combustion, which are summarised I the following list:

The ignition delay is shorter with OME, as is expected with higher cetane number.

The premixed portion is reduced with OME due to two reasons: First, the ignition delay is slightly shorter and the injected fuel volume (with the assumption of similar injection behaviour) during the ignition delay, which is prepared for premixed combustion, is smaller. Second, the volumetric heating value of OME is smaller, thus, the effective heat release even within a similar volume is smaller.

The diffusion combustion with OME is apparently faster, and shows a particularly short burn out phase.

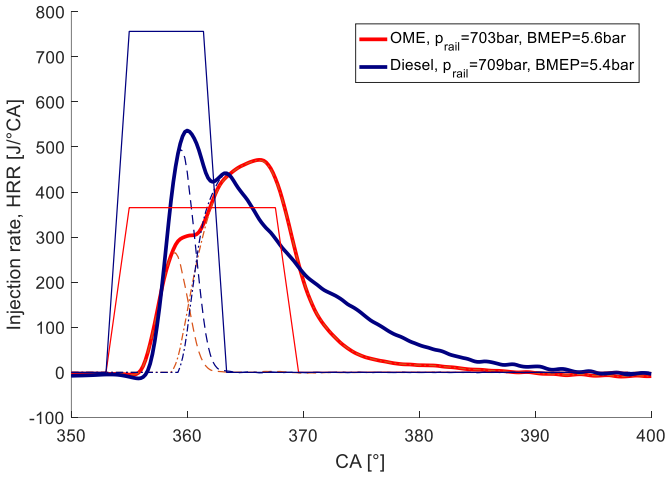

Figure 25: HRR of OME and of Diesel, SOI=10°BTDC, EGR=0%. Red: OME, blue: Diesel, solid thick: heat release rate, solid thin: injected energy rate, dashed: premixed heat release rate, dashed-dotted: diffusion heat release rate.

The speed of the diffusion combustion and the role of the fuel oxygen content need to be investigated more in detail. To explain this fact, the concept of characteristic mixing time

introduced earlier is used. The speed of diffusion combustion can be shown using the inverse of the characteristic mixing time (i.e. the char. mixing rate or frequency). Figure 26 shows the characteristic mixing frequency of OME and Diesel. The dashed lines indicate the conventional mixing rate. The solid lines use only the fuel which is already mixed to λ= 0.3 and higher, as calculated using the Musculus-Kattke model. This is done in order to account for the effect that both the fuel supply as well as the air entrainment can be the rate liming factor, particularly at the start of diffusion combustion. The cases with diesel (blue) show particularly high difference at the beginning of combustion. The difference in the OME combustion (red) is smaller, since the mixing with air to a certain stoichiometry is faster due to the lower oxygen demand from air because of the oxygen content of the fuel. The difference between OME and Diesel combustion is very high and cannot be explained solely by the oxygen content.

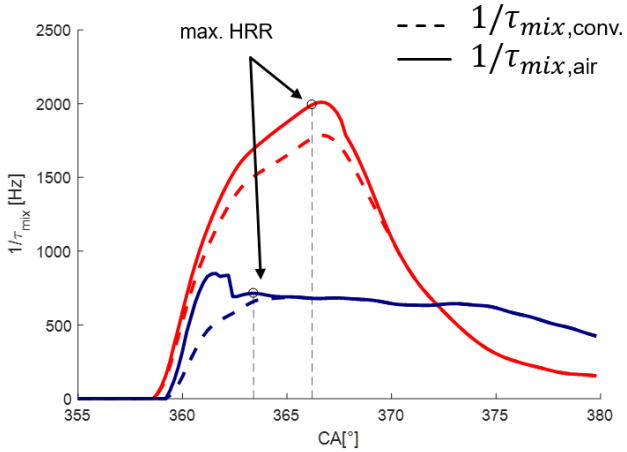

Figure 26: Characteristic mixing frequency for Diesel and OME, p_{rail}=700bar, BMEP=5.5bar. Red: OME, blue: Diesel, dashed: conventional, solid: including flammability limit.

However, the accuracy of the calculation of mixing rate at the beginning of diffusion combustion depends on the accuracy of the distribution of premixed and diffusion combustion portion. To further explain why the mixing of OME is faster than the mixing of Diesel, the role of turbulence needs to be discussed. Mixing speed is controlled mainly by two drivers; turbulence and concentration difference. As shown in Figure 27, the spray-generated turbulence is reduced with increasing distance from the nozzle due to lower dissipation rate of kinetic energy as source of turbulence, calculated using the Musculus-Kattke model (previously described).

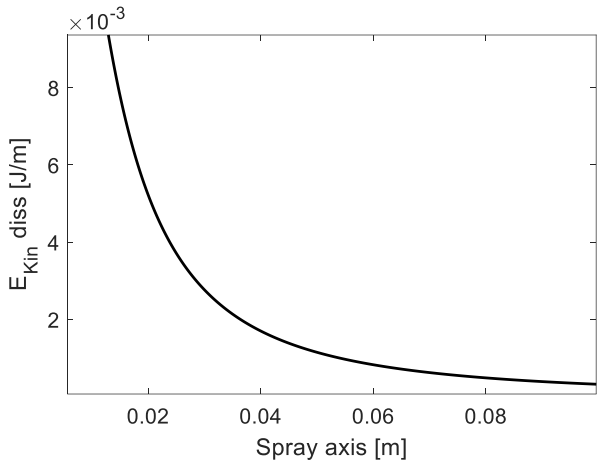

Figure 27: Dissipation of kinetic energy along the spray axis of a sample operating condition.

Assuming stoichiometric conditions as a representative combustion zone, the combustion of a type of fuel with less oxygen demand (e.g. OME, because of its inter-molecular oxygen content) is located closer to the nozzle tip, where turbulence intensity is higher and mixing can occur faster. Figure 28 shows a comparison of the dissipation rate of kinetic energy at the end of injection as a representative of turbulence level and the position of stoichiometric mixing, calculated using the Musculus-Kattke spray model and the characteristic time to mix until the spray tip reaches stoichiometric conditions (τ_{spray}). This quantity can be calculated with the abovementioned Naber-Siebers spray model, which requires much less computational effort than the Musculus-Kattke approach. Time is chosen rather than axial distance to also account for changing fuel pressures. The figure shows a visible correlation between the dissipation of kinetic energy and the characteristic time τ_{spray}. The operating condition with diesel (blue dots) show generally lower turbulence and longer time to mix. The spread of turbulence levels and τ_{spray} is due to changes in EGR conditions ranging from 0 to 60% under stoichiometric conditions. However, the trends of Diesel and OME show a shift. The reason for this is assumed to be the simplified description of the spray models, using a constant spray angle for the two fuels and nozzle geometries and constant fuel density over time.

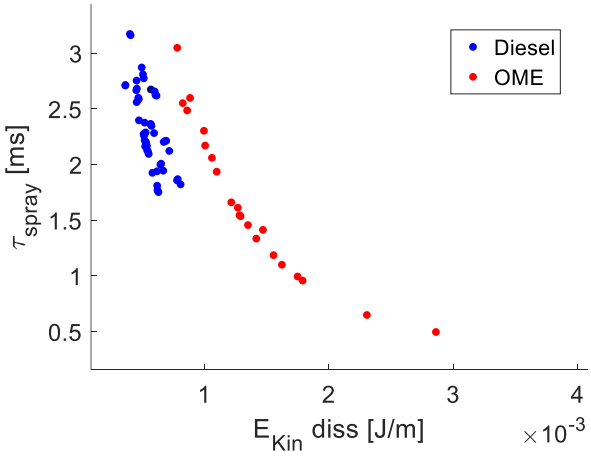

Figure 28: Comparison of dissipation of kinetic energy at end of injection versus τ_{spray} for all operating conditions. Red OME, blue Diesel

Figure 29 shows a comparison between the spray characteristic time τ_{spray} and the mixing characteristic time τ_{mix}. The figure supports the simplified relation: with longer time that the spray

needs to reach a certain equivalence ratio (in this work, an equivalence ratio of one has been chosen for all cases), less turbulence is available, indicated by the lower dissipation rate. A good correlation between these quantities is visible with a particular regard of the absolute level. The correlation supports the theory that the faster combustion of OME is caused by the higher turbulence level due to the position of the stoichiometric conditions, taken as the representative combustion zone, which is closer to the injector nozzle tip. Since τ_{spray} is a modelled quantity and allows an approximate prediction of diffusion combustion rate for a wide variation of engine operation and design parameters, ranging from injector nozzle diameter to different fuels under varying EGR conditions.

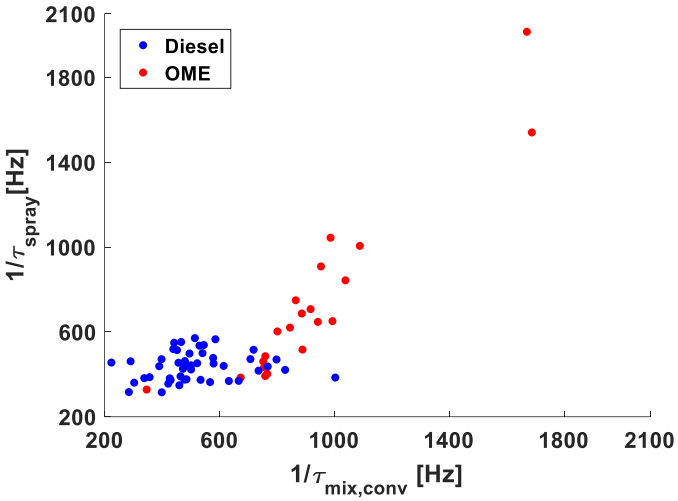

Figure 29: correlation between τ_{mix} and τ_{spray} for all recorded operating conditions. Red: OME, blue: Diesel.

The spread of the OME cases is larger than the cases with diesel. The main driver for this is the choice of the operating conditions. As previously mentioned, numerous operating points have been acquired under globally stoichiometric conditions. Using the later described operation strategy, the spread of the applied EGR rates and therefore, the spread in charge oxygen content is very high. This results in high differences in stoichiometric air fuel ratios, which allows a high variation of the axial stoichiometric position with respect to the nozzle tip and therefore large variations in and τ_{spray} and τ_{mix}.

In order to investigate the combustion process under globally stoichiometric conditions, the EGR rate was increased in order to replace the intake oxygen and lower the λ-value towards 1. Figure 30 shows a comparison of heat release rate at λ = 1.4, λ = 1.2 and λ = 1. With increasing EGR, the ignition delay is also increasing. This also results in a higher peak of premixed combustion. The peak diffusion combustion is lower and the late-phase combustion is slower with increasing EGR. Both are attributed to decreasing oxygen content in the background with increasing EGR rate. The reduction in diffusion peak can be explained by slower mixing due to decreased turbulence according to Figure 28 and Figure 29. The reducing charge oxygen content results in increasing stoichiometric air fuel ratio, which moves the representative combustion zone further away from the spray tip, where the turbulence level is lower and τ_{spray} and therefore, also τ_{mix} are longer . The late-phase-combustion is rather depending on the background turbulence and the oxygen availability, since the turbulence of the injection has already dissipated. The late-phase-combustion is still sufficiently fast even under stoichiometric conditions due to the availability of the oxygen bonded in the fuel.

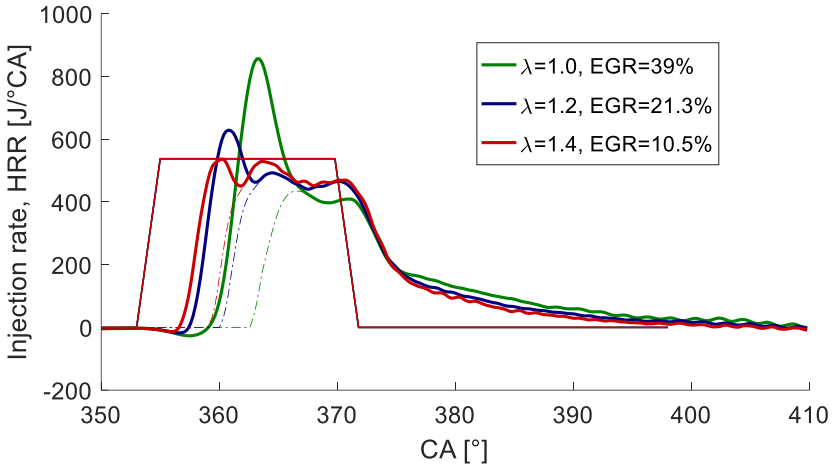

Figure 30: Heat release rate of OME with increasing EGR rate to reach λ=1.0. The rail pressure is constant at $1000bar$ and BMEP at $8.7bar$. Red: λ=1.4, blue: λ=1.2, green: λ=1.0, solid thick: heat release rate, solid thin: injected energy rate, dashed-dotted: diffusion heat release rate.

At stoichiometric conditions, the load can be varied by changing the boost pressure or the EGR rate, with the corresponding change in fuel supply.

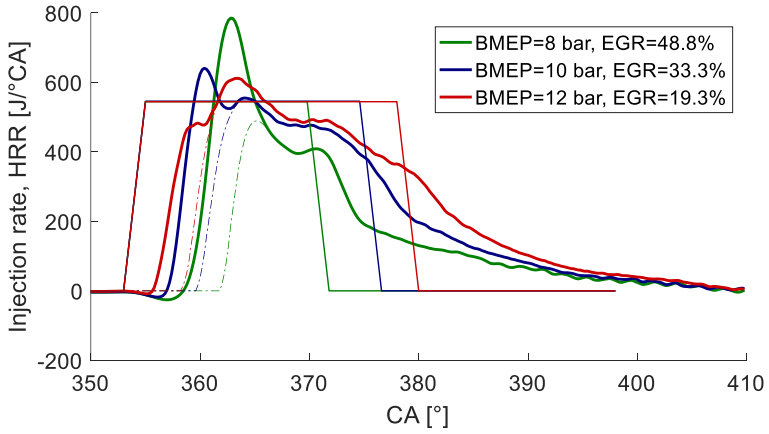

Figure 31: Heat release rate of load variation using OME at λ=1.0 with constant fuel pressure of 1000 bar. Red: 8 bar BMEP, blue: 10 bar BMEP, green: 12 bar BMEP, solid thick: heat release rate, solid thin: injected energy rate, dashed-dotted: diffusion heat release rate.

Figure 31 shows the heat release rate of a load variation with different EGR rates at stoichiometric conditions. The increasing fuel demand has been supplied with prolonged duration of injection at constant fuel and boost pressure as well as a simultaneous reduction of the EGR rate. Therefore, the intake oxygen content is increased with increasing load. It can be observed, as seen already in Figure 30, ignition delay is increasing with increasing EGR and the premixed fraction is increased accordingly. Regarding the diffusion combustion part of the heat release rate, it is observed that the later diffusion part of the combustion decreases even before the end of injection. This may be explained by cavitation occurring where the fuel leaves the injector sac to enter the nozzle duct that reduces the fuel mass flow rate. Therefore, the attention is drawn to a crank angle degree, where the diffusion combustion can be considered in stationary regime for all three cases (i.e. around 370 °CA). At this point, the burning rate diminishes with increasing EGR rate as in Figure 30. The effect can be

explained with longer τ_{spray} in the cases with lower load, resulting in lower charge oxygen content and higher stoichiometric air fuel ratio.

Pollutant Emissions

Gaseous Emissions

The pollutant emissions of an OME fired engine are of particular interest, since the λ=1- operation without excessive soot emission offers to simplify the exhaust gas aftertreatment architecture to a three-way-catalyst and possibly a DPF.

Carbon Monoxide

Carbon monoxide in Diesel engines can originate from the fuel dripping from the injector nozzles after the end of injection, from those regions that during the ignition delay which are overmixed and therefore not flammable and from local combustion zones under fuel rich conditions, which do not have the ability to be oxidized in the late phase combustion. The first effect is mainly depending on the size of the injectors sack hole and the number of injections. The second effect scales with the premixed portion and is therefore strongly depending on the cetane number of the fuel and all other effects, which influence the ignition delay. Under globally stoichiometric or even fuel rich conditions, the emissions of carbon monoxide are expected to rise due the third mentioned effect.

Figure 32 shows the level of carbon monoxide emission against the BMEP at low load conditions and high λ-values (~ 4, resp. equivalence ratio φ ~ 0.25). Under these lean and low load conditions, the sum of the abovementioned effects are in the same order of magnitude for the two fuels.

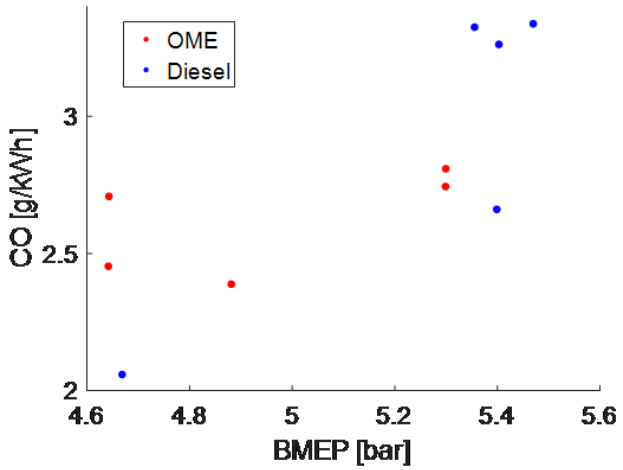

Figure 32: CO emissions for different BMEP at high λ (>4).

Figure 33 shows the carbon monoxide emissions of all recorded operating conditions. When introducing exhaust gas in the intake (EGR) to lower the air-to-fuel ratio for similar load conditions, as soon as a global oxygen limitation occurs, mixing of air and fuel is reduced (see characteristic mixing rate as mentioned above) and the fuel rich zones become larger. For this reason, the emissions of CO increase. The behaviour of the emissions is almost digital. As soon as λ is at stoichiometry or below, the values rise massively. The EURO 6 standard, lying at 1.5 g/kWh for the WHSC and at 4g/kWh for the WHTC, is largely exceeded.

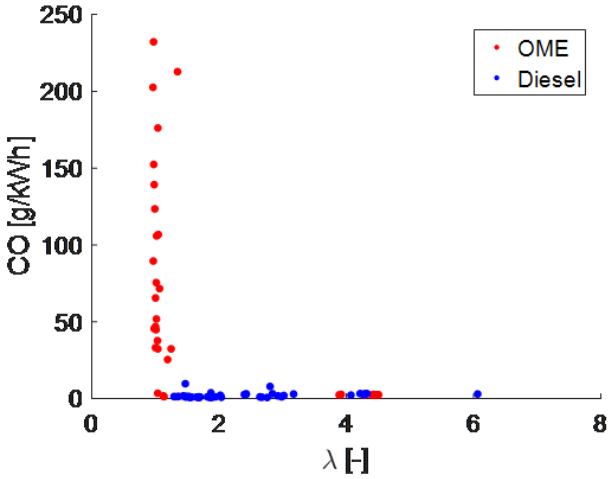

Figure 33: CO emissions for different λ.

Unburned Hydrocarbons

sSimilar to the carbon monoxide, unburnt hydrocarbons in Diesel engines originate from injector dripping and from too lean and fuel rich zones. Figure 34 compares the HC emissions versus λ. The trend of decreasing values approaching stoichiometric conditions from the lean side are attributed to mainly increasing load. Hydrocarbon emissions also increase massively at and below stoichiometric conditions, similar to carbon monoxide emissions. The reason is also expected in incomplete combustion. The EURO 6 limits of unburnt hydrocarbons for heavy duty engine that are 130mg/kWh for the WHSC and 160mg/kWh for the WHTC.

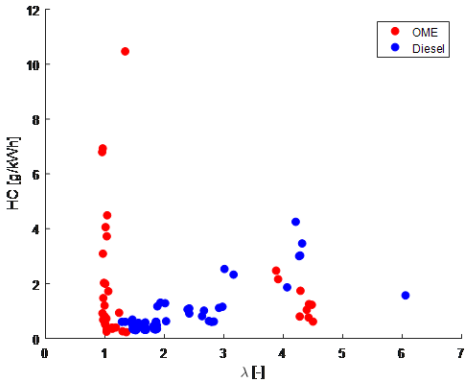

Figure 34: HC emissions for different λ.

Another important investigation is the composition of the hydrocarbon. Since OME does not contain any C-C bonds, short exhaust HC are expected. Figure 35 shows a comparison of measurements with the standard FID, calibrated for propane and a fast spectrometer, calibrated for methane. The figure shows that a considerable amount of total hydrocarbon is methane, which is more difficult to oxidize in a catalyst. However, the question of the composition of the remaining HC rests unanswered. Due to the architecture of OME, the presence of formaldehyde has a high probability.

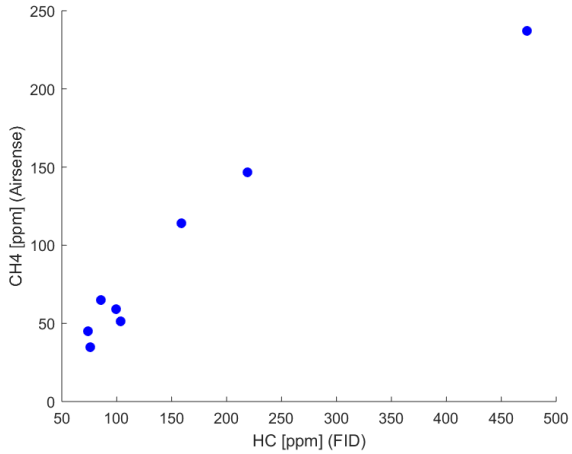

Figure 35: HC recorded with FID versus CH4 emissions, recorded with the fast mass spectrometer

Nitrous Oxides

NOx emissions are a result of residence time at high temperature. The residence time is dependent of the char. mixing time, the temperature is a result of compression ratio, pressure rise due to premixed combustion, pressure addition due to fast diffusion combustion (inverse mixing time) and adiabatic flame temperature. A comparison between the emissions of Diesel and OME is therefore very difficult since all the abovementioned parameters are changed simultaneously.

Figure 36 shows a comparison of NOx emissions versus intake oxygen concentration. The majority of the points with less than 14% intake oxygen content are below the indicated EURO 6 limit (WHSC: 400mg/kWh, WHTC: 460mg/kWh). All these points are recorded under globally stoichiometric conditions. Remembering carbon monoxide and hydrocarbon emission under these conditions, even a small increase in λ would help to reduce these emissions without exceeding the legislative emission limit, since in those conditions, NOx does not need a further reduction in the three-way-catalyst. For operating conditions above 14% intake oxygen content, a carful λ = 1 feedback control is required to prevent spikes in CO and HC.

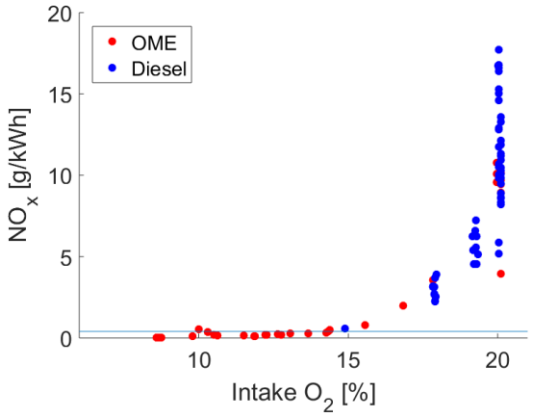

Figure 36: NOx emissions of OME and Diesel versus intake oxygen concentration. The line represents the EURO 6 limit for NOx according to the WHSC which lies at 400 mg / kWh.

Particle Emissions

Particle Spectrometer

The potential of reducing soot emissions is the main reason why OME is investigated. Due to its particular molecular structure in fact (no C-C-bonds), in contrary to fuels with similar oxygen content, OME has a very low tendency to form soot particles.

Figure 37 shows a comparison of the particulate number (PN) emitted using Diesel and OME. The operating conditions are at relatively low load (~ 5 bar BMEP) without EGR. The Diesel operating condition show both, nucleation mode and agglomeration mode. The nucleation mode is most likely of volatile nature and only the agglomeration mode (particles above 23 nm diameter) is restricted by PN legislation. The recorded particulate mass for these operating conditions is extremely low for both the fuels. The OME fired operating conditions do not show an agglomeration mode in the expected size distribution, but a nucleation mode in similar manner than the diesel operating condition. The nucleation mode is expected to be condensates of heavy hydrocarbons. This is acceptable for the diesel case, but questionable for the operation with OME since the formed hydrocarbons are not expected to be heavy (as shown in Figure 35). Therefore, the particle composition also needs to be investigated. The two operating conditions with OME uses different fuel pressures. The effect on the particle size distribution is very small.

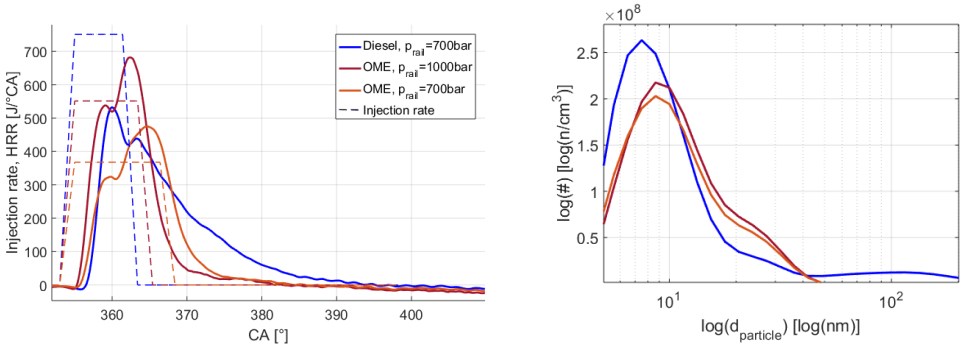

Figure 37: Comparison of OME and Diesel at high λ and low loads: left: heat release- and injection rate; right: particle size distribution.

Figure 38 shows the results of two cases, fired with OME, one under globally lean and one under globally stoichiometric conditions. The combustion process under very high EGR rates is slower and colder in comparison to the corresponding condition without EGR. The lower temperature reduces both, soot formation and oxidation. The slower combustion mainly increase the residence time of the soot particle in the hot zone and increases soot formation and especially particle diameter. These phenomena indicate that there is a maximum particle formation at a certain EGR rate, where PN does not show a significant contribution above 23 nm but still shows large number of nucleation mode particles.

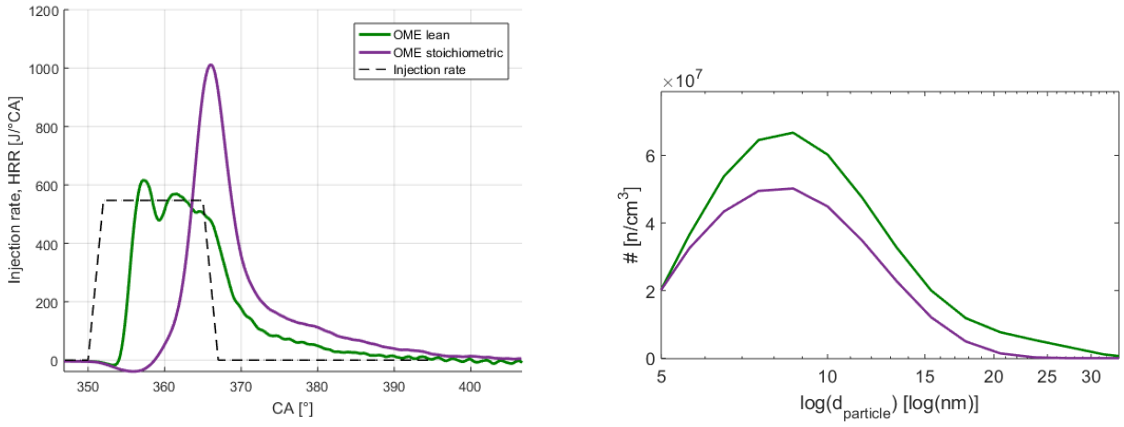

Figure 38: Comparison of OME and Diesel at stoichiometric conditions: left: heat release- and injection rate; right: particle size distribution.

Transmission Electron Microscopy

Figure 39 shows images of an exhaust sample on a grid for transmission electron microscopy (TEM). The operating condition corresponds to the one in purple in Figure 38. Figure 39A shows widespread soot mostly enclosing metal particles (dark 'spots'). The different highlighted areas are as follows: the blue correspond to small particles of metal compounds, the green indicate agglomerates of soot with enclosed metal–bearing particles, possibly acting as nucleation cores for soot growth. The red area is similar to the green but the metal-bearing soot particles are captured in a hole of the carbon film of the TEM grid (blue and green areas show particles lying on the carbon film itself). The large amount of small particles is corresponding to the size distribution measurements in Figure 38. Figure 39B corresponds to the red circle of Figure 39A and is taken in high resolution mode. It shows a soot agglomerate enclosing metal compounds, a few nanometers large (examples encircled in red). The metal compounds exhibit lattice fringes, which points to their crystalline structure.

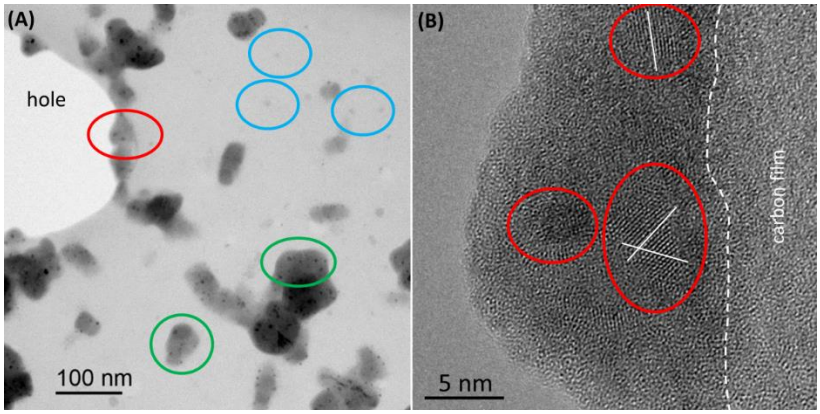

Figure 39: (A) Bright-field Scanning TEM (BF-STEM) and (B) High Resolution TEM (HRTEM) images of particles collected under a stoichiometric OME operating condition. In (B), the metal compound(s) are indicated also by the regular lattice fringes (parallel lines marked partly with white color for clarity; examples encircled). Dashed line separates the soot particle on the left from the carbon film of the grid. Collection time, ca. 5 min during steady state engine operation.

Apparently soot is formed in the presence of minute metal-bearing particles which act as nucleation cores for soot surface growth. The origin of the metal particles is not understood for all of them. Based on energy dispersive X-ray analysis (EDX, Figure 40) carried out simultaneously with TEM imaging they consist of different elements or compounds of them: Ca, P, Cl, S, Zn, Pb, Fe, Al, K, O. A chemical analysis of the neat fuel has been performed by ICP OES (inductively coupled plasma optical emission spectrometry) and did not show any of the abovementioned elements above the detection limit of the method. However, the limit of detection is at 2 mg/kg for Phosphorus and Potassium, 10 mg/kg for Chlorine and 1mg/kg for all other elements. TEM and scanning electron microscopy (SEM) combined with EDX analysis of the return line fuel also showed predominantly Ca, some S, Pb and minor Ti and Zn, indicating the prevalence of possibly CaO, or CaSO4. The origin of these metals is either from wear of injection system components or from the neat fuel below the abovementioned detection limit. The contribution of the lubrication oil is not precisely known but seems to provide most of P and Zn.

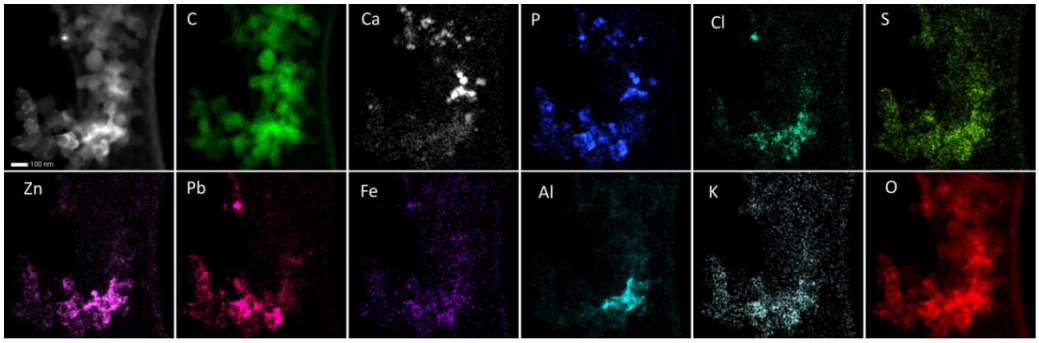

Figure 40: Scanning TEM image (upper row left; white bar: 100nm) and element mapping of a metal-bearing soot agglomerate. The colour intensity correlates with the amount of the element present and/or the particle thickness.

However, as it is difficult to remove all sources of small particles that can favour soot growth, it can be expected that a certain amount of soot can be formed even with fuels without C-C bonds. The emitted PN concentration above 23 nm is well below the EU6 PN limit and would not require a DPF. However, the genotoxicity of these particles is unknown but the appearance of the small particles in Figure 39 show that the nucleation mode particles from OME combustion (Figure 37 & Figure 38) are certainly not of volatile nature, in comparison with what is assumed in the nucleation mode of the Diesel combustion in Figure 37.

1.1.6. Conclusion

The experimental work conducted within a cylindrical constant volume, temperature and pressure controlled cell, has focused on several highly oxygenated fuels belonging to the poly(oxymethylene)dimethilethers family. The effect of increasing oxygen content on combustion and soot formation and oxidation processes has been studied and results demonstrated that:

- A massive reduction of the soot formation dominated phase when increasing the oxygenated fraction in the blend is achieved.
- 2D-2-colour-pyrometry images gave the possibility of determining a specific area of soot formation showing its reduction with increasing oxygen content in the blend.
- In-chamber flame luminosities of pure oxygenated fuels are extremely diminished in comparison with diesel fuel probably because of no contribution from soot radiation.

- Pure oxygenated fuels are characterized by a nearly smokeless combustion and an increase of O_2 content in blends is associated to a not linear soot reduction. In fact an addition of just 5% of oxygenated fuel within commercial diesel permits a reduction in soot emissions of about 30%.
- Further soot reduction could be achieved if operating towards a premixed dominated combustion mode.
- Particulate matter in oxygenated fuels is characterized by far smaller dimensions with respect to those from commercial diesel combustion probably because of an oxidation effect on nucleation cores.

The experimental activity conducted on a single cylinder heavy-duty diesel engine had the aim of investigating the achievable benefits in performance and exhaust emissions that could derive from the use of POMDME in diesel blends. Since the particular investigated mixture of POMDME is characterized by similar physical properties to diesel thus not requiring substantial modifications to the engine infrastructure, it could be produced on industrial scale to be blended with commercial diesel. In this way the blend could take the advantages of both fuels: diesel high energy content and POMDME strong capability of reducing soot formation. In particular, a 5% and a 10% POMDME in diesel have been selected for the experimental activity. The investigation focused on particulate matter as well as nitrogen oxides, unburned hydrocarbons, carbon monoxide and carbon dioxide evaluation. The main conclusions that can be drawn from the analysis of the experimental activity are listed in the following:

- A reduction in soot emissions up to 34% has been detected with the 10% POMDME in diesel blend, investigating operating conditions with similar premixed – diffusive combustion mode ratios.

- NO_X emissions have not been significantly affected by the adoption of blends containing a percentage of oxygenated fuel up to 10%.

- No significant decay in combustion efficiency has been detected operating the engine with the 5% POMDME and 10% POMDME blends. This result is confirmed by similar values, detected for the different investigated fuels, in carbon dioxide.

- An increase in BSFC has been detected for any investigated fuel when retarding the start of injection from -12 to -6 cad atdc and with increased EGR rates because of a lower efficiency. In addition, with respect to the comparison commercial diesel – investigated blends, a 2.2% and a 4% increase in BSFC has been detected with 5% POMDME and 10% POMDME respectively. Therefore fuel economy could be the main reason for considering, in a hypothetical industrial scale production, 10% as a maximum percentage of POMDME to be blended in commercial diesel.

In the third part, the combustion behaviour of neat OME in a composition of approximately 80% OME_3 and 20% OME_4 has been investigated using again the single cylinder heavy duty engine. For the operation with neat OME, the injector nozzle diameter has been increased from 0.24 mm to 0.29 mm.

It was observed that the ignition delay of OME is shorter than the one of Diesel; this is due to the higher cetane number of the oxygenated fuel. Moreover OME showed a faster combustion, which is in agreement with previous studies available in literature. The reason for this fast combustion behaviour has not been found in the lower demand on air directly, but mainly in the higher turbulence level for mixing due to combustion closer to the injector nozzle tip. The turbulence level has been estimated with the Musculus-Kattke spray model. In addition, the computationally less expensive Naber-Siebers description for steady state sprays has been used to express a characteristic time which the fuel

requires to mix until stoichiometric conditions. The resulting characteristic number τ_{spray} correlates well with the inverse dissipation rate from the Musculus-Kattke model as well as with the characteristic mixing rate τ_{mix}, calculated from the measurement data. For this reason it can be concluded that a fast and easy way to estimate the relative intensity of the molecular mixing using the Naber-Siebers model was found. This description offers the possibility to predict the diffusion combustion rate in a very wide range of engine operation parameter variation, including changes in nozzle size, fuel pressure or fuel composition even with a strongly changing air demand. Furthermore, it has been demonstrated, that the ability for fast fuel conversion of OME can be used to reduce background oxygen content to very low levels and operate the engine globally stoichiometric. In Addition, the total HC emissions contain a substantial amount of methane. NOx emissions within the recorded operating conditions have shown a strong dependence on the applied EGR rate. The particle emissions using OME demonstrate high number in a size range mainly below 20 nm. The particles are assumed to be of solid nature, even though, the particle measurement device does not remove volatile particles. This assumption is due to the high amount of light unburned hydrocarbons, indicated with the high methane portion. TEM imaging combined with EDX analysis showed that these particles are soot mostly with metal inclusions and/or purely metal particles (not enclosed in soot). Some of the non-organic compounds of the particles are found in the return fuel (predominantly Ca, some S, Pb, P, Cl and minor Ti and Zn). These compounds possibly derive from the fuel (in low concentration) and from the injection system while part of Zn and P, as well as K are assumed to come from the engine lube oil. Finally, at least part of the analysed Fe and Al may originate from engine wear.

1.2. Development of a Flexible Rapid Compression Machine (FRCM)

1.2.1. Management Summary

WP2 co-funds the CCEM investment proposal “Flex-FI-Dual” supporting the development of the new test rig which will be used for generation of validation data of dual fuel combustion processes. Initially intended to be a new type of a hydraulically driven rapid compression machine the design target had to be shifted in 2015 due to the unexpectedly high costs of the hydraulic piston drive system. The new design target is based on a large bore Diesel engine block with a new valve train and customized cylinder heads. The mayor designs are complete, manufacturing of the parts and assembly of the test rig is well underway; the new rig is expected to be operational in March 2017.

1.2.2. Scope

To further advance gas- and dual-fuel combustion engine technology both numerical and experimental investigations into the relevant in-cylinder processes are needed. However, not all test rigs are suitable for experimental in-depth studies at engine like conditions (mixture, pressures, temperatures and turbulence levels) for both gaseous and liquid fuel combustion. This project aims therefore at the development of a new test rig that combines excellent optical access of constant volume cells with internal compression and in-cylinder flow fields resp. turbulence levels of real engines; it is hence especially suitable for (but not limited to) investigations into dual-fuel combustion processes.

1.2.3. Status and Results

After the switch of the design target from a hydraulically operated rapid compression machine to a crank based, more engine like configuration in 2015 the project work in this year concentrated on finalizing the new design, manufacturing resp. ordering of the machine components and then finally the assembly of the test rig itself.

The new design target for the flexible facility for the investigation of gas, Diesel and dual-fuel combustion is based on a motor block from a “truck-size” Diesel engine (Liebherr D944, donated by Liebherr SA, Bulle) where only one cylinder, equipped with a special cylinder head that forms a combustion chamber with excellent optical access, is used. This combustion chamber (which can be easily exchanged to suit different experimental needs) is one of the key components of the new test rig: The initial combustion chamber type that will be realized during this project has a circular combustion chamber of 60mm diameter with a depth of 20mm. The circular diameter is fully optically accessible from both sides, two additional elongated windows on the chamber side provide additional optical access (for example for Laser sheets). The design of the cylinder head is very complex, the many holes for windows, valves, mounting bolts, heating elements, temperature and pressure sensors must fit together and preserve the space needed for the cylinder head mounting bolts at the fixed positions prescribed by the engine block. After the initial design underwent a review process the design was finalized in May, manufacturing was completed in November. Figure 41 shows the bare cylinder head after manufacturing, but before its surface was burnished (black oxidized) to minimize Laser light reflections; Figure 42 shows the burnished and fully assembled cylinder head with all cables required for heating and temperature measurements. The head itself is almost hidden behind the twelve pneumatic valves required to control the intake- and exhaust valves.

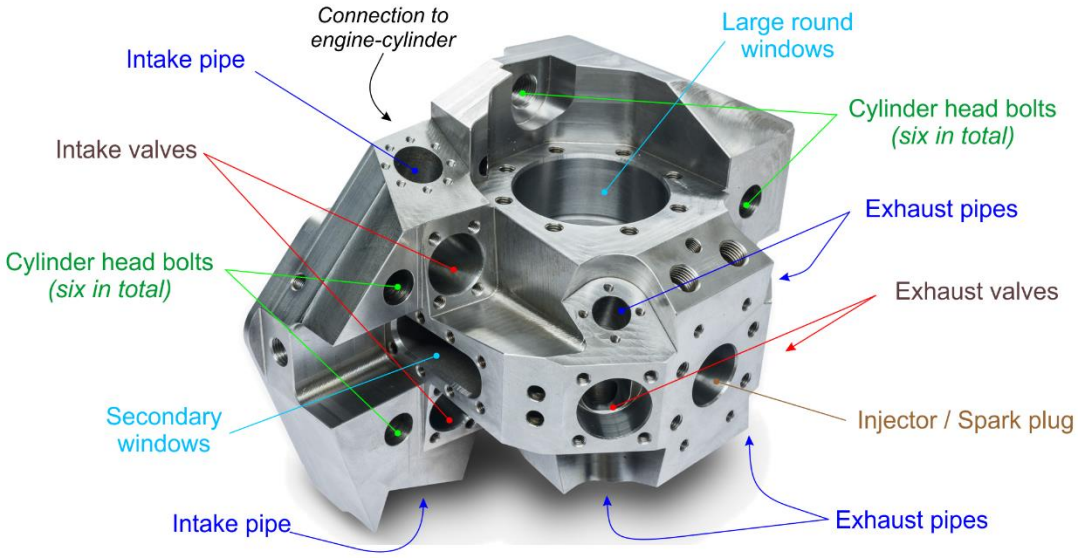

Figure 41: *The “car type” cylinder head realized in the context of this project after manufacturing. The surface of the head will be burnished (black-oxidized) before use.*

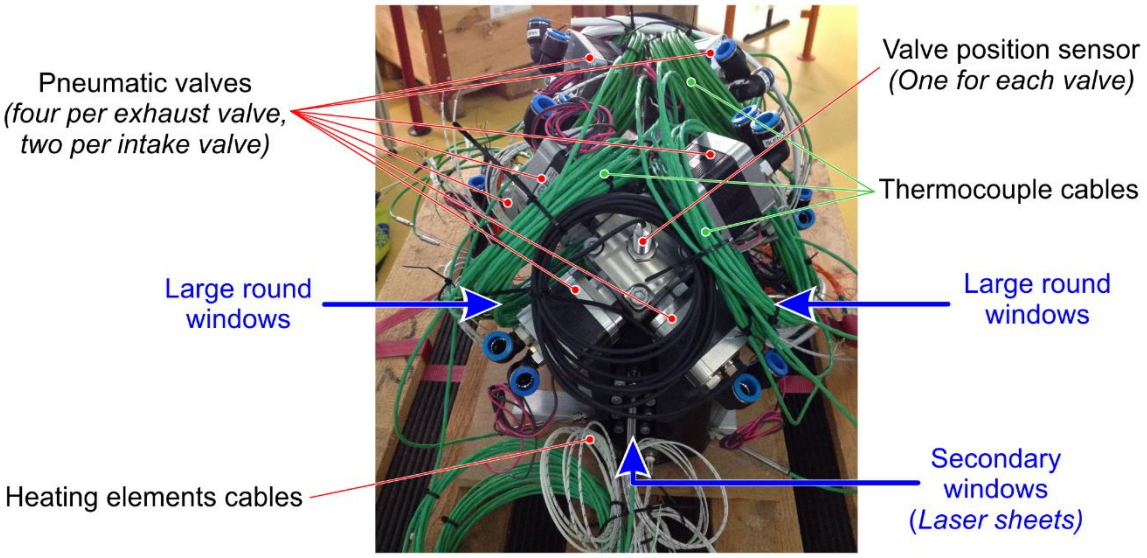

Figure 42: *The burnished and fully assembled cylinder head ready to be mounted on the engine block.*

Due to the space constraints in the cylinder head relatively small gas exchange valves must to be used. To compensate for this the test rig is supplied with pressurized (and preheated) air resp. air-gas mixtures. The pneumatically driven valves allow for completely unrestricted valve timings; apart from simply changing intake air pressure and temperature different experimental conditions in the combustion chamber (pressure, temperature, gas mixture) can also be achieved by varying valve timings over a number of consecutive intake/exhaust cycles before the actual “experiment cycle” with ignition and successive combustion takes place. The valves are controlled by a customized FPGA system which operates independently of the PLC based test rig control and monitoring system. To prevent possible crashes between valves and the engine piston in case of valve control or operation errors new valve pockets have been manufactured into the piston of the working cylinder. Figure 43 shows the setup that is used for testing and the run-in procedure of the valves.

Another important part with a long lead time is the base frame of the test rig. Intended to provide a rigid base for the instalment of the other drive train parts it is firmly mounted on the already existing concrete base plate in the lab. The drive train consist of an electric motor / brake, a connecting shaft that also carries the large and heavy flywheel (to dampen rotational speed oscillations) and the engine block itself. All couplings in-between are flexible to allow for slight shaft misalignments. Figure 44 shows a picture of the ongoing drive train assembly in the lab.

Work currently focusses on completing the drive train assembly and the run-in procedure of the valves that is required before the assembly of the cylinder head can be started. In parallel the instalment of the air supply system (pressure control, preheating) and the design, manufacturing and instalment electrical equipment of the test bed is also in the works. The first run of the test rig is planned for March next year; after a commissioning phase it will be ready for the first experimental campaign in summer 2017.

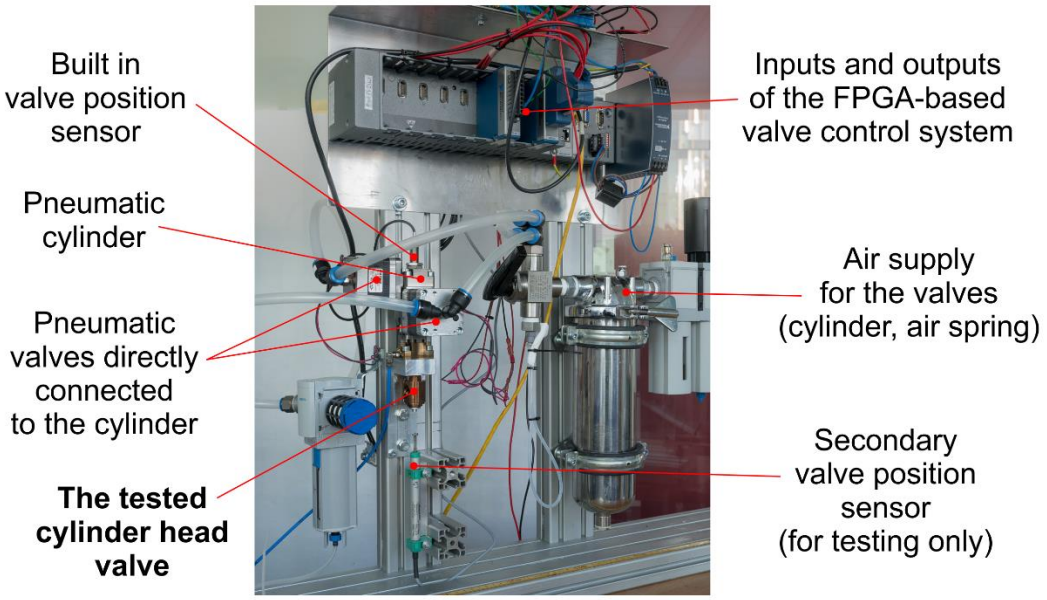

Figure 43: *Setup used for testing and run-in procedure of the valves.*

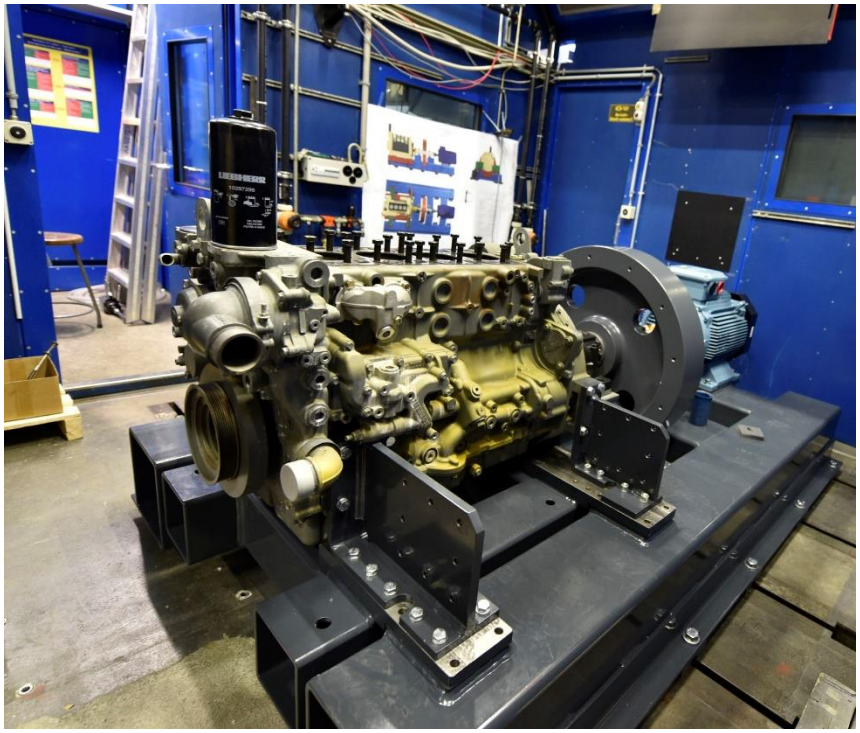

Figure 44: *An image from the lab during assembly of the test rig drive train. The combustion chamber / cylinder head is not yet mounted on the engine block.*

A view of the built-up test rig as it can be seen from the adjacent control room is shown in Figure 45. Although many cables and flexible pipes seem to cover the cylinder head / combustion chamber completely the optical access through the four windows is not obstructed by anything.

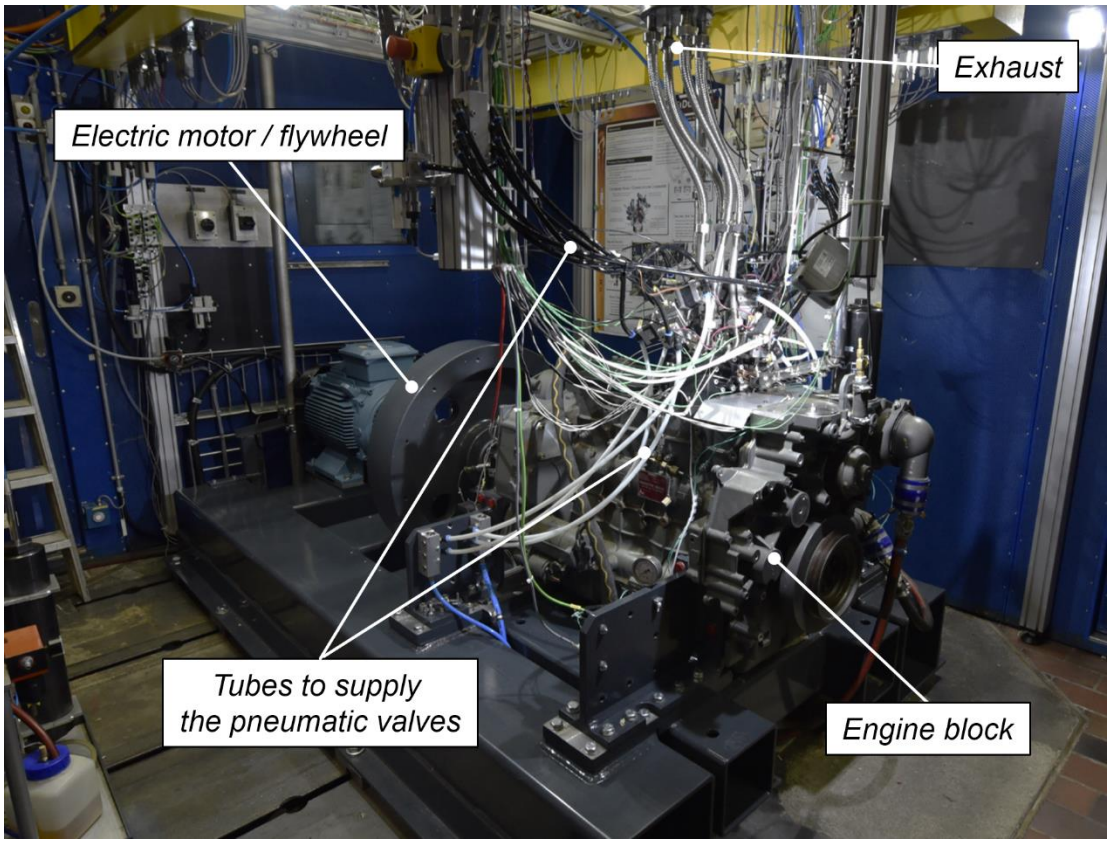

Figure 45 A view of the built-up test rig in the lab at LAV / ETHZ.

Still missing on this picture is the housing for the flywheel and the shaft between electrical motor / generator and the engine block, and the insulation of the heated intake pipes.

Commissioning of the pneumatic valve actuators

An important goal during commissioning was to achieve repeatable, stable valve lift curves at all engine speeds. Unexpected effects found during this process was on one side valve bouncing at low engine speed (200…400rpm), and on the other side an unexpected dependence of the valve lift opening resp. closing curves on the engine speed. However, these undesired effects could be successfully corrected with a new system (shown on the right side in Figure 46) that provides a regulated backpressure at the outflow of the pneumatic valves (thereby also rendering the orifices in the pneumatic valve exhausts obsolete).

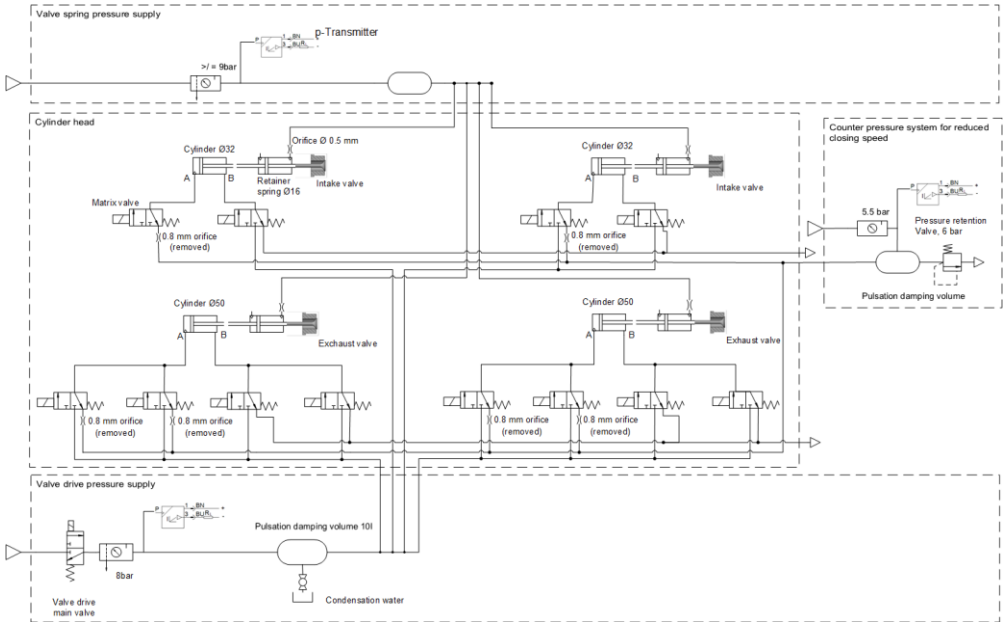

Figure 46 Pneumatic valve drive diagram.

After the modifications, highly repeatable and stable valve lift curves can be realised as shown in Figure 47. Since the valve opening and closing speeds are only time and not crank angle dependent the valves seem to open / close faster at slower engine speeds if drawn on a crank angle scale as shown in Figure 47.

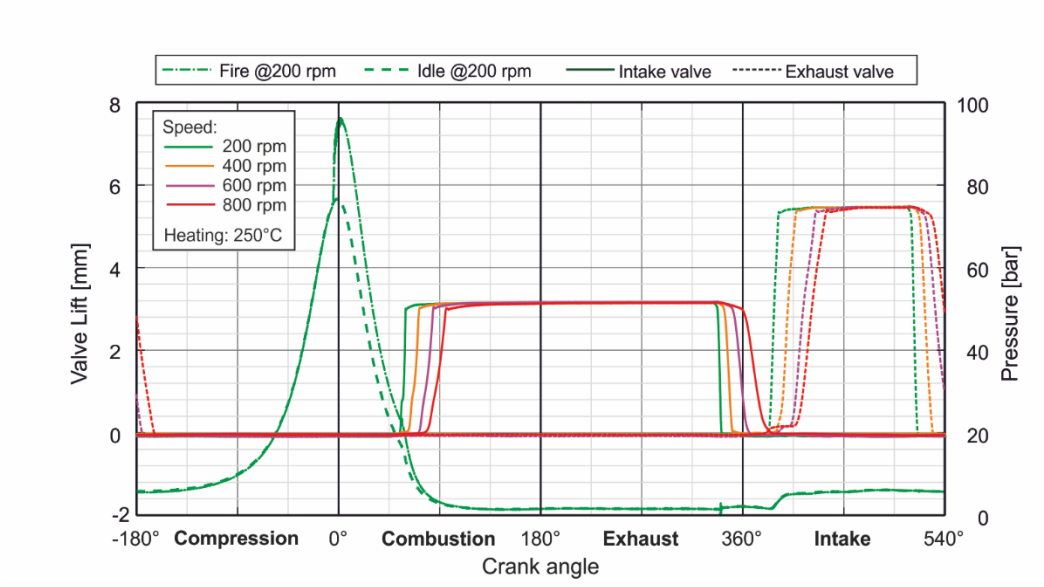

Figure 47 Valve lift curves in the final test rig at different engine speeds.

Because of manufacturing tolerances and the elastic (pneumatic-) piston stop, there is a gap of about 0.3mm between the pneumatic cylinder and the valve shaft. This leads to the effect of a short flat passage in the valve lift traces (around 405°CA) during intake valve opening at higher engine speeds (600rpm and 800rpm). At this point, the pneumatic piston is already in contact with the engine valve, but the pneumatic pressure force is not yet high enough to open the engine valve against the valve spring (and in-cylinder gas pressure).

For the researchers using the test rig it is therefore important to know that the sensor detects the pneumatic piston position only, and that the gap between pneumatic piston and engine valve must be taken into account to get the effective engine valve opening time.

First cylinder pressure measurements

For commissioning the cylinder head / combustion chamber was equipped with a single hole Diesel injector (Ø0.24mm) mounted on top of the head for radial fuel injection. Since the piston has not been modified yet the compression ratio was very low (8.2) which leads to rather low end of compression gas pressures and temperatures. Since it is mandatory to keep component temperatures in a safe range the temperatures of the cylinder head and intake pipes have also been kept in a conservative range during the initial phases of commissioning which further lowered the achievable end of compression air temperatures. However, the achieved air temperatures where still high enough to ignite the Diesel fuel spray!

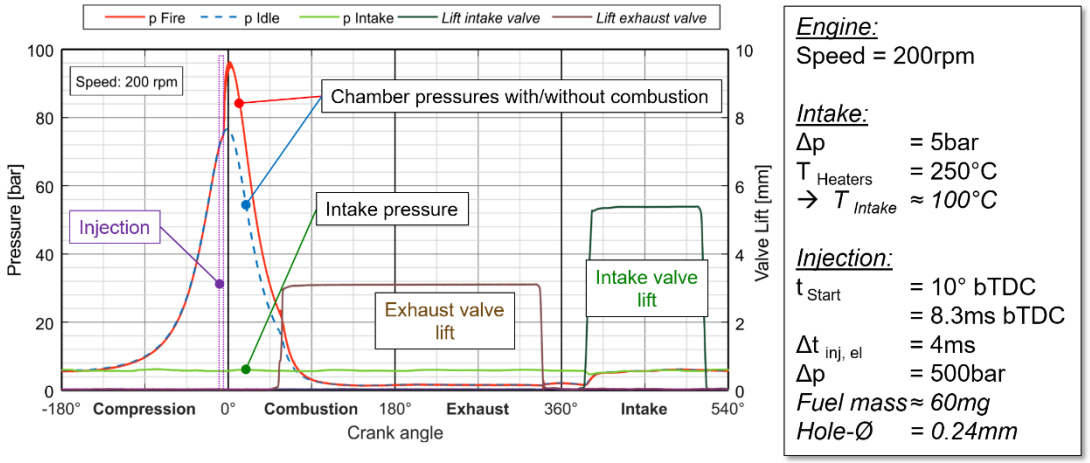

Figure 48 Example of a combustion chamber pressure trace recorded during commissioning. Radial Diesel fuel injection with a single hole Diesel fuel injector.

As can be seen in Figure 48 an end of compression gas pressure of ~75bar can be reached with an intake air pressure of 6bar (absolute). The small amount of injected fuel leads to a pressure increase of only about 20bar during combustion. Clearly visible the pressure drop when the exhaust valves open (~60°CA after TDC) and the pressure increase when the intake valves open (~390°CA).

Figure 49 shows cylinder pressure traces for three different air-preheating temperatures. Since the hot air coming from the intake pipes passes through the cooler cylinder head and intake valve housing the effect of the air preheating temperature on the effective in-cylinder gas temperature is reduced (further measurements and a careful set up of the heat release / heat losses calculation model is projected to quantify this effect).

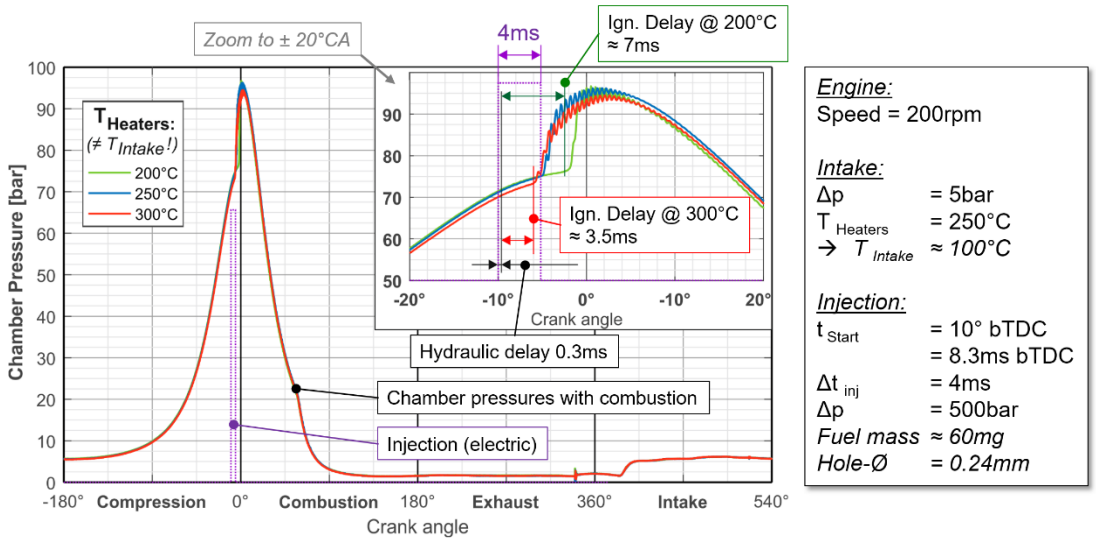

Figure 49 Combustion chamber pressure traces for three different air-preheating temperatures. The effective in-cylinder gas temperature variation is much smaller than the air preheating temperature change.

The measured ignition delay of about 3.5ms with the highest air-preheating temperature indicates an end of compression gas temperature in the order of 750K. Not shown in the two previous figures is the pressure measured in the actual engine cylinder (below the neck that connects the combustion chamber to the engine cylinder). For low engine speeds (as shown here) the difference is negligible, but for higher speeds it must be taken into account in the heat release calculations.

WP 2 (IDSC)

In WP2, the IDSC is concerned with the thermal management of the exhaust aftertreatment system of the Diesel-ignited gas engine as an example of a highly efficient drive system. The aim is to create optimum conditions for effective exhaust aftertreatment by means of intelligent engine control. The subject of the investigation is a four-cylinder engine operated in a dual-fuel combustion process with natural gas/diesel. With this engine, it has already been demonstrated at the IDSC that this technology is also suitable for dynamic operation in a passenger car engine. One of the challenges of this concept is the complete oxidation of the natural gas and thus the prevention of methane escaping into the environment. Combustion of natural gas proves to be a demanding process both inside the engine and in the catalytic converter, especially under partial load.

1.1. Hardware Setup

The Diesel-ignited gas engine is based on a conventional 2L Diesel engine. A port fuel injection system for natural gas are mounted in the swirl flap adapter of the engine. In addition we installed a natural gas three way catalyst in the exhaust gas downstream of the turbine. Some characteristic parameters of the hardware are outlined in Table 4.

Table 4: Parameters of Engine and Catalyst.

Description	**Symbol**	**Value**
Displacement volume	cm^3	1986
Number of cylinders	–	4
Bore/Stroke	mm	81/95.5
Compression Ratio	-	16.5
Catalyst dimension	mm	118 x 152
Cell density	$cells/in^2$	600
PML Pd/Rd	g/ft^3	147/3

The engine is equipped with cylinder pressure sensors in all four cylinders. The engine control unit is a rapid-prototyping system that allows convenient deployment of code based on Simulink. Figure 45 shows the photographs of selected components as the gas injector mount, the three-way catalyst and the electrical control cabinet.

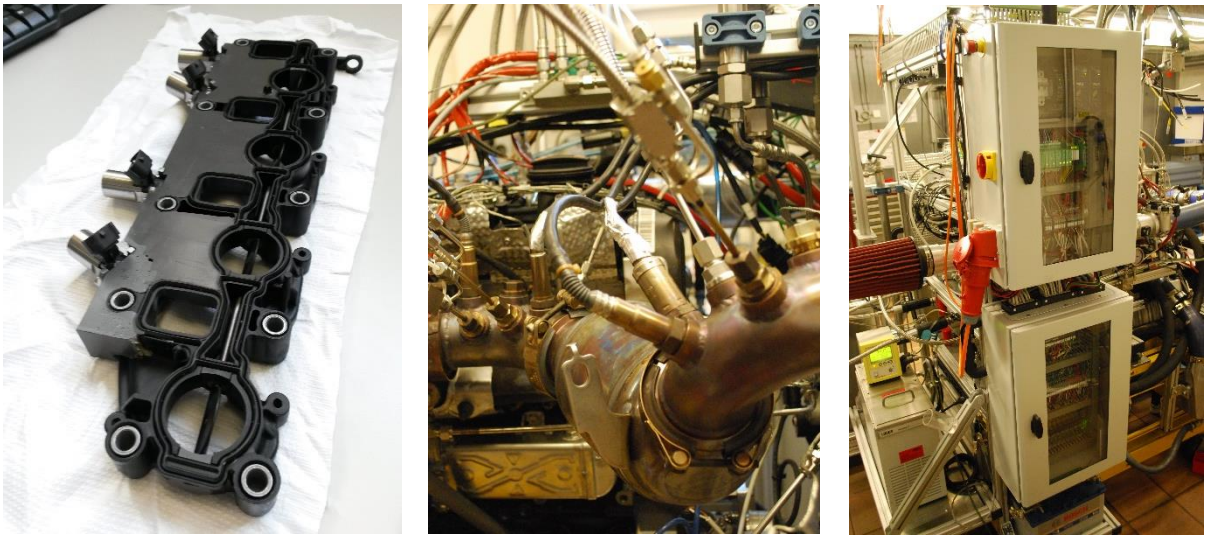

Figure 45: Some key hardware components of the Diesel-ignited gas engine testbnech: Swirl flap plate with cylinder-specific gas injection (left), three-way catalytic converter (center), control cabinet (right).

A schematic overview of the hardware setup is shown in Figure 46. The natural gas (massflow $\dot{m}_g$) is injected into the intake ports, while the Diesel (massflow $\dot{m}_d$) is injected directly into the cylinders by a common rail injection system. Some relevant input variables are indicated in green and in addition some pressure signals (p), massflows $\dot{m}$ and oxygen mass fraction signals (F) are introduced. The latter variable is defined as

$$F_y = [O_2]_y \frac{M_{O_2}}{M_y}$$

with the oxygen concentration $[O_2]_y$ and the molar weights of oxygen M_{O_2} and of the gas M_y at location y.

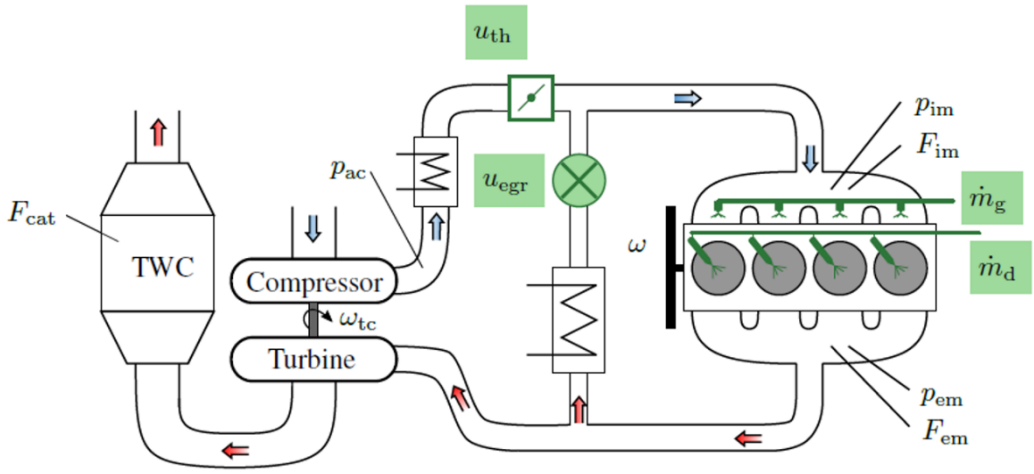

Figure 46: Schematic diagram of the hardware setup

1.2. Problem Description

The number of degrees of freedom of modern combustion engines is increasing as additional actuators are introduced or the functionality of the existing actuators is extended. The driving force behind the demand for greater complexity is often found in new challenging legal emission standards. The application process for modern engines becomes then more and more challenging. The work package 2 deals mainly with a particular engine, namely the Diesel-ignited gas engine. This engine is a dual-fuel type engine that runs on two different fuels. The principle fuel is natural gas, that is port-injected, while the second fuel is Diesel, that is directly injected into the cylinders. The main degrees of freedom of this engine are listed in the following.

- Fuel Ratio: how should we distribute the desired chemical energy between natural gas andDiesel?
- Timing of fuel injection: when do we inject the pilot Diesel injection?
- Air/fuel ratio: lean or stoichiometric operation?
- External EGR: How much exhaust gas is recirculated?

Setting these parameters has a big effect on the performance and emissions of the engine. In addition, we need to think about the exhaust gas aftertreatment system. The catalyst will only work efficiently under certain circumstances. Here the oxidation of unburnt methane gas is a major problem the engine control has to deal with. The oxidation of methane proves to be far more demanding than it

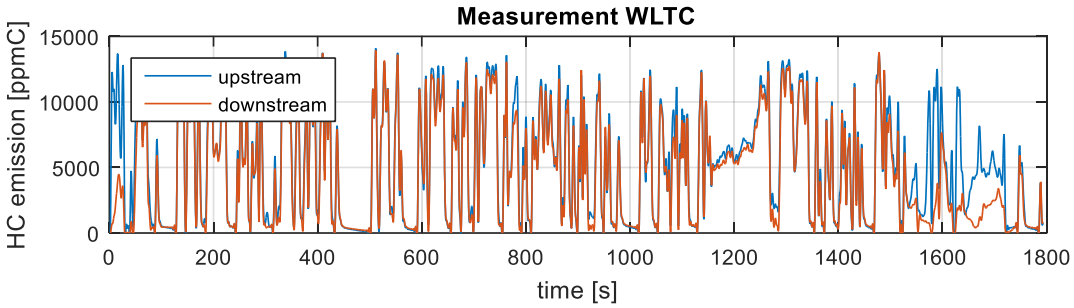

Figure 47: Measured concentration of unburnt hydrocarbons upstream (raw) and downstream (tailpipe) of the three way catalyst.

is the case with longer-chain hydrocarbons such as petrol. Due to the high molecular stability of methane, a significantly higher temperature is required for oxidation. This can be seen impressively in the HC measurements during a driving cycle in Figure 47. The measured concentration of unburned hydrocarbons before the catalyst deviate from the concentration after the catalyst only after 25 minutes. Consequently, there is no significant HC oxidation up to this point. The reason for the insufficient emission values lies in the setting of the engine control system that is designed for low NO_X and low CO_2 emissions by applying high EGR rates. Obviously, the Diesel-ignited gas engine requires a control approach that leads to acceptable HC and NOx tailpipe emissions with the best possible CO_2 emissions.

We find first insights into this control problem by solving a simplified version by dynamic programming. Solving for the global optimum of the full control problem that contains all the mentioned degrees of freedom would require a lot of computational power. With the simplified problem that comprise a static

engine model and a simplified dynamic model of the aftertreatment system, we learn about the relevant effects the inputs have on pollutant and CO_2 emissions. Optimality is defined by a cost function. This contains the pollutant emissions of HC and NO_x as well as the CO_2 emission that are weighted by two free parameters (α and β) in the following way.

$$\min_u \{\alpha m_{CO2} + (1-\alpha)[\beta m_{NOx} + (1-\beta) m_{HC}]\}$$

In the simplified problem, we distinguish three different combustion modes: Diesel-only combustion, stoichiometric dual-fuel combustion and lean dual-fuel combustion. Figure 48 shows the resulting optimal strategy for a parameter set (α,β) in the case of the WLTC drive cycle.

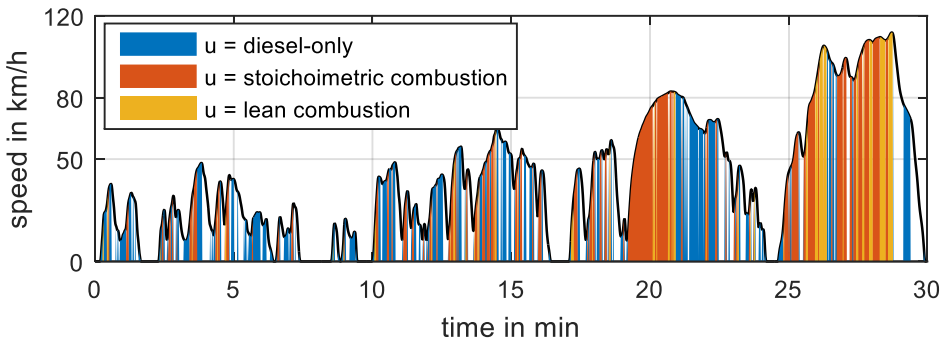

Figure 48: Simulative solution of the simplified control problem with optimization parameters α=0.85 and β=0.35.

Finally, the parameters were systematically varied over 441 different sets of parameters (α,β) on the WLTC drive cycle. Figure 49 shows the results of this parameter variation. The CO_2 advantage over the original diesel engine is plotted on the horizontal axis. Different colours show different fuel ratios. Blue corresponds to operation with only diesel, i.e. 100% of the chemical energy used comes from diesel fuel. Results with a yellow colour indicate an average diesel content of only 30% over the entire cycle. Consequently, 70% of the chemical energy is accounted for by natural gas.

Two conclusions to be drawn from Figure 49:

- The substitution of diesel with natural gas enables CO_2 savings of up to 16% as well as the reduction of NO_x emissions of up to 77%.
- The CO_2 advantage of lean strategies is countered by the low conversion efficiency of exhaust aftertreatment. The reduction of CO_2 emissions leads to increased HC emissions..

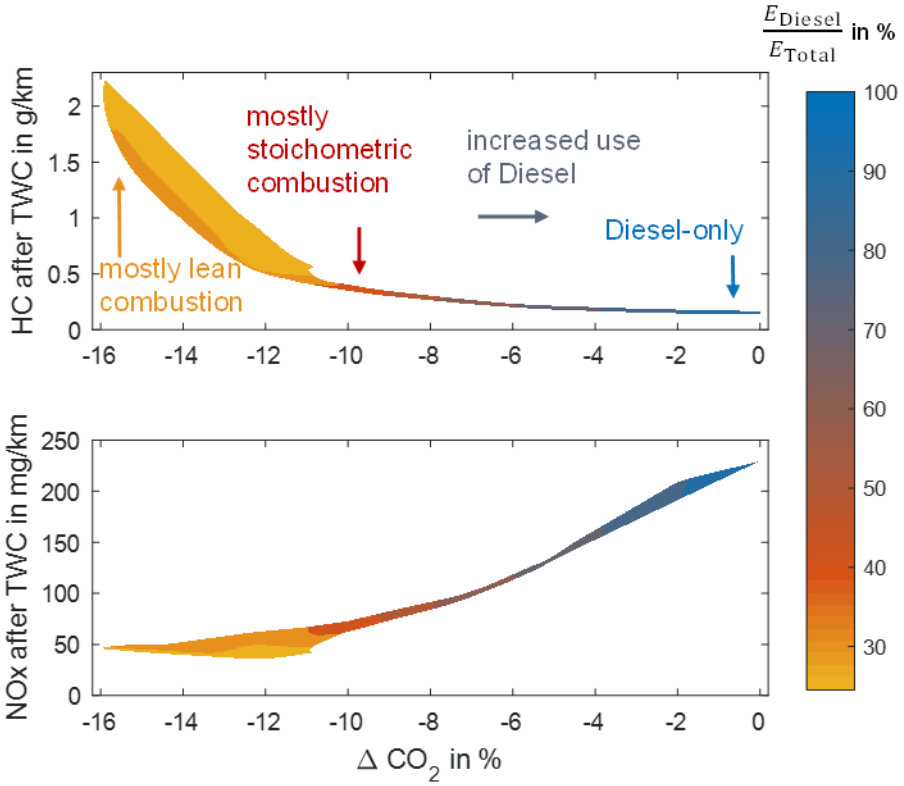

Figure 49: Simulative Solution of the simplified optimal control problem for 441 combinations of the parameters α and β.

1.2.1. Research Fields

In consequence of the presented simulation study the following three research fields are identified that are crucial for the development of a suitable engine control approach that accounts not only for the sensitivities of standard actuators as throttle, valves or injectors but also takes the current state of the exhaust aftertreatment system into consideration.

1. CO_2-optimal Diesel injection: In contrast to conventional, single-fuel engines the amount of Diesel that is injected in a Diesel-ignited gas engine is not solely linked to the torque production as additional chemical energy is introduced by the natural gas. We can therefore choose the main parameters of the Diesel injection (start and duration) such that the given torque and combustion phasing is achieved with the lowest possible CO_2 emissions.

Zurbriggen, F.; Hutter, R.; Onder, C. Diesel-Minimal Combustion Control of a Natural Gas-Diesel Engine. Energies 2016, 9(1), 58; doi:10.3390/en9010058.

Hutter, R.; Zurbriggen, F.; Onder, C. Diesel-Minimal Combustion Control with Constraints in a Diesel-Ignited Gas Engine, FISITA automotive conference 2016, FISITA, 2016

2. Low-load feasibility of dual-fuel combustion: At low loads, the combustion mode has to be switched from dual-fuel combustion to Diesel-only combustion equivalent to that in a conventional diesel engine. The particular torque level, at which the combustion modes are switched highly

affect the performance in terms of pollutant emissions and CO2 emission of the engine. Thus, the low-load operation has to be investigated thoroughly. The following two studies are conducted in this context. They cover both the stationary and the dynamic viewpoint.

- Stationary optimization of low-load operation:

Hutter, R.; Ritzmann, J.; Elbert, P.; Onder, C. Low-load Limit in a Diesel-ignited Gas Engine, Energies, Volume 10; 2017

- Dynamic transition control between combustion modes

Hutter, R.; Hänggi, S.; Albin, T.; Onder, C. Optimal Transition Control between Combustion Modes in a Diesel-ignited Gas Engine, not yet published

3. Catalyst of a lean-burn natural gas engine: The catalytic oxidation of unburnt methane is drastically impaired in lean conditions, even when the inlet exhaust gas temperature is high. We link this effect to the availability of carbon monoxide in the exhaust gas and provide a control-oriented model that predicts the methane conversion efficiency under lean operation.

Hutter, R.; De Libero, L.; Elbert, P.; F.; Onder, C. Catalytic Methane Oxidation in the Exhaust Gas Aftertreatment of a Lean-burn Natural Gas Engine, Chemical Engineering Journal, Volume 349, 2018

1.3. CO_2-optimal Diesel injection

Unique to dual-fuel engines is the fact that the amount of fuel injected does not have to be directly related to the resulting force. In the diesel-ignited natural gas engine, for example, the combustion position is defined by the amount of diesel injected. However, as much of the chemical energy released as possible should come from natural gas. This is the only way to exploit the maximum potential for CO2 savings. The timing of diesel injection represents an additional degree of freedom. For each operating point there is a point in time at which the smallest possible amount of diesel results. Consequently, the intelligent selection of the injection point ensures that more natural gas and less diesel are consumed.

Under constant operating conditions, the combustion phasing is manipulated by changing the start and the duration of the diesel injection. These are referred to as SOI and DOI respectively. The combustion phasing is indicated by the center of combustion COC. Measurements for variations of SOI and DOI are shown in Figure 50.

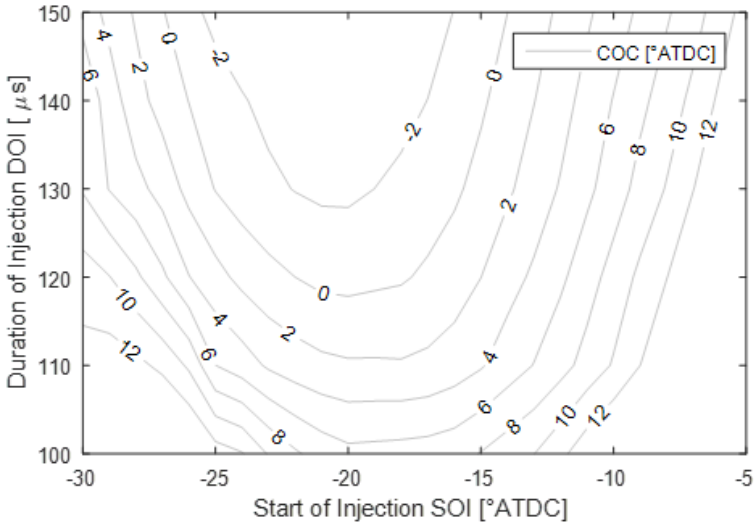

Figure 50: Measured center-of-combustion COC depending on diesel start of injection SOI and duration of injection DOI at 10 bar BMEP, 1500 rpm and stoichiometric conditions

The relationship between the duration DOI and the center of combustion COC is unique, as increasing the duration DOI, for a given start of injection SOI, always advances the center of combustion COC. However, the relationship between the start of injection SOI and the center of combustion COC for a constant duration DOI is more complicated. There exists a minimum achievable center of combustion COC for each chosen duration of injection DOI. For late crank angles the center of combustion COC is retarded if the start of injection SOI is retarded. On the other hand, for early crank angles the COC is retarded if the start SOI is advanced. In other words, there exists an injection timing, which leads to the smallest possible diesel quantity for a particular combustion phasing.

Figure 51 shows a vartiation in SOI at different fuel-to-air equivalence ϕ but constant combustion phasing such that the injected diesel quantity DOI has to be varied. In order to keep the load constant, the injected quantity of natural gas was also adjusted. The injection parameters with which the required operating point (combustion position, load, fuel-to-air ratio) is reached with the minimum diesel quantity are marked with a red star in Figure 51.

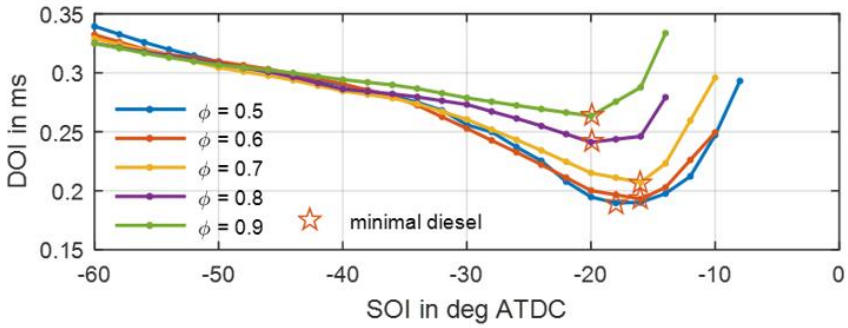

Figure 51: Variation of SOI at various fuel/air equivalence ratios for a constant COC=6°ATDC.

Finally, the effect of the Diesel injection strategy on HC and CO_2 emission is shown in Figure 52. With a constant fuel-to-air ratio, lower HC emissions can be achieved if the diesel is injected earlier (about 40° before TDC) than would be the case with the minimum diesel strategy.

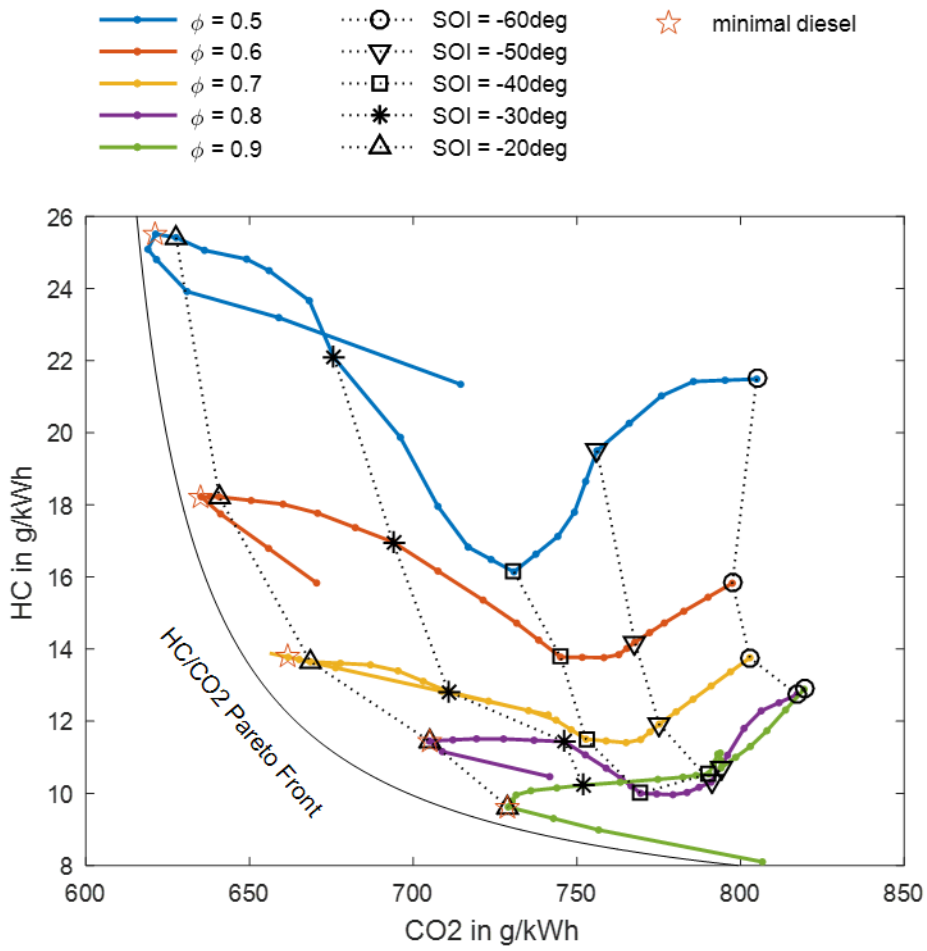

Figure 52: Measured HC and CO2 emissions that result with different injection timings and fuel/air equivalence ratios. All measurements are conducted at the same center of combustion COC=6°ATDC and the same load $p_{me} = 4$ bar at 2000 rpm.

If, however, it is assumed that the fuel-to-air ratio is available as degrees of freedom and can therefore be used for optimization, the diesel minimum injection points turn out to be optimal as HC/CO2. Because these measuring points run along the Pareto front which results from minimum CO2 or HC emissions. A Pareto Front is defined as a series of operating points in which one size cannot be improved without simultaneously worsening the other size. Consequently, the engine is operated HC/CO2-optimally if the injection strategy is selected according to the Diesel-minimal approach, i.e. with the smallest possible amount of injected diesel.

1.3.1. Diesel Minimal Control based on Extremum Seeking Technique

A method was developed at the IDSC which sets diesel injection at this "optimum" point in time at all operating points. The method is based on an "Extremum Seeking" algorithm. It makes it possible to minimize the amount of diesel at any operating point without the combustion position deviating from its target value. The Diesel Minimal Control (DMC) adapts the injected quantity of diesel as well as the injection point of the diesel to the given conditions in such a way that a stable and efficient combustion is achieved. This closed-loop system has proven to be very useful as it keeps the combustion phasing constant even under drastically changed charge conditions, for example with EGR or in throttled operation. Figure 53 shows two measurements with different initial SOI values that converges to the same SOI as DMC activated at time = 0 s.

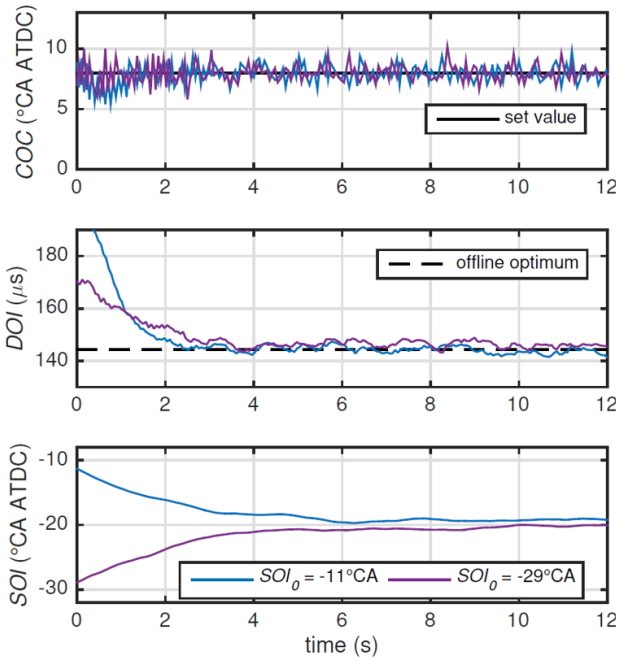

Figure 53: Measured online-optimizations of the Diesel injection parameters SOI and DOI while keeping the COC at 8° ATDC.

1.3.2. Extended Algorithm

The DMC algorithm has been extended to deal with limitations in the feasbile quantity of Diesel that can be injected. In the diesel ignited gas engine only very small quantities of diesel are needed for a successful ignition, especially with high load demands. Figure 54 shows how the diesel share of the total chemically supplied energy decreases over the load. This is also reflected in the reduced Duration of Injection (DOI). However, the original diesel injectors have a minimum injection time. If the injection time falls below this value, the actual quantity injected can vary greatly from cycle to cycle and consequently affect the control of the center of combustion.

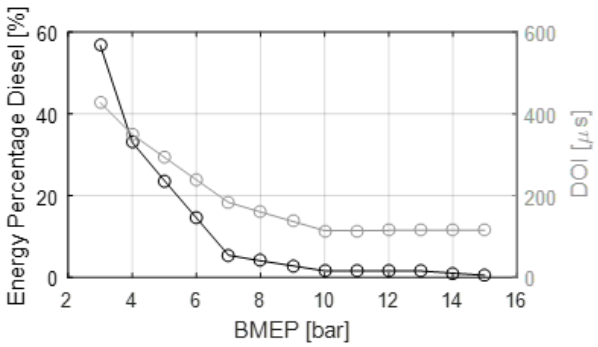

Figure 54: Energetic share of diesel fuel in the total chemical energy supplied in relation to the effective mean pressure BMEP. Operating conditions: 2000rpm, stoichiometric.

The injection limits mentioned above must be taken into account in the DMC, otherwise deviations in the combustion centre will result. As soon as such a limit is reached, the control loop that uses the injection time loses its ability to influence the system. As a result of the ongoing optimization, the combustion position is shifted to early crank angle, which can have higher NO_x emissions and pressure gradients as consequence. The extension ensures that when the limit is reached, the injection timing is no longer optimized, but maintained at the crank angle at which the desired combustion position can be achieved. A signal flow diagram of the extended DMC algorithm can be seen in Figure 55.

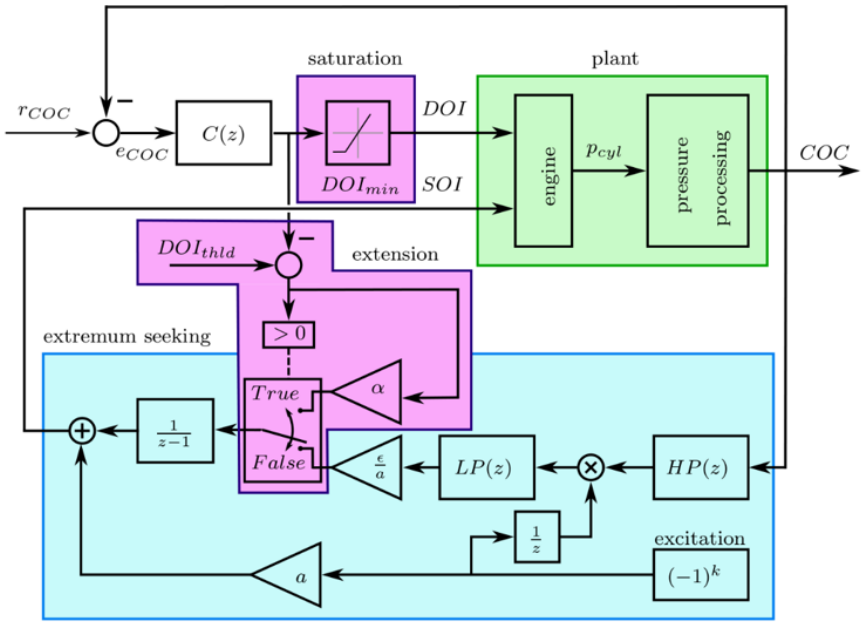

Figure 55: Signal flow diagram of the extended Diesel Minimum Control.

1.4. The Low-Load Feasibility of Dual-Fuel Combustion

The capability of the diesel ignited gas engine to cover low load conditions is only partially given. For low torque requirements, the engine must be operated with pure diesel. It is therefore important to understand the physical phenomenon that implies this low load limit in order to assess the usability of this engine in conventional operation, i.e. without electrical hybridisation, since in this case the entire load spectrum must be covered. In the following investigation, we develop optimal low-load operation strategies for the input variables equivalence ratio and exhaust gas recirculation (EGR) rate. A physical engine model helps to investigate three important limitations, namely maximum acceptable HC emissions, minimal CO_2 reduction, and minimal exhaust gas temperature.

1.4.1. The Low-Load Constraints

The low-load limit $p_{me,min}$ of a Diesel-ignited gas engine is defined as the minimal load at which dual-fuel combustion is still feasible. The three low-load constraints considered here are introduced in the following.

A major driving force in the development of the Diesel-ignited gas engine is its potential to reduce CO_2 emissions. The first criterion is therefore given by the CO_2 reduction over the base Diesel engine Δm_{CO_2}. This quantity describes the relative difference in CO_2 emission between a base (Diesel-only) operation $m_{CO_2,base}$ and a dual-fuel operation $m_{CO_2,dual}$.

$$\Delta m_{CO_2} = \frac{m_{CO_2,base} - m_{CO_2,dual}}{m_{CO_2,base}}$$

Throughout this study, hypothetical tailpipe CO_2 emissions are considered, i.e. the CO_2 emission that result in the case of the complete oxidation of all unburnt hydrocarbons (HC) and carbon monoxide (CO) in the exhaust. Increased CO and HC emissions thus have no diminishing effect on the CO_2 values considered.

The other two criteria are related to the complete oxidation of unburnt methane in the engine's exhaust gas. In general, lean-burn gas engines feature significant emissions of unburnt methane fuel. It is a crucial challenge to limit the engine-out hydrocarbon emissions $m_{HC}$to a level such that a well working catalyst with 95% efficiency is able to oxidize the hydrocarbons according to current (Euro VI) limits set by legislation for tailpipe emissions. The catalyst is only capable to comply with this requirement if the exhaust gas temperature ϑ_{exh} is high enough, which constitutes the third criterion. As reported in literature, the exhaust gas temperature required to oxidize methane is significantly higher than for typical unburnt hydrocarbons produced in a gasoline or Diesel engine. A summary of the three constraints is presented in Table 5.

Table 5: Low-Load Contraints

Description	**Symbol**	**Value**
CO2 reduction	Δm_{CO_2}	>0%
HC engine-out emission	m_{HC}	<13 g/kWh
Exhaust gas temperature	ϑ_{exh}	>450° C

1.4.2. The Static Engine Model

The structure of the model is special in that it incorporates knowledge about the engine performance in the base Diesel configuration, i.e. the operation using only Diesel, the way the engine was operated before the dual-fuel capability was added. The model input and output variables are given in Table 6.

Table 6: Overview input and output variables of the engine model.

Model Inputs		**Model Outputs**	
Symbol	Description	Symbol	Description
p_{me}	Brake mean effective pressure	Δm_{CO_2}	CO2 reduction
ϕ	Fuel/air equivalence ratio	m_{HC}	HC engine-out emission
x_{egr}	Exhaust gas recirculation rate	ϑ_{exh}	Exhaust gas temperature

The detailed model equations are not given here, but can be found in the aforementioned publication[1].

[1] Hutter, R.; Ritzmann, J.; Elbert, P.; Onder, C. Low-load Limit in a Diesel-ignited Gas Engine, Energies, Volume 10; 2017

1.4.3. Results

The major results of the stationary low-load study comprise

- The validation of the engine model
- The determination of the low-load limit $p_{me,min}$
- Three optimal low-load operation strategies

1.4.3.1. Model Validation

The comparison of the modeled and the measured constraint variables in throttled operation shown in Figure 56 demonstrates that the engine model is capable of reproducing the main trends of all three variables.

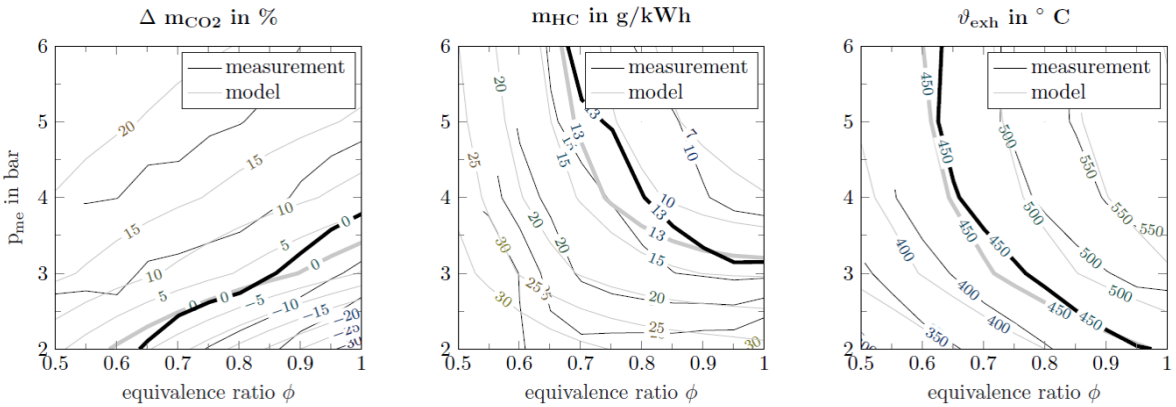

Figure 56: Comparison of the measured and modeled low-load constraints for the case $x_{EGR} = 0\%$.

1.4.3.2. The Low-Load Limit

Figure 57 illustrates the conditions that lead to the minimum feasible load in dual-fuel mode, i.e. the global low-load limit. The low load limit $p_{me,min} \approx 3.2$ bar results under the slightly lean conditions $\phi \approx 0.96$ and without EGR $x_{EGR} = 0\%$. As a consequence, the operation has to be switched to Diesel-only whenever a load is required that is lower than $p_{me,min}$. Within the feasible space Λ the engine can be operated with excess air, i.e. under lean conditions, down to an equivalence ratio of approximately $\phi_{min,min} = 0.65$ at $p_{me} = 6$ bar. The maximum applicable EGR rate $x_{EGR,max}$ is mainly limited by the minimum exhaust gas temperature. The higher the equivalence ratio is, the higher the maximum EGR rate $x_{EGR,max}$ becomes.

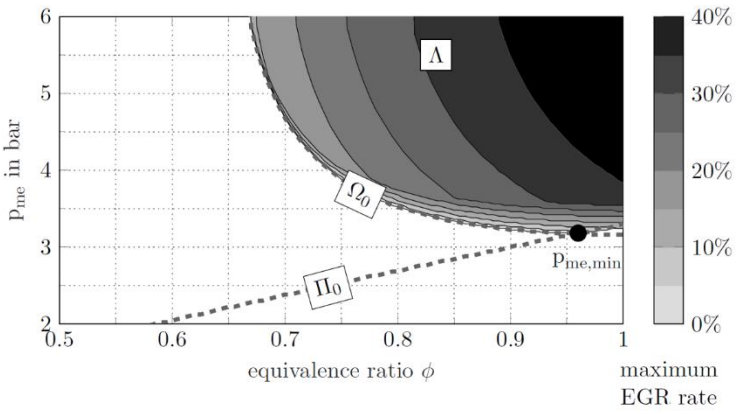

Figure 57: The global feasible set Λ.

1.4.3.3. Optimal Low-Load Strategies

Three strategies minimizing different cost functions $f_S()$ are derived. The three strategies minimize the engine-out HC emissions, minimize the CO_2 emissions, and maximize the total engine efficiency, respectively. The particular cost functions are listed in Table 7.

Table 7: The cost functions f_S oft he three strategies considered.

Name	$\boldsymbol{f_S(\phi, x_{EGR})}$	**Goal**
S_{HC}	$m_{HC}(\phi, x_{EGR})$	Minimize engine-out HC emission
S_{CO_2}	$m_{CO_2}(\phi, x_{EGR})$	Minimize CO_2 emissions
S_η	$-\eta(\phi, x_{EGR})$	Maximize engine efficiency

The optimization problem is as follows:

$$\min_{\phi\in[0.5,1], x_{EGR}\in[0,0.4]} f_S(\phi, x_{EGR})$$
$$s.t. \quad m_{HC} < 13\ \mathrm{g/kWh}$$
$$\Delta m_{CO_2} > 0$$
$$\vartheta_{exh} > 450\ ^\circ\mathrm{C}$$

Figure 58 outlines the resulting optimal input variables $\phi^*(p_{me})$ and $x^*_{EGR}(p_{me})$ as functions of the third input variable p_{me}. For loads lower than the minimal load $p_{me,min}$ no optimal inputs can be found as at least one of the constraints is active. At $p_{me,min}$ only one feasible solution exists. Therefore, all strategies merge at $p_{me,min}$. The CO_2-optimal strategy S_{CO_2} is the only strategy operating with a lean equivalence ratio, $\phi < 1$, exclusively. The excess air enables the highest substitution rates while the pumping losses are minimized. The efficiency-optimal strategy S_η on the other hand minimizes pumping losses by stoichiometric combustion with a high EGR ratio x_{EGR}. Stoichiometric combustion *without* EGR (S_{HC}) minimizes the HC emissions m_{HC} while the exhaust gas temperature ϑ_{exh} is maximized at the same time. In agreement with the HC-to-CO_2 tradeoff presented previously this strategy leads to the highest CO_2 emissions. Table 8 shows a very simplified view of the optimal input

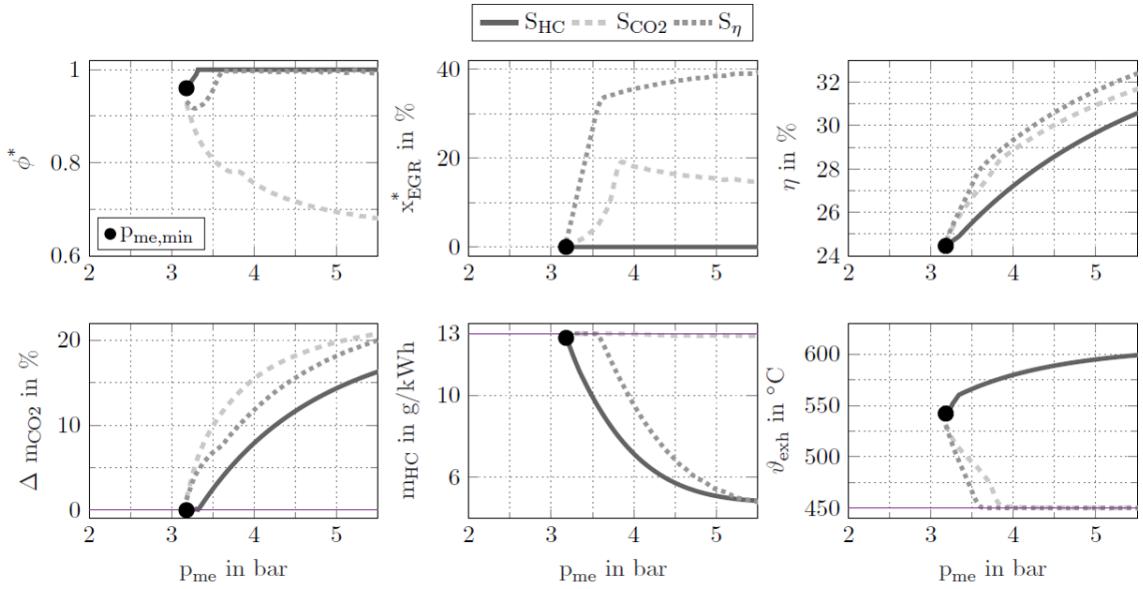

Figure 58: Simulation results for the three optimal strategies in terms of HC emissions (S_{HC}), minimal CO_2 emissions (S_{HC}), and maximum efficiency (S_η).

properties.

Table 8: Simplified optimal strategies.

Strategy	$\boldsymbol{\phi^*}$	$\boldsymbol{x^*_{EGR}}$
S_{HC}	1	0
S_{CO_2}	<1	>0
S_η	1	>0

1.4.4. Discussion

The reason for the high HC emissions at lean mixtures and low loads is strongly linked to the gas-to-air equivalence ratio ϕ_{gas}.

$$\phi_{gas} = \frac{m_{gas}}{m_{air}} \cdot \sigma_{0,gas}$$

It describes the gas-to-air ratio of the homogeneous cylinder charge that is present before the diesel is injected. Figure 59 shows that the gas conversion rate η_{gas} can be well described as a function of ϕ_{gas}. The increase of the gas-to-air equivalence ratio ϕ_{gas}, is accompanied by a reduction of the excess air, clearly leads to a higher gas conversion rate and thus to better gas combustion. One way to achieve this increase is to throttle the air mass flow into the intake manifold. The pressure in the inlet is thus reduced. The ignition characteristic of the Diesel, however, depends strongly on the prevailing inlet pressure. The injected quantity of diesel has to be increased in order to maintain the desired combustion phasing at a lower intake pressure.

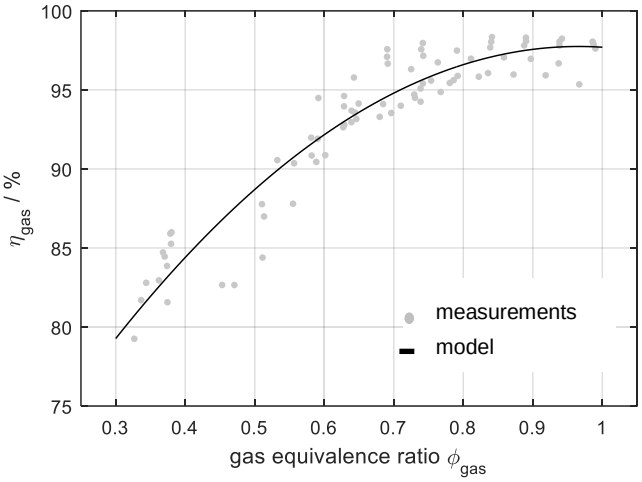

Figure 59: Relation between gas equivlance ratio ϕ_{gas} and the gas conversion efficiency η_{gas}.

The technique of throttling, however, is only effective if the increase in the total equivalence ratio ϕ leads to an increase in the gas equivalence ratio ϕ_{gas}. Under high-load operation (approximately $p_{me} > 4$ bar) this is the case, while for throttled low-load operation this condition is not fulfilled. As a consequence of the impaired Diesel ignition at lower intake pressure, significantly more Diesel fuel has to be injected in order to assure a proper ignition. In other words, the ignition delay rises disproportionally to the decrease in intake manifold pressure. Since the higher amount of Diesel requires more air for combustion, the resulting gas equivalence ratio ϕ_{gas} is not increased. Figure 60 shows that below approximately 4 bar brake mean effective pressure p_{me}, the gas equivalence ratio ϕ_{gas} is independent of the total equivalence ratio ϕ. In conclusion, below a certain load, the technique of throttling cannot raise the gas equivalence ratio ϕ_{gas}.

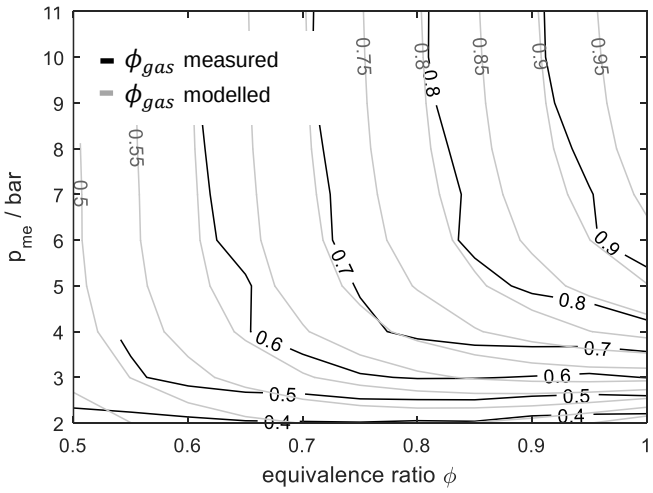

Figure 60: Measured and simulated gas equivalence ratio ϕ_{gas}.

The observed phenomenon that the gas conversion rate η_{gas} is very poor at low loads, regardless of the total fuel-to-air ratio ϕ, is thus due to two properties.

1. The gas conversion rate η_{gas} is related closely to the gas-to-air equivalence ratio ϕ_{gas}
2. At low loads, it is not possible to increase the gas-to-air equivalence ratio ϕ_{gas} by throttling.

1.5. Optimal Combustion Mode Transition

The previous section shows that under certain low-load conditions the dual-fuel mode is not feasible, such that the engine requires inherently two combustion modes: At low loads, the engine is operated with Diesel fuel only (Diesel-only mode), while at medium and high loads both fuels are injected (dual-fuel mode). The capability to perform the transition between these combustion modes in a smooth manner is crucial in terms of the practicability of this engine type. The transition should not lead to a noticeable deviation from the nominal torque level, neither should the transition lead to a penalty in CO_2 or tailpipe pollutant emissions like NO_x or CH_4. These requirements result in the transition being a challenging task as various actuator settings, from both the fuel and the air paths, change during the transition largely.

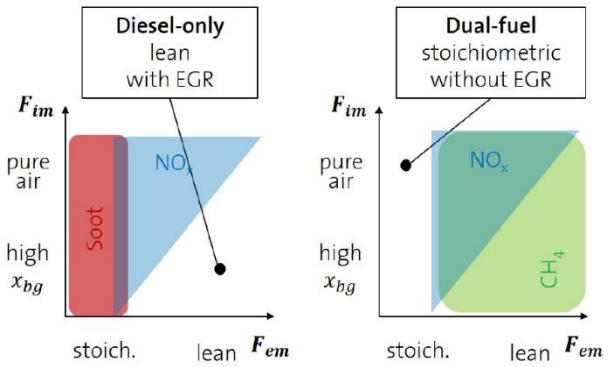

Figure 61: Schematic overview about the mode-dependent conditions imposed on the oxygen mass fractions in the intake (F_{im})and exhaust manifold (F_{em}).

In particular, the two modes impose significantly different requirements on the air path conditions. The Diesel-only mode requires lean exhaust conditions ($F_{em} > 0\%$) due to the excessive soot formulation with air/fuel ratios close to stoichiometric conditions. In addition, the lack of any lean NO_x exhaust aftertreatment system requires the NO_x abatement to take place in-cylinder with EGR, i.e. by reducing the oxygen content inside the intake manifold ($F_{im} < F_{air}$). In contrast, the dual-fuel operation is only feasible with stoichiometric conditions ($F_{em} = 0\%$). This is a result from the limitations of today's three-way catalysts. At low load, they offer only effective methane oxidation in stoichiometric. Figure 61 summarizes the mentioned requirements on the airpath conditions $F_{im}$and F_{em}.

Figure 62 shows a measurement of two combustion mode transitions: from dual-fuel to Diesel-only mode at$t = t_1$, then back to dual-fuel mode$t = t_2$. At the time instances t_1 and t_2, respectively, all input signals change to the steady-state values of the new combustion mode (static transition). In both caes the transition leads to a deviation from the nominal torque as well as additional pollutant emissions. The transition from Diesel-only to dual-fuel is the transition with the larger deviations. In comparison to the transition in the reverse direction, the torque deviation is by a factor of 5 higher and the additional emissions by a factor of 16 and 30, respectively. Consequently, the focus of this investigation lies on the transition from Diesel-only to dual-fuel mode exclusively as it appears to be the critical case.

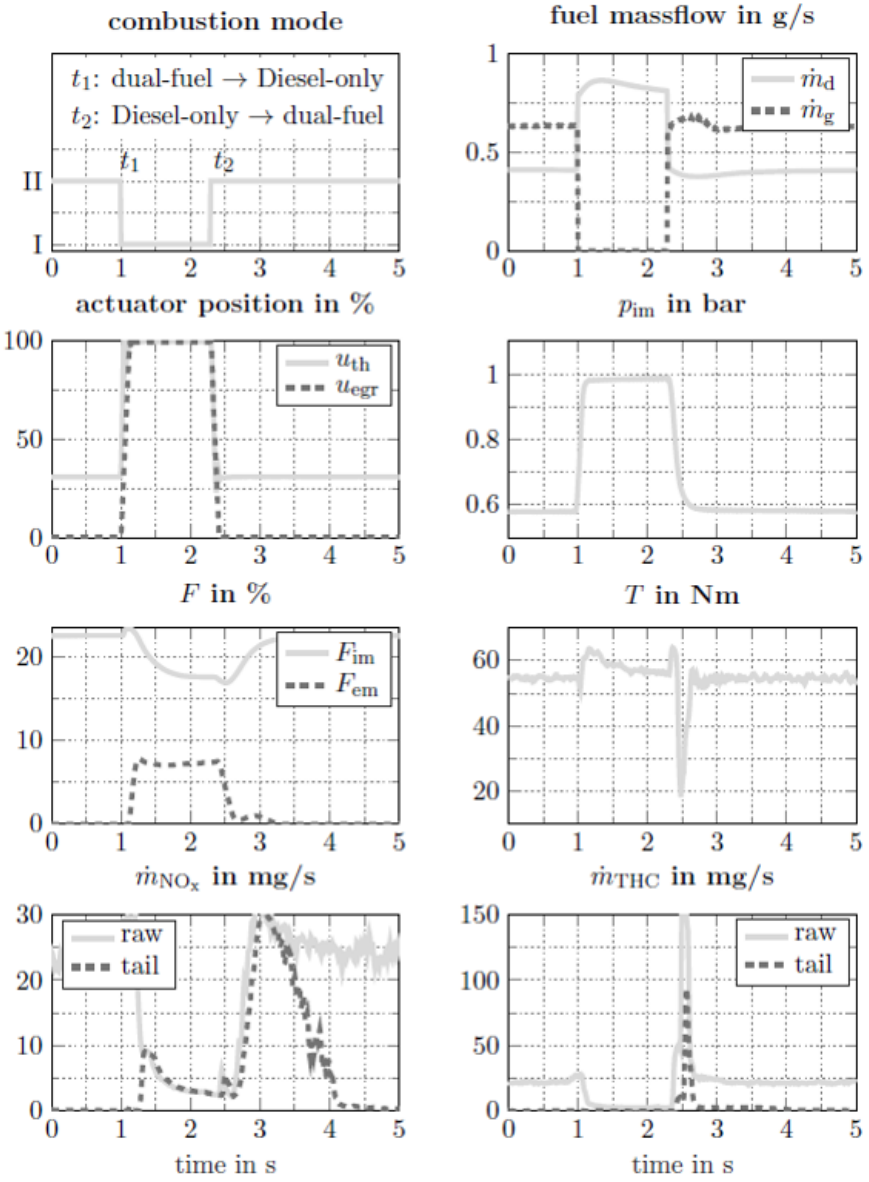

Figure 62: Measurement of the static transition between the combustion modes.

The objective is the synthesis of the optimal actuator commands for the smooth transition between the combustion modes of a Diesel-ignited gas engine using a nonlinear integrated model of the engine and of the aftertreatment system. Optimality is defined in this context in terms of torque deviation, NOx and HC tailpipe emissions. The setup includes four control inputs, namely the two fuel massflows, the position of the air throttle and the position of the EGR valve. The engine performance of the presented method is tested by implementing the optimal actuator commands in a feedforward controller. A focus lies on the mathematical model used for optimization to be of low order such that it is suitable for the use in online optimization.

1.5.1. Dynamic Engine Model

The dynamic model that is used for optimization subsequently, is outlined here briefly. First, we introduce input, output and state variables. Then we present the main dynamic equations. The input vector contains the following signals.

$$u(t) = \begin{bmatrix} \dot{m}_{\mathrm{d,T}}(t) \\ \dot{m}_{\mathrm{g}}(t) \\ u_{\mathrm{th}}(t) \\ u_{\mathrm{egr}}(t) \end{bmatrix} \quad \begin{array}{l} \text{massflow Diesel-torque} \\ \text{massflow natural gas} \\ \text{position air throttle} \\ \text{position EGR valve} \end{array}$$

The output $\boldsymbol{y}(t)$ contains signals that are part of the cost function of the optimization problem introduced later.

$$y(t) = \begin{bmatrix} T(t) \\ \dot{m}_{\mathrm{CO_2}}(t) \\ \dot{m}_{\mathrm{NO_x,tail}}(t) \\ F_{\mathrm{im}}(t) \\ F_{\mathrm{em}}(t) \end{bmatrix} \quad \begin{array}{l} \text{engine torque} \\ \mathrm{CO_2}\ \text{massflow} \\ \mathrm{NO}_x\ \text{massflow tailpipe} \\ \text{oxygen fraction intake manifold} \\ \text{oxygen fraction exhaust manifold} \end{array}$$

The dynamic model is based on the seven state variables as follows.

$$x(t) = \begin{bmatrix} \omega_{\mathrm{tc}}(t) \\ p_{\mathrm{im}}(t) \\ p_{\mathrm{ac}}(t) \\ p_{\mathrm{em}}(t) \\ F_{\mathrm{im}}(t) \\ F_{\mathrm{em}}(t) \\ F_{\mathrm{cat}}(t) \end{bmatrix} \quad \begin{array}{l} \text{speed turbocharger} \\ \text{pressure intake manifold} \\ \text{pressure after compressor} \\ \text{pressure exhaust manifold} \\ \text{oxygen fraction intake manifold} \\ \text{oxygen fraction exhaust manifold} \\ \text{oxygen fraction catalyst} \end{array}$$

The core equation of the model are given in the following.

$$
\begin{aligned}
\dot{\omega}_{\mathrm{tc}}(t) =& \frac{1}{\omega_{\mathrm{tc}}(t) J_{\mathrm{tc}}} \Big(P_t(t) - P_c(t) - P_f(t) \Big) \\
\dot{p}_{\mathrm{im}}(t) =& \frac{\kappa_{\mathrm{air}} R_{\mathrm{air}}}{V_{\mathrm{im}}} \Big(\dot{m}_{\mathrm{th}}(t) \vartheta_{\mathrm{ic}} + \dot{m}_{\mathrm{egr}}(t) \vartheta_{\mathrm{egr}} - \dot{m}_{\beta}(t) \vartheta_{\mathrm{im}}(t) \Big) \\
\\
\dot{p}_{\mathrm{ac}}(t) =& \frac{R_{\mathrm{air}} \vartheta_{\mathrm{ac}}}{V_{\mathrm{ac}}} \Big(\dot{m}_{\mathrm{c}}(t) - \dot{m}_{\mathrm{th}}(t) \Big) \\
\dot{p}_{\mathrm{em}}(t) =& \frac{R_{\mathrm{eg}} \vartheta_{\mathrm{em}}}{V_{\mathrm{em}}} \Big(\dot{m}_{\mathrm{eo}}(t) - \dot{m}_{\mathrm{egr}}(t) - \dot{m}_{\mathrm{t}}(t) \Big) \\
\dot{F}_{\mathrm{im}}(t) =& \frac{R_{\mathrm{air}} \vartheta_{\mathrm{im}}}{V_{\mathrm{im}} p_{\mathrm{im}}} \Big(\dot{m}_{\mathrm{th}}(t) (F_{\mathrm{air}} - F_{\mathrm{im}}(t)) + \\
& \dot{m}_{\mathrm{egr}}(t) (F_{\mathrm{em}}(t) - F_{\mathrm{im}}(t)) \Big) \\
\dot{F}_{\mathrm{em}}(t) =& \frac{R_{\mathrm{eg}} \vartheta_{\mathrm{em}}}{V_{\mathrm{em}} p_{\mathrm{em}}(t)} \Big(\dot{m}_{\mathrm{eo}}(t) (F_{\mathrm{eo}}(t) - F_{\mathrm{em}}(t)) \Big) \\
\dot{F}_{\mathrm{cat}}(t) =& - \frac{1}{\tau_{\mathrm{cat}}} (F_{\mathrm{cat}}(t) + F_{\mathrm{em}}(t))
\end{aligned}
$$

1.5.2. Optimal Control Problem

The task is interpreted as an optimal control problem. The goal is to find the optimal actuator signals for switching from Diesel-only to dual-fuel mode at time $t = t_{switch}$. Based on the mathematical model $\dot{x}(t) = f(\boldsymbol{x}(t), \boldsymbol{u}(t))$ introduced in the previous sections, we set up the continuous time formulation of the optimal control problem with finite horizont_H. The cost function is composed of three terms. The first term relates to the time period $t_0 \rightarrow t_{switch}$ in Diesel-only mode, the second term relates to the time period $t_{switch} \rightarrow t_H$ in dual-fuel mode and the thir term introduces a final cost.

$$
\begin{aligned}
\min_{\boldsymbol{x}(\cdot), \boldsymbol{u}(\cdot)} & \int_{t_0}^{t_{\mathrm{switch}}} ||y_{\mathrm{r}}(t) - y(t)||^2_{R_{\mathrm{I}}} + ||\dot{u}(t)||^2_{Q_{\mathrm{I}}} \, \mathrm{d}t \\
& + \int_{t_{\mathrm{switch}}}^{t_{\mathrm{H}}} ||y_{\mathrm{r}}(t) - y(t)||^2_{R_{\mathrm{II}}} + ||\dot{u}(t)||^2_{Q_{\mathrm{II}}} \, \mathrm{d}t \\
& + ||y_{\mathrm{r},k} - y_k||^2_{R_{\mathrm{N}}} \\
\text{s. t.} \quad & \dot{x}(t) = f\big(x(t), u(t)\big), \qquad t \in [0, t_{\mathrm{H}}] \\
& x(t_0) = X_0 \\
& g_i(x(t), u(t)) \leq 0, \qquad i = 1, .., q
\end{aligned}
$$

Various constraints on input, state or output variables are combined in the term $g_i(\boldsymbol{x}(t), \boldsymbol{u}(t))$. We discuss the specific terms in the following.

- Prevent the excessive formulation of soot by restricting the in-cylinder oxygen mass fraction in Diesel-only mode to stay lean ($> 4\%$, approximately $\lambda > 1.3$). In dual-fuel mode this lower bound shifts stoichiometric conditions, i.e. 0%.

$$\left.\begin{matrix} Diesel-only & 4\% \\ dual-fuel & 0\% \end{matrix}\right\} \leq F_{eo}(t)$$

- Account for injector characteristics at small opening durations. Given a certain rail pressure, not an arbitrary small fuel mass can be injected.

$$\left.\begin{matrix} 0\ mg/s \\ 4\ mg/s \end{matrix}\right\} \leq m_g(t) \leq \begin{cases} 0\dfrac{mg}{s} & Diesel-only \\ \infty & dual-fuel \end{cases}$$

- Limit actuators as throttles and valves by fully-open and fully-closed position

$$0\% \leq u_{th}(t) \leq 100\%$$
$$0\% \leq u_{egr}(t) \leq 100\%$$

- Limit the rate with which throttles and valves can move.

$$-1000\ \frac{\%}{s} \leq \dot{u}_{th}(t) \leq 1000\ \frac{\%}{s}$$
$$-700\ \frac{\%}{s} \leq \dot{u}_{egr}(t) \leq 700\ \frac{\%}{s}$$

- Introduce lower bound on oxygen mass fraction in the intake manifold as too much burnt gas concentrations increase combustion variations and eventually leads to misfires. The lower bound of $F_{im}(t) = 15\%$ corresponds to a burnt gas ratio of approximately $x_{bg} = 35\%$.

$$\left.\begin{matrix} Diesel-only & 17\% \\ dual-fuel & 15\% \end{matrix}\right\} \leq F_{im}(t)$$

1.5.3. Results

We compare the optimization result to the non-optimized static transitions. For this purpose, the optimized trajectory is applied as a feedforward control on the testbench. Figure 63 shows the empirical results. The striking characteristic of the optimal trajectory is the closing of the air throttle in Diesel-only mode prior to the activation of the gas injection at $t = t_{switch}$. The drop in the intake manifold pressure leads to a reduced oxygen concentration in the exhaust, which is still high enough to prevent excessive soot formation, but improves at the same time the in-cylinder conversion of the natural gas that is injected after t_{switch}. In accordance the THC raw emissions do not show the peak we see in the baseline measurement as a result from the very lean methane-air mixture in the cylinders. In addition, the EGR valve is kept open for approximately 2:5 s after the switch. The dilution leads to low NOx raw emission during the period of time in which the catalyst's reduction capability is impaired due to the full catalyst oxygen storage. Not until the storage is depleted the reduction of NOx takes place. We account for the oxygen storage in the model by the state variable F_{cat}, whose dynamics is described by a low pass filter. Figure 64 shows the mean cumulative tailpipe emissions, determined over 10 measurements. The quantitive results are outline in Table 9.

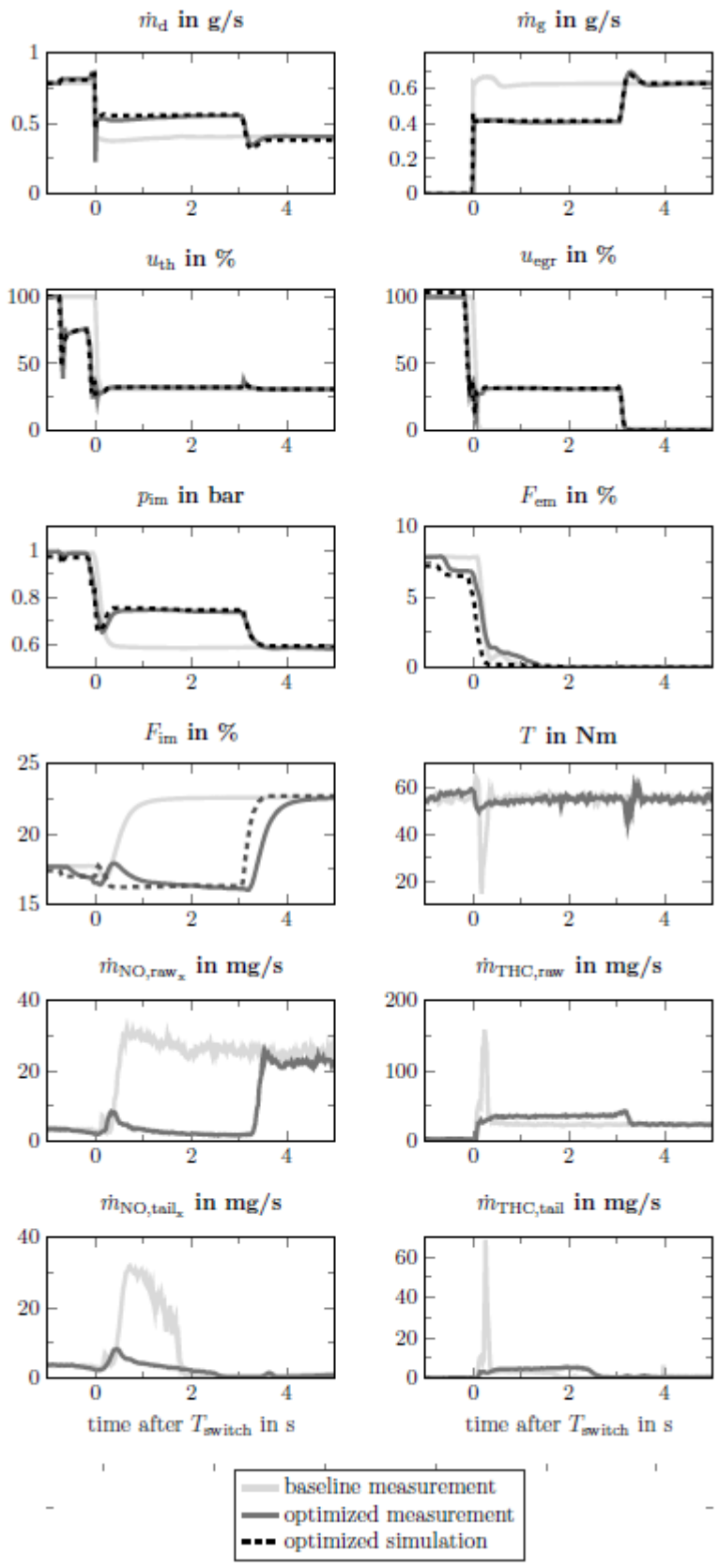

Figure 63: Measurement of optimized trajectory and static trajectory.

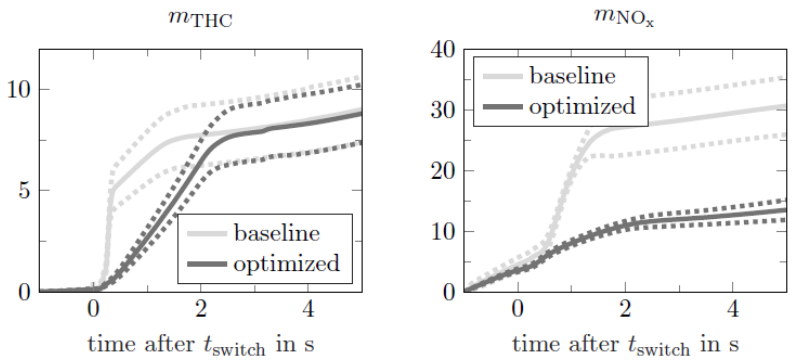

Figure 64: Measured cumulative THC and NO_x tailpipe emissions The solid lines indicate the mean value over 10 measurements and the area between the dotted lines the standard deviations.

Table 9: Evaluation of 10 Measurements

Deviation	Unit	Baseline	Optimized	Improvement
T_{max}	Nm	40.3 (4.90)	14.2 (3.19)	-65%
$m_{\mathrm{NO_x}}$	mg	30.6 (4.74)	13.5 (1.63)	-56%
m_{THC}	mg	9.03 (1.61)	8.81 (1.43)	-2.4%

1.5.4. Discussion

The oxygen diagram in Figure 65 outlines the simulation results oft he optimized transition. The main difference between the static and the optimized trajectory lies in the different values of the exhaust oxygen mass fraction at the moment of switching, i.e. $F_{em}(t_{switch})$. The switching time denotes the moment where the injection of natural gas is activated. While in the baseline case the exhaust oxygen level is at this moment still at the level of Diesel-only mode steady-state operation ($F_{em}(t_{switch}) = F_{em}(t_0)$), in the optimized case the fraction is reduced beforehand to 5:5%. This reduction prevents the excessive HC emission that occur with very lean CNG-air mixtures that we observe with the static translation trajectory. To what extend the exhaust oxygen level can be decreased in the Diesel-only mode is imposed by the contraint on F_{eo}. At t_{switch} the oxygen mass fraction at engine-out F_{eo} hits the contraint of 4%. While with the baseline trajectory both oxygen fractions changes at the same time, (reduction of $F_{em}$and raise ofF_{im}), the optimized solution shows a sequential strategy – reduce F_{em}first, then increase F_{im}.

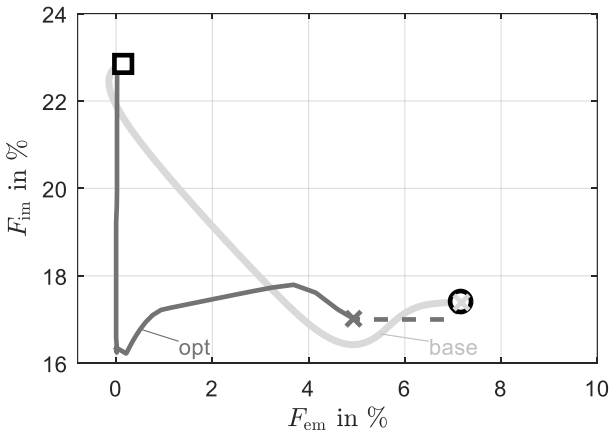

Figure 65: Oxygen diagram shows simulation with static (base) and optimized trajectory (opt).

1.6. Catalytic Methane Oxidation in Lean Exhaust Gas

Internal combustion engines that run on compressed natural gas with lean-burn combustion instead of stoichiometric combustion have the potential to reach a high overall efficiency. However, the aftertreatment of unburnt methane under such conditions is problematic as the methane conversion efficiency η_{CH_4} is impaired in lean exhaust gas mixtures. The conversion efficiency is defined as

$$\eta_{CH_4} = 1 - \frac{\dot{m}_{CH_4,ds}}{\dot{m}_{CH_4,us}}$$

with methane massflow downstream of the catalyst $\dot{m}_{CH_4,ds}$, and upstream, $\dot{m}_{CH_4,us}$. Figure 66 shows the exhaust gas temperature measured upstream of the catalyst as well as the methane conversion efficiency η_{CH_4} at various equivalence ratios ϕ and with two different engine loads. A perfect conversion efficiency close to 100% is achieved for both loads only with a stoichiometric mixture. By decreasing the fuel/air equivalence ratio, methane is converted less efficiently for both engine loads, whereby methane conversion drops more rapidly at high loads than at lower loads, even though the measured upstream temperature is always higher. Thus, the observed drop in methane conversion cannot be explained by the upstream temperature of the exhaust gas alone.

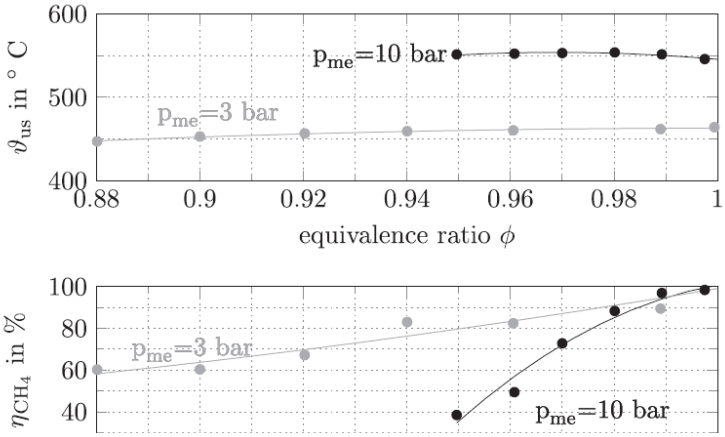

Figure 66: Exhaust gas temperature upstream oft he catalyst and methane conversion efficiency at two loads.

An alternative approach for explaining the conversion drop with lean mixtures considers the reactive heat that originates from the catalytic oxidation of the CO in the exhaust gas. Figure 67 shows the CO raw emissions $\dot{m}_{CO,us}$ as a function of the equivalence ratio. The amount of thermal energy released during the catalytic oxidation of CO, $\dot{Q}_{CO}$, depends on the lower heating value $H_{l,CO} = 10\,Mg/kg$ and on the amount of converted CO emissions inside the catalyst as

$$\dot{Q}_{CO} = \left(\dot{m}_{CO,us} - \dot{m}_{CO,ds}\right) H_{l,CO}$$

In stoichiometric conditions, the enthalpy released is around 1.5 kW while for only slightly lean conditions it reduces steeply. From the observation presented, the hypothesis is derived according to which the reaction heat $\dot{Q}_{CO}$ provides the crucial energy for methane conversion at stoichiometric conditions. This locally released energy is very effective as both the oxidations of methane and CO take place at the same or at similar catalytic sites on the substrate.

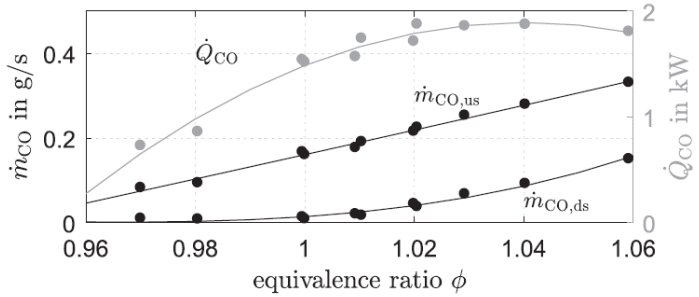

Figure 67: Measured carbon monoxide massflow upstream and downstream of the catalyst. The reaction heat released during the oxidation of carbon monoxide $\dot{Q}_{CO}$ is calculated.

1.6.1. Experimental Setup

In order to investigate the hypothesis, a CO-injection is added to the setup of the Diesel-ignited gas enigne. Bottled CO (50% in N2) can be injected into the exhaust gas upstream of the turbine.

1.6.2. Catalyst Model

The model distinguishes among the three following unburnt products

- CH_4 methane
- NMHC non-methane hydrocarbons
- CO carbon monoxide.

The core element of the catalyst model is the single-cell model with state variable ϑ that is defined by the energy balance, an ordinary differential equation, as follows:

$$\frac{d}{dt}\vartheta(t) = \frac{\vartheta(t)}{\tau}\left(c_p\dot{m}_{exh}(t)\vartheta_{us}(t) - c_p\dot{m}_{exh}(t)\vartheta(t) + \dot{Q}_{react}(t) + \dot{Q}_{loss}(t)\right).$$

Upon conversion, the incoming pollutant species release into the catalyst cell the chemical reaction heat $\dot{Q}_{react}$, which is defined as

$$\dot{Q}_{react}(t) = \sum \dot{Q}_x(t) = \sum \dot{m}_{x,us}(t)\, H_{l,x}\, \eta_x(t) \quad \text{with } x \in \{CH_4, NMHC, CO\}$$

with the massflow $\dot{m}_{x,us}$, the lower heating value $H_{l,x}$, and conversion efficiency η_x of specie x. Only the conversion efficiency of CH_4 is not constant but a function of $\dot{m}_{exh}$ and the state variable ϑ.

$$\eta_{CH_4}(t) = 1 - \exp\left(\frac{-a}{\dot{m}_{exh}(t)}\left(\frac{\vartheta(t) - \vartheta_0}{\Delta\vartheta}\right)^m\right)$$

Finally, the multi-cell model is composed of an arbitrary number of single-cell models that are stacked in series. The inlet conditions in terms of temperature and pollutant species of the subsequent cell are defined by the outlet conditions of the previous one. The downstream temperature ϑ_{ds} and the methane tailpipe emissions $\dot{m}_{CH_4,ds}$ of the multi-cell model are defined by the outlet conditions of the

last cell (see Figure 68). The NMHC and CO emissions are always oxidated completely but not necessarily in the first cell.

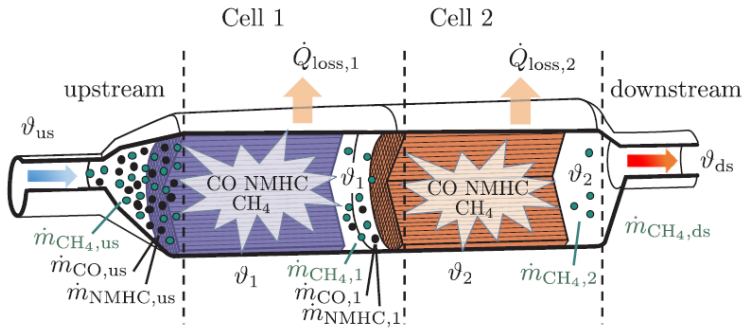

Figure 68: Schematic representation of the two-cell model.

1.6.3. Results

Figure 69 shows the effects of a CO injection on the measured ϕ_{us}, exhaust gas temperature and methane emissions. The equivalence ratio stays lean during the CO pulse and the upstream exhaust gas temperature remains constant. The methane downstream emissions $\dot{m}_{CH_4,ds}$ drop as the inflowing methane starts to oxidize. After 60 s a complete methane conversion is achieved, and after the CO injection is turned off again, the catalyst is still able to fully convert methane for another 30 s. The more cells used, the better the modelled emissions correspond to the measured values. The modell with the highest cell number uses 40 cells and reproduces the measured emission values best.

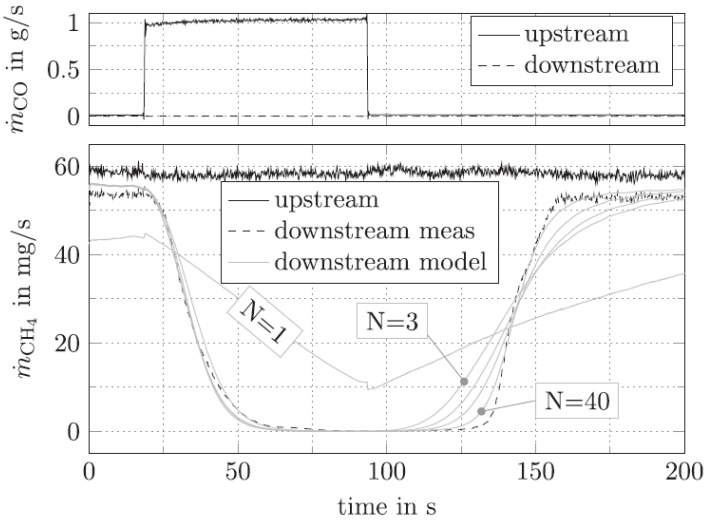

Figure 69: Injection of CO into the exhaust gas at lean conditions with $\phi = 0.5$ and $p_{me} = 3.2$ bar

1.6.4. Discussion

An effective catalytic methane conversion is achieved with the techniques of CO injection even with an upstream exhaust gas temperature as low as 300 °C. In general, conversion can be achieved by diverting energy to the catalyst by two paths: Either through the exhaust gas enthalpy path or by the reaction heat path. The simulation results shown in Figure 70 demonstrate that, in general, achieving a high methane conversion efficiency is a result of the combination of the exhaust gas enthalpy and the partially burnt or unburnt fuel contained in the exhaust gas. Good conversion as observed in stoichiometric engines is only possible if these two factors add up to provide enough local energy. In the case of stoichiometric operation, the relatively high CO concentration in the exhaust gas promotes the methane conversion. An exemplary sweep in the fuel/air equivalence ratio ϕ is also shown in Figure 70. In addition to the reaction heat released upon the CO oxidation at $\phi = 1$, an exhaust gas temperature of around 480 °C is required. A much higher exhaust gas temperature of approximately 700 °C is required if no chemical energy is available in the exhaust gas (see ”exhaust enthalpy path” in Figure 70). This case corresponds to the lean exhaust gas conditions, i.e. the reaction heat originating from the CO oxidation falls away. However, given the low exhaust gas temperature at $\phi = 0.5$ one way to achieve a high methane conversion is to provide more chemically-bonded energy to the catalyst.

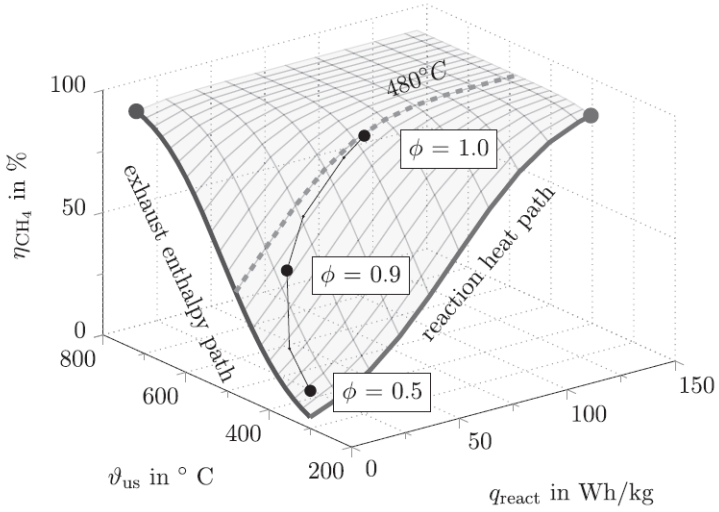

Figure 70: Simulation result of the catalyst model with 10 cells and with stationary inputs. An exemplary sweep in the fuel/air equivalence ratio ϕ from lean (0.5) to stoichiometric conditions (1) is outlined.

Figure 71 shows a dynamic CO-injection measurement, where once the CO injection is finished, the conversion efficiency stays at a high level for a certain period of time. Since at the beginning of the CO injection the conversion efficiency rises with only little delay on the CO pulse, this observation cannot be explained by a simple single-state thermal inertia of the catalyst. In addition to the measured variables, Figure 71-left shows the simulated outlet conditions of six particular cells. The cool-down of the last cell temperature coincides with the conversion loss 30 s after the end of the CO injection. Figure 71-rigth shows how the active zone, i.e., the region where most of the methane oxidation takes place, moves from the front to the back. It outlines the spatial activity of the catalyst at four time instances ($t_1, t_2. t_3$ and t_4) as indicated in Figure 71-left.. After a transient phase (time t_1), the CH_4 conversion reaches steady-state conditions at time t_2. In this moment, all CH_4 is converted and the

downstream CH_4 mass flow vanishes. The most active cell, meaning the cell where the most CH_4 is converted, is cell number 8. After the deactivation of the CO injection, the active zone starts to move towards the back of the catalyst. At time t_3 the most active cell is cell number 16 and 35 s later, at time t_4, it is cell number 39. Methane is converted by the catalyst until the active zone reaches the last cell. In conclusion, the reason for the delay with which the CH_4 downstream conditions rise after the stop of the CO injection lies in the movement of the active zone inside the catalyst.

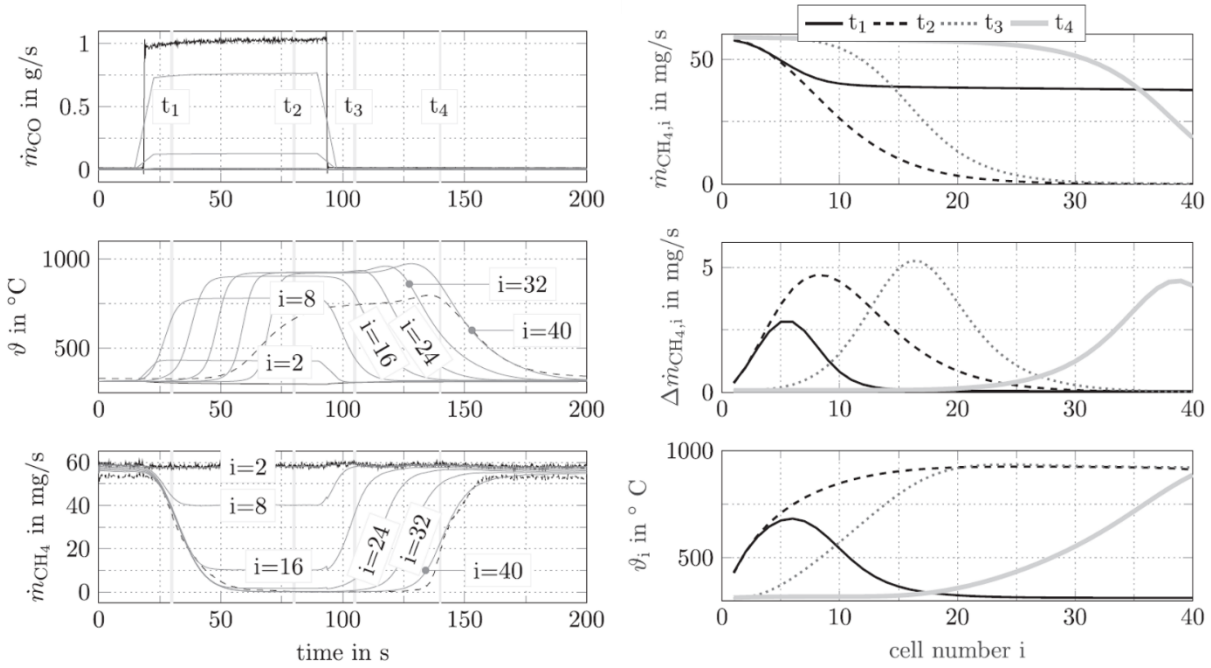

Figure 71: Simulation result with a 40 cell model over time (left) and space (right).

1.7. WP2 Conclusions

The research that was conducted withing the WP2 has yielded many important findings in the areas of combustion feedback control, stationary operating point optimization and combustion mode switching control in a Diesel-ignited gas engine. In addition, contributions were made on the subject of the oxidation of unburnt methane in the exhaust gas of lean-burn natural gas engines. All these topics represent components which are essential for a successful introduction of a thermal management for a Diesel-ignited gas engine. We summarize the major findings in the following.

- The Diesel-ignited gas engine is operated CO_2/HC-optimal in case the injection timing of the Diesel fuel is chosen according to the Diesel-minimal approach. A possibility to persue this approach is the use of the online optimization method “Diesel Minimal Control” that minimizes the injected Diesel fuel mass while keeping the combustion phasing at the desired level.
- The high HC emissions under low-load and lean conditions are a consequence of the inability to raise the gas equivalence ratio resulting in a poor flame propagation. There is a conflicting demand of lean combustion with low CO_2 emissions and stoichiometric operation with low HC emissions.
- The minimal feasible dual-fuel load is at 3.2 bar brake mean effective pressure. For lower torque levels, the operation has to be switched to Diesel-only combustion.

- Switching between the combustion modes lead to unacceptable torque deviation and additional pollutant emissions (NO_x and CH_4). The transition from Diesel-only to dual-fuel combustion is thereby the critical case with more pronounced disturbances.
- By using a nonlinear mathematical optimization method, the transition penalties can be reduced significantly (65% reduction in maximum torque deviation, 56% reduction in cumulative NO_x emissions with comparable HC emissions).
- The addition of chemical-bound energy to the exhaust gas of a lean-burn natural gas engine using CO injection enables good conversion results even with low exhaust gas temperatures. An effective catalytic methane conversion is a result of arranging the exhaust gas enthalpy and the partially burnt or unburnt fuel contained in the exhaust gas in such a way that locally enough energy is available. In comparison to stoichiometric engines, lean-burn engines require very high exhaust gas temperatures as the reaction heat originating from the CO oxidation under stoichiometric conditions falls away.

WP 3 (Empa)

Valves of all serial-production internal combustion engines are actuated using camshafts, which are mechanically coupled to the crankshaft. This setup is comparably simple, fail-save and robust, but it is very inflexible. Valvetrains with some flexibility are on the market, but all of them modify the movement provided by a cam using meachincal or hydraulical coupling devices such as cam phasers, adjustable mechanical links (e.g. BMW Valvetronic) or hydraulic coupling (e.g. Fiat Multiair). However, full flexibility is desired to enable new combustion concepts, efficient gas exchange processes, the control of internal EGR, the control of charging devices, better cold start stragegies, enhanced power, adaptation to changing fuel qualities or to changing ambient conditions, for the complete deactivation of cylinders, and so on. So, a fully flexible valve actuation mechanism, which itself must be energy-efficient, has been requested for a long time. Numerous publications and patents exist on this field, but none of these ideas could find its way into serial production. Accourding to our assessment, the reason for this is that all existing ideas are either to complex (and therefore to expensive) or simple but not energy-efficient.

Empa has invented, in close collaboration with the Wolfgang Schneider Ingenieurbüro, a fully flexible electro-hydraulic actuation system for gas exchange valves whch we believe solves the drawbacks or restrictions which known electro-hydraulical valvetrains have. The innovations of this concept are:

- The control of the movement is given by the hydraulic setup, no expensive sensors and fast closed-loop-control of the valve movement is necessary,
- The system is fail-save, the valves are closed in case of loss of hydraulic pressure or electric actuation,
- The hydraulic actuation valves switch only at conditions where the hydraulic fluid has no movement, this omits the demand for expensive fast-switching valves and omits dissipation,
- The system is able to recuperate a large anount of the kinetic energy of all moving parts as well as the potential energy from valve spring compression hydraulically,
- A damping element is integrated which enables a slow and controlled seating of the valve to the valve seat,
- The pressure of the hydraulic fluid gives the maximum valve lift, so the valve lift can easily be controlled by controlling the pressure level.

Additionally, we used as the first researchers (to our knowledge) a water/ethylene-glycole mixture as the hydraulic fluid for an electrohydraulic valvetrain. Normally, oil is used. The use of a water/ethylene-glycole mixture has the advantage that the cylinder head remains completely oil-free and that the engine oil can be optimized for the lubrication of the lower engine parts only. This leads to lower additivation of oils, and therefore less catalyst poisioning components. Additionally, water/ethylene-glycole (e-module of 28‘000 bar) is stiffer than oil (e-module of 17’000 bar) which reduced the so-called capacitive hydraulic losses. The layout has been patended with a common patent of Empa and the Wolfgang Schneider Ingenieurbüro.

The system was first layed-out and simulated using a 1D multiphysics simulation tool (Simcenter Amesim). Figure 72 shows the graphical representation of the intake valve actuation mechanism where the main elements can be seen, namely:

- The check valve which automatically blocks the mechanism in its open position (Rückschlagventil Öffnung),
- The main electromagnetically actuated valve which controls the flow to the high pressure source for engine valve opening and recuperation during closing (Öffnungs- und Rekuperationsventil),
- The valve which is actuated with the same electromagnet as the valve mentionned above; this valve initiates the full closing of the engine valve after the end of the recuperation phase (Ablasssteuerung),
- A valve which is activated by the movement of the engine valve and enables a slow seating “integrierte Aufsetzbremse”.

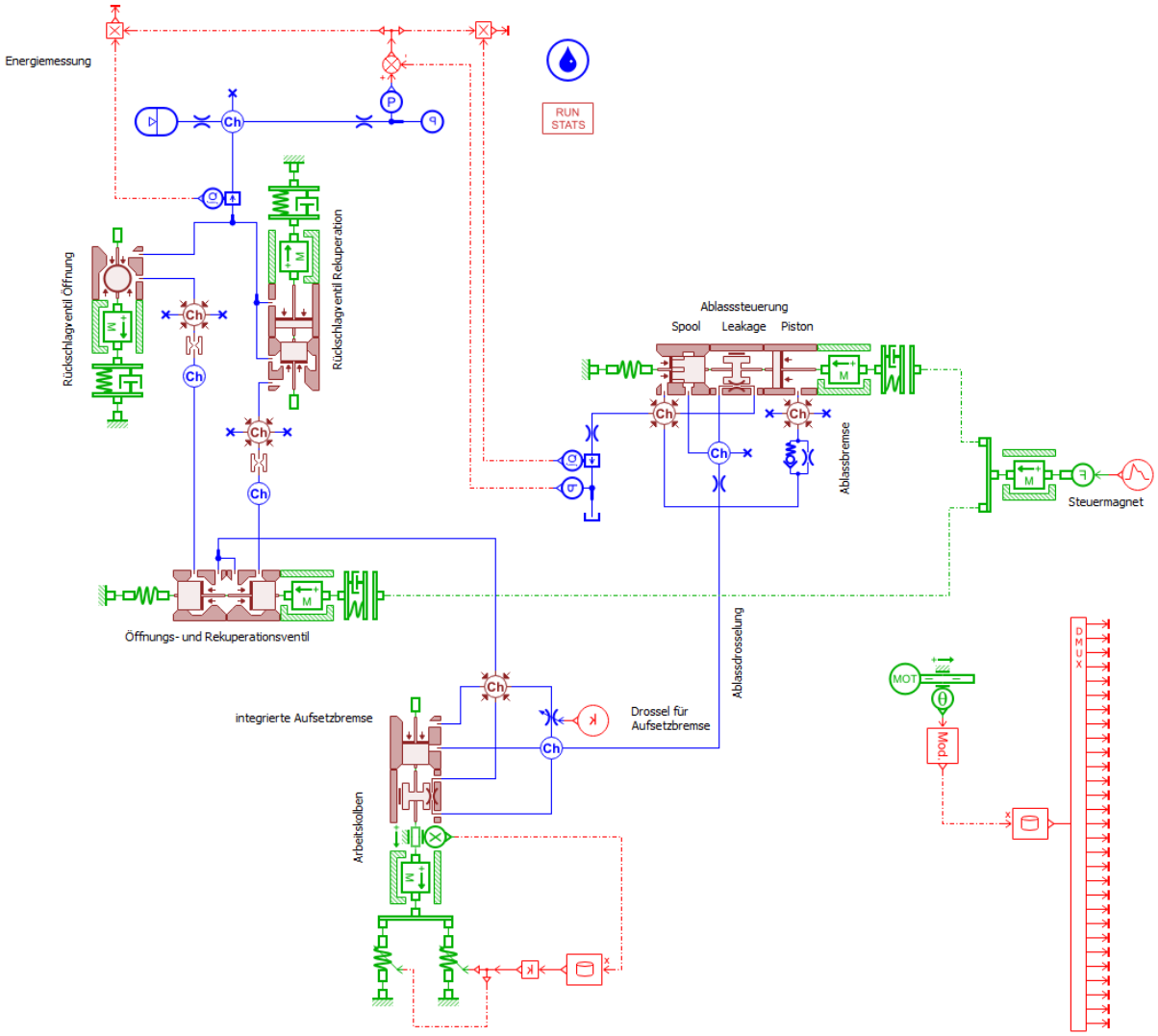

Figure 72: 1D simulation layout of the intake vale actuation mechanism

1.8. First prototype (intake side)

A first prototype has been built which operated both intake valves of one cylinder on a cylinder head of a Volkswagen 1.4 TSI (EA111) engine. Figure 73 shows the corresponding experimental set-up. The mechanism and valves shown in Figure 72 are placed in the black body in the upper-left part of the picture. Hydraulic accumulators are placed on each side of the mechanism to dampen the hydraulic pressure-waves which are generaed by the fast accelerations of the hydraulic fluid. Below the cylinder head, a plexiglass cylinder can be seen which can be pressurized to simulate cylinder pressure. An air filter is placed on the intake of the corresponding cylinder to dampen the noise of the gases when the pressure is released. This first prototype was built with the focus of a good access for measurement of the valve lift and pressure levels and pressure waves at several points. The valve lift was measures using a high-grade laboratory-type Micro-Epsilon position sensor.

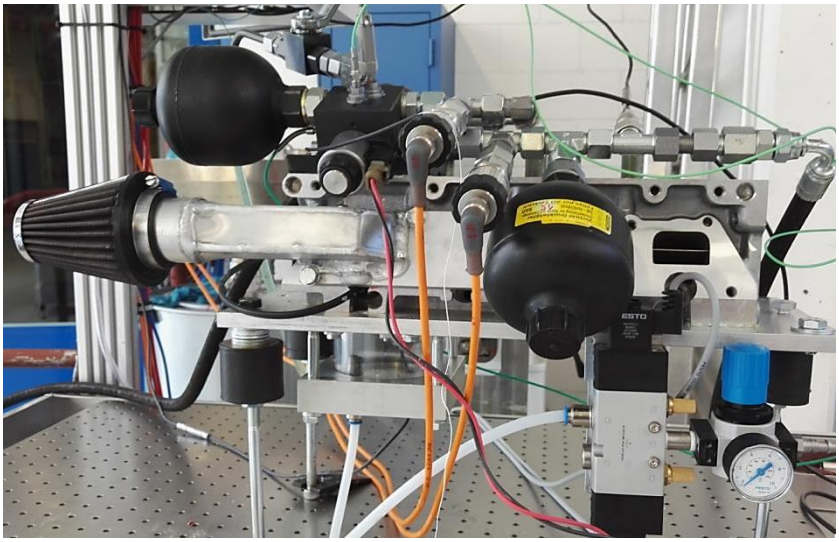

Figure 73: First prototype on a Volkswagen EA111 cylinder head

Figure 74 shows a comparison of simulation and experiments performed with the first prototype. It can clearly be seen that the agreement between simulation and experiment is excellent. So, this first prototype could be used for a in-depth validation and calibration of all hydraulical components.

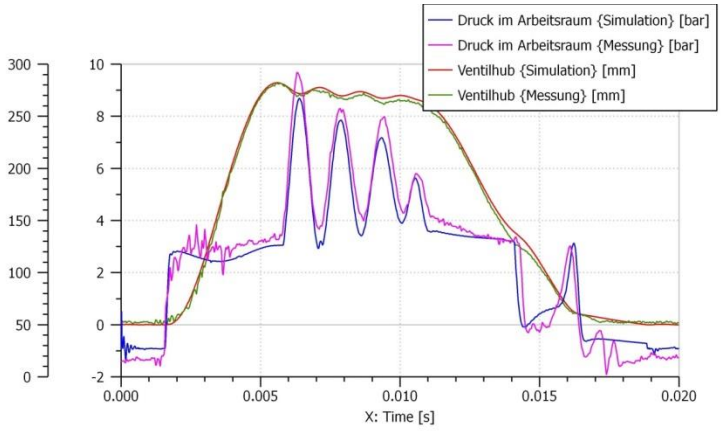

Figure 74: Comparison of simulation and experiment

Beside of the valve actuation mechism, an adequalte supply of pressurized water/ethylene-glycole had to been built. For that, a common-rail pump was accordingly modfied and tested. The test pump and the pump test-bench has been supplied by LAV-ETH. Figure 75 shows the experimental set-up.

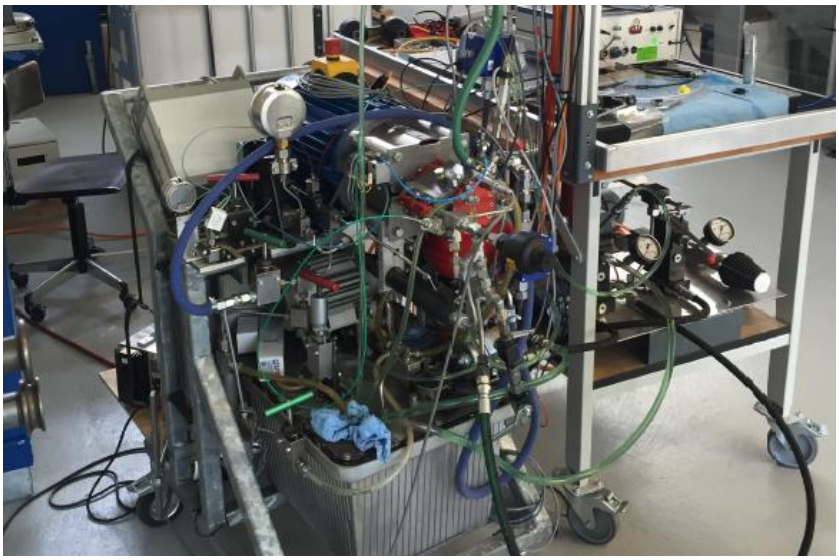

Figure 75: Test-bench for pump experiments

1.9. Second prototype (intake side)

After validation of the simulation model with the first prototype, a second prototype was designed This prototype has less access for measurement but is so compact that all cylinders can be equipped. Figure 76 shows CAD renderings of a fully equipped cylinder head and the cross-section through one intake side module. In the cross-section, the two spring-loaded intake valves can be seen which are actuated via a bridge from a hydraulic piston. The hydraulic valves are positionned parallel to this actuation axis, the magnetic coil is not shown. Additionally, one check valve is visible.

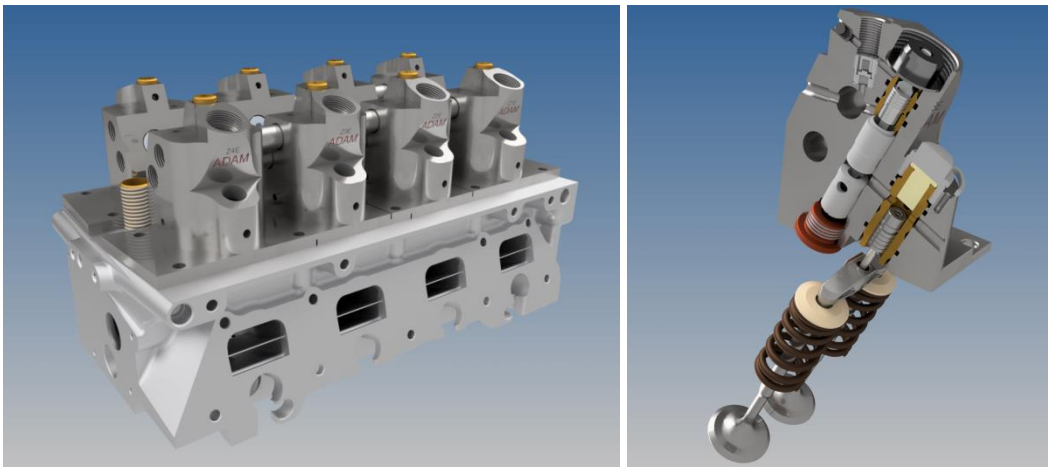

Figure 76: CAD rendering of the fully equipped cylinder head and a cross-section of one module

Figure 77 shows such an intake module, before being equipped with its inner parts, positionned on the cylinder head. In order to measure the lift of the valves, an affordable industry-grade position sensor has been implemented. The sensor head measures the signal of a magnetically coded stripe attached to the bridge. This low-cost position measurement is not used for real-time control but for checking and recording the lift profile.

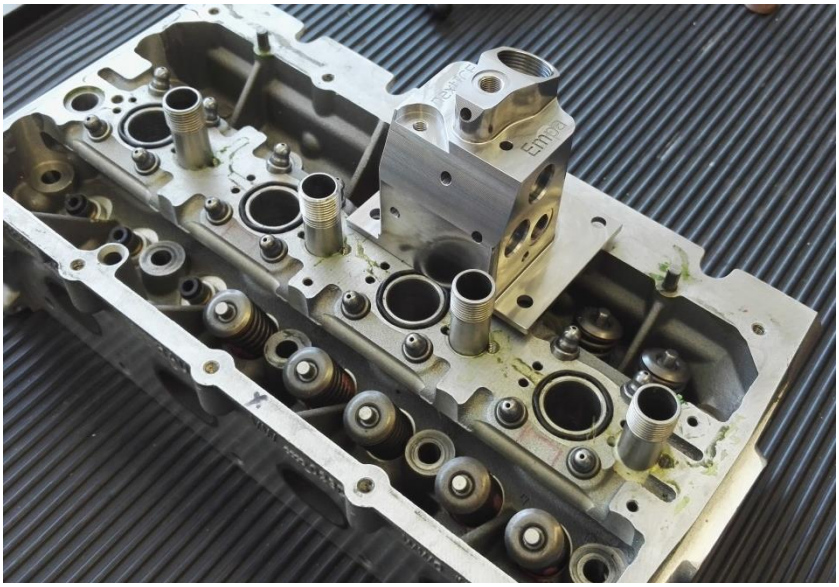

Figure 77: One module positonned on the cylinder head

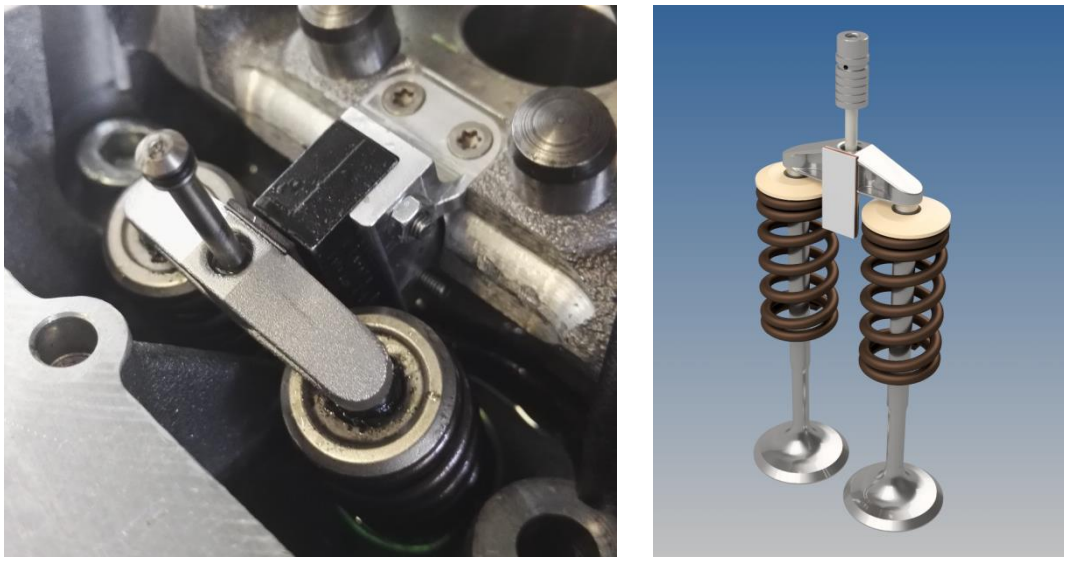

Figure 78: Lift measurement sensor placement

Figure 90 shows the cylinder head, fully equipped on the intake side including the actuation coils and the hydraulic accumulators. Figure 80 (left) shows the measured valve lift profiles for different

maximum lifts. The maximum lift can easily be adjusted by setting the supply pressure at the desired level. Figure 80 (right) show the corresponding relationship.

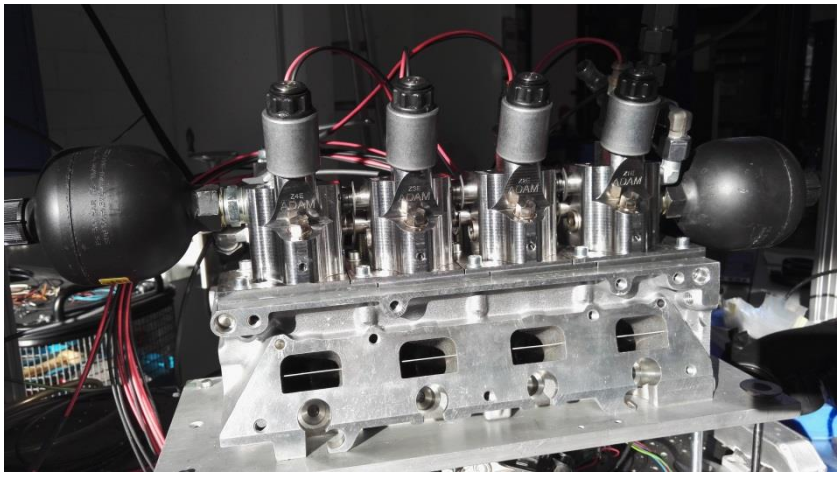

Figure 79: Cylinder head with fully equipped intake side

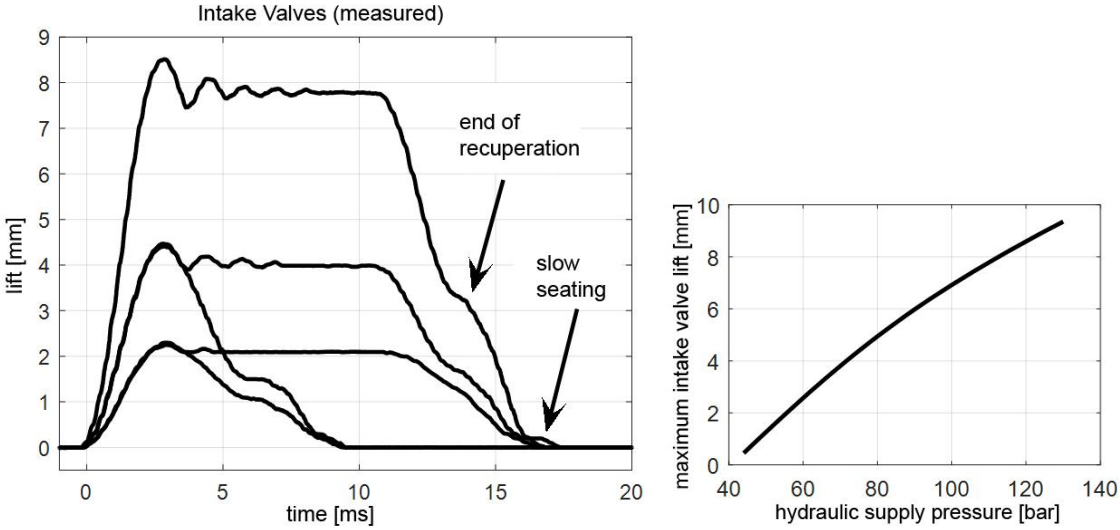

Figure 80: Mesured valve lift profiles (left), correlation between pressure and maximum lift (right)

1.10. Second prototype (exhaust side)

During the simulations it became evident, that the hydraulical principle of the intake side cannot safely be used on the exhaust side. On the intake side of an engine, the valves open after the exhaust gases have been pushed-out and fresh gas has to flow to the combustion chamber. Therefore, the pressure situation is that in the cylinder a pressure of about the backpressure before turbine or before catalysts is present and in the intake, the intake manifold pressure is present. The pressure situation is very stable, an engine misfire for example does not drastically change the pressure situation of the intake valve. For the exhaust valves, the situation is much more severe. They have to open against

potentially high pressure (typically up to 10 bar) but if a cylinder shows delayed combustion or a complete misfire, the pressure can be much lower. If the actuation pressure is set at a level for robust opening against the expected cylinder pressure but this pressure is different, the system can mechanically fail. So, we had to invent an energy efficient way to stop the exhaut valve at a desired maximum lift at all possible conditions. The resulting functioning principle for the exhaust valves is different to the one discussed so far: the actuation pressure remains at a constantly high level that guarantees a robust opening againgsall cylinder pressures that can occur. The recuperation in the fully open position is not done in such a way that the energy is stored in the spring but the excess energy is already in the opening phase recuperated hydraulically. A mechnism is introduced which twists the actuating pistons which themselves have a control edge to cut the hydraulic supply. Figure 81 show the CAD rendering for the exhaust valve actuation mechanism. The mechanism to twist the piston is made with a worm gear transmission. This invention has been patented. Figure 82 and Figure 83 show the fully equipped cylinder head whith the servo motor to adjust the desired exhaust gas valve lift mounted on the right side.

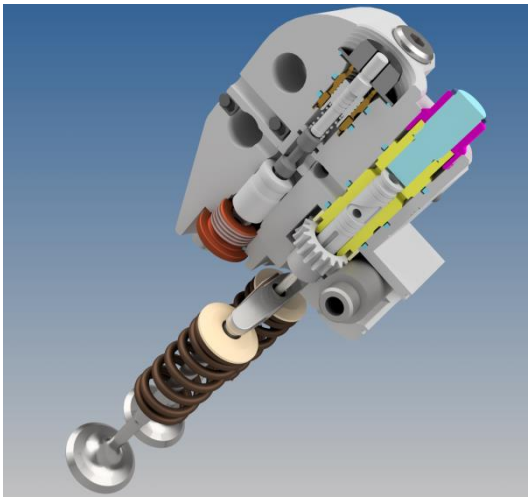

Figure 81: CAD rendering of the cross-section of one exhaust vale actuation module

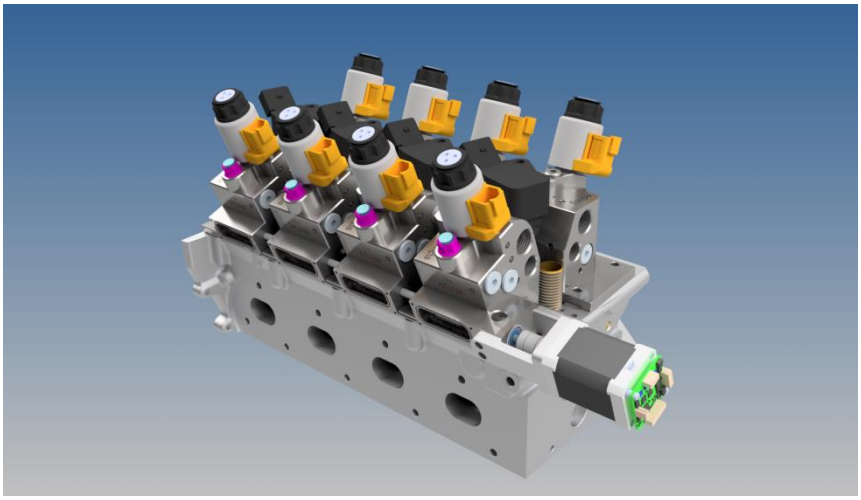

Figure 82: CAD rendering of the fully equipped cylinder head

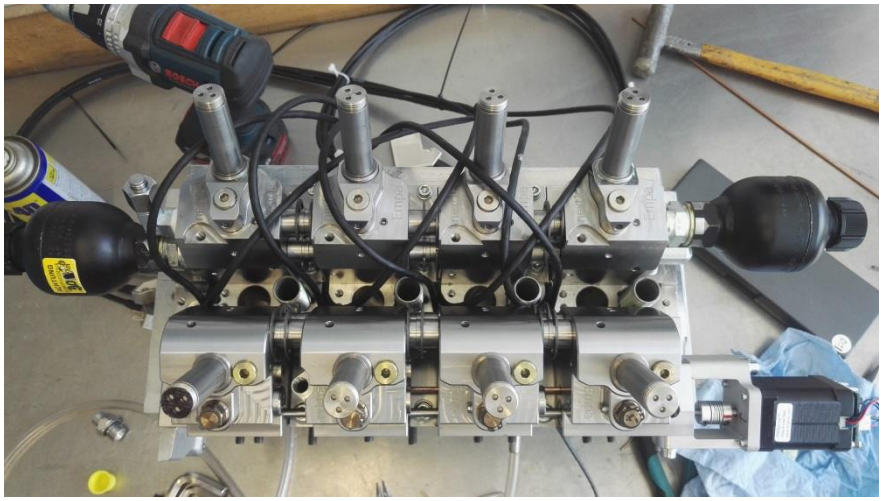

Figure 83: Assembly of the fully equipped cylinder head

The fully equipped cylinder head was extensively tested in cold operation, Figure 84 shows the setup.

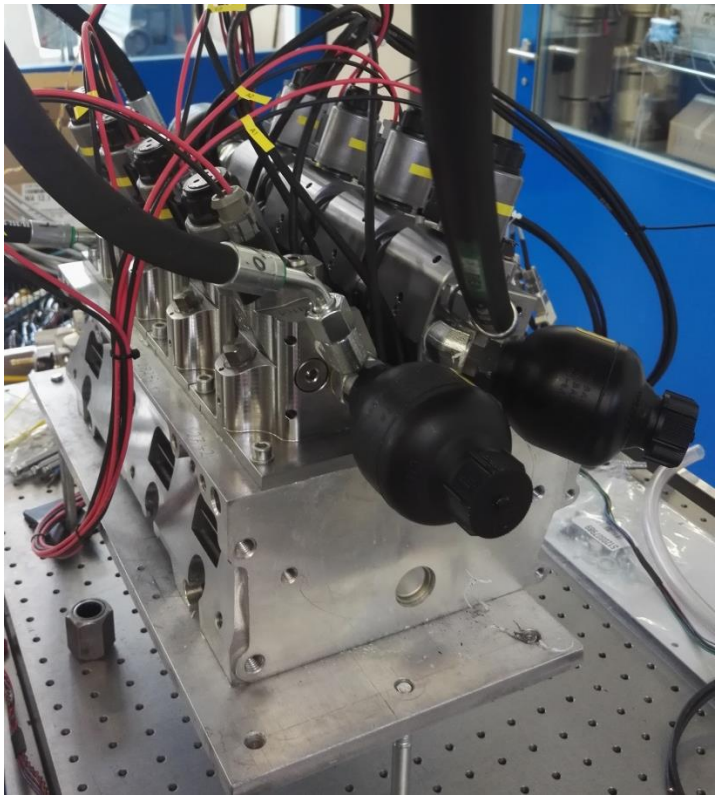

Figure 84: Cylinder head test bench

Figure 85 shows the system is able to open fast against cylinder pressure and without hitting a mechaincal stop. The lift overshoot at the beginning is a wanted feature as the system opens fast to release cylinder pressure and swings back to its static lift position while recuperating hydraulic energy. The closing phase is shown in Figure 85 for maximum recuperation which means that first, all energy is recuperated to the high pressure side of the hydraulic system until the valves come to a complete

stop and then, for the rest of the lift, hydraulic fluid is dumped to the low pressure side of the hydraulic system. The behavior in this transition beween recuperation and dissipation can be tuned for a faster closing of the valves, if needed. In the setup used for engine operation, an energy recuperation of 60% is achieved.

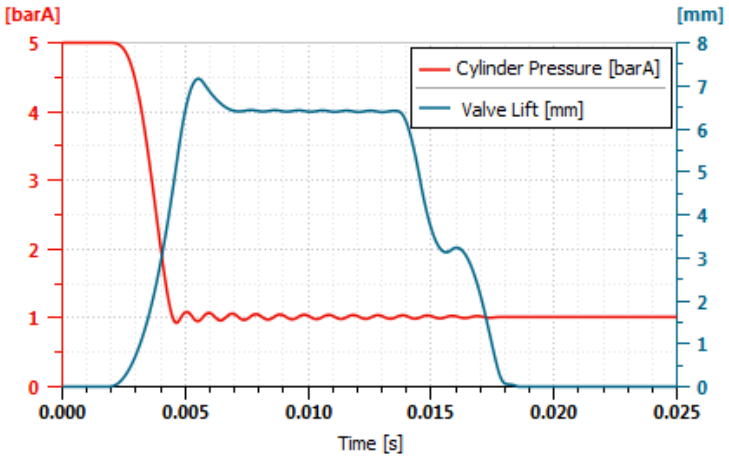

Figure 85: Valve lift and the pressure in the cylinder

1.11. Energy demand

The electrohydraulic valvetrain needs hydraulical power for the actuation plus electrical power for the electromagnetic valves. Hydraulical power is provided by pumps. A classical camshaft is coupled, via a belt or a chaindrive, to the crankshaft. A fully variable valvetrain has distinct advantages regarding the efficiency of the thermodynamical cycle but its own energy demand should be as low as possible in order to not create a drawback. A mechanical camshaft is quite efficient as it opens the valves versus springs and recovers a large part of this enery when the valves are closed again. Our electrohydraulic valvetrain operated also in combination with springs and is able to recuperate a large fraction of this energy hydraulically so that the hydraulic pump has to cover only the losses.

In order to asses the energy demand for our electrohydraulic valvetrain, its dissipation has been computed taking into account the energy needed to drive the pumps plus the energy needed to activate the electromagnetic coils. Figure 86 shows the comparison with a classical camshaft drive for four-stroke operation of an engine at a low load operating point of 2 bar brake mean effektive pressure. The dissipation is expressed in the diagram, as it is usual in engine technology, as a friction mean effective pressure, which is defined as work divided by the engine displacement volume. A classical camshaft has a friction mean effective pressure at this load of about 0.16 bar. As Figure 86 shows, the electrohydraulic valvetrain outperforms a classical camshaft almost across the whole engine speed range.

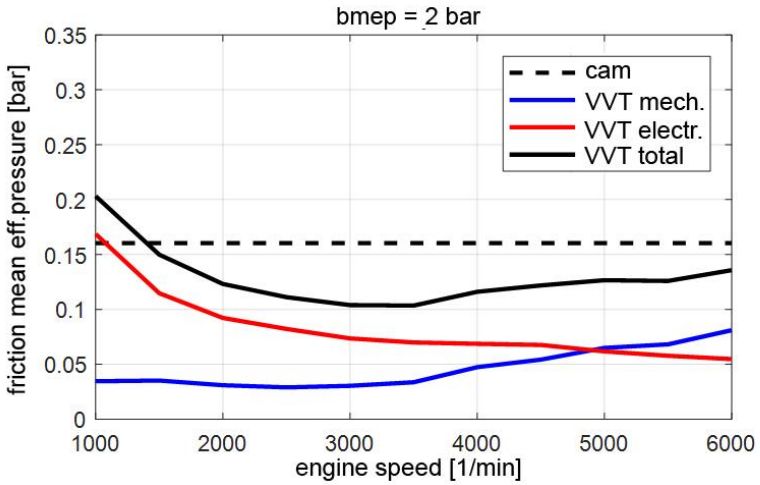

Figure 86: Comparison of friction mean effective pressure for the variable valvetrain (VVT) versus a camshaft

1.12. Conclusion and outlook of WP3

The goal of WP3 was to develop a new, fully flexible electrohydraulic valvetrain and to build a prototype for a full engine. This goal could be successfully achieved. The electrohydraulic valvetrain shows an excellent mechanical performance, it is able to run with an unusual fluid without any problems, and its energy demand is low. Within the project we realized, that we have to invent a new solution for an energy-efficient and safe limitation of the maximum valve lift for the exhaust side, which led to a consiberably-increased effort for this new task in terms of simulation, design, construction and testing. The consequence was that we were not able to transfer the valvetrain to an engine and do fired tests on the engine, as it was initially planned for the NextICE WP3. However, a follow-up-project named “FlexWork” (BFE contract SI/501020-01) was initialized with the goal to transfer the valvetrain to a running engine and to perform combustion strategy research. Within the FlexWork project, we were able to build-up the full engine by Autumn 2018. The careful preparation has paid out – the engine could be successfully fired and the valvetrain has reached nearly one million valve actuations by end of 2018. Figure 87 shows the setup of the engine on the test bench. Figure 88 shows a measured p(V) diagram of a low load operating point with an indicated mean effective pressure of 2.25 bar. The gas exchange mean effective pressure is at an extremely low level of 0.026 bar since the load was controlled without any throttling but by an early closure of the intake valve.

In conclusion, an electrohydraulic valvetrain could be invented and build. It shows excellent performance and its effenct on a internal combustion engine is investigated in a follow-up project. In parallel, Empa is seeking cooperation with a automotive manufacturer or supplier who is interested to transfer this system into production. First results have recently been published, more publications will follow.

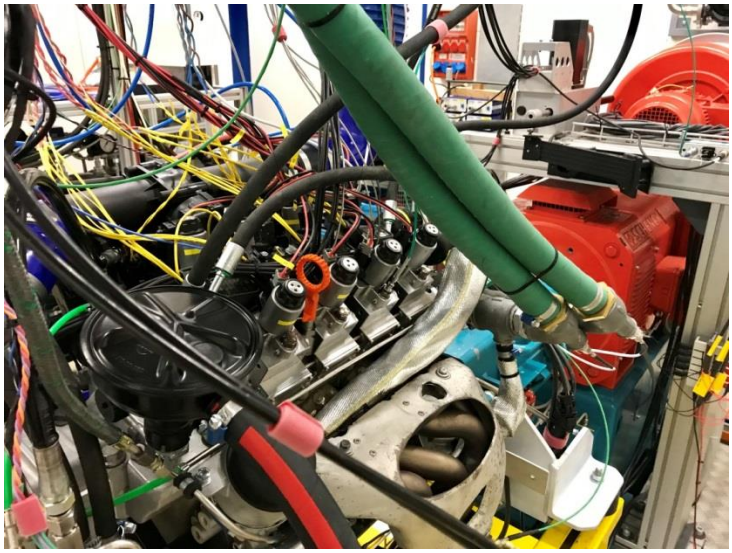

Figure 87: VW EA111 engine with the electrohydraulic valvetrain on the engine test bench

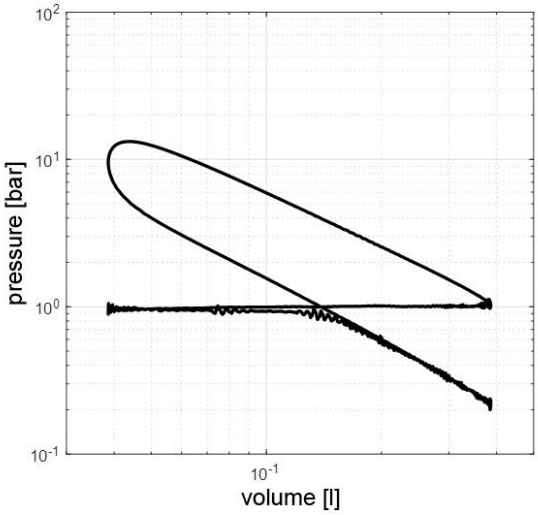

Figure 88: Measured p(V) diagram at an indicated mean effective pressure of 2.25 bar

Colaboration Between Work Package: A Study on POMDME

In a collaboration between the two ETH institutes LAV and IDSC, a NextICE project investigated whether the fuel POMDME (or OME for short) can be used in pilot-ignition combustion. For this purpose measurements with OME were carried out on the pilot-ignition engine of the IDSC.

1.13. Closed-Loop Comparison

In a first attempt the Diesel was replaced with OME, leaving all feedback controls on the test bench activated. Measurements were taken at identical operating points, i.e. with the same values for the following parameters:

- Load
- Fuel/air equivalence ratio
- Combustion phasing

The Figure 89 shows an exemplary heating curves of two measurements, one with Diesel and one with OME, at the same operating point. Obviously, the measured heat release rates of OME and

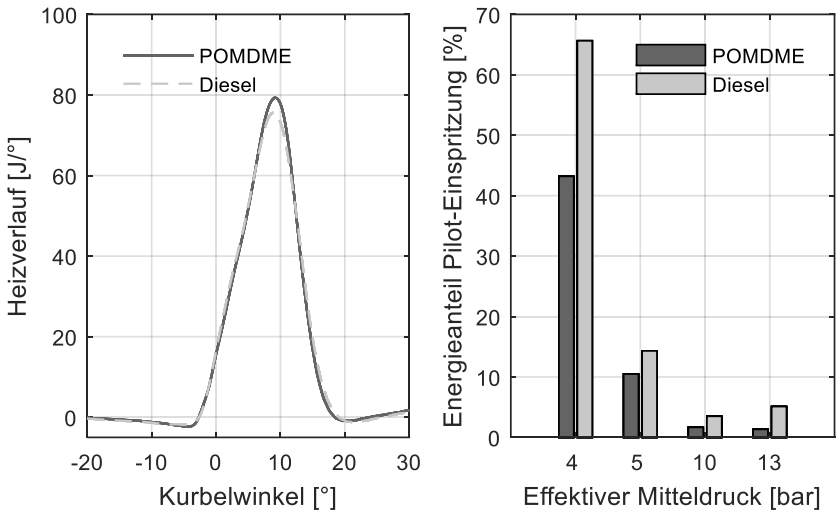

Figure 89: (left) Heat release curves of the two pilot fuels OME and Diesel at the same operating point. (right) Energetic share of the fuel injected by the pilot injection in the total fuel energy.

Diesel are very similar at the same operating point. However, the two fuels differ significantly in the amount that has to be injected to achieve this desired combustion. Figure 89 shows that at all investigated operating points the energy share of pilot injection in the total fuel energy is smaller in the case of OME than in the case of diesel. The investigations in WP2 suggest that this property can have a positive effect on HC emissions in the low load range.

1.14. Open-Loop Comparison of POMDME and Diesel

Figure 90 compares the heat release rates of an operating condition at 1600 rpm and 8 bar brake mean effective pressure (BMEP) with either Diesel or OME as pilot fuel with similar injection settings (This means: similar fuel mass but different energy share) The global stoichiometry λ is one for both pilot fuels. At this load, the percentage of pilot fuel is already very low, thus, lower energy content of

OME only minor influence the stoichiometry of the premixed natural gas. However, the impact of the pilot fuel on the combustion is very high. The ignition delay is lower due to the higher cetane number and the natural gas combustion is faster. The latter effect can be attributed to the higher temperature, since the combustion is closer to top dead center. Furthermore, the stoichiometry of the natural gas is closer to 1 which increases the flame speed.

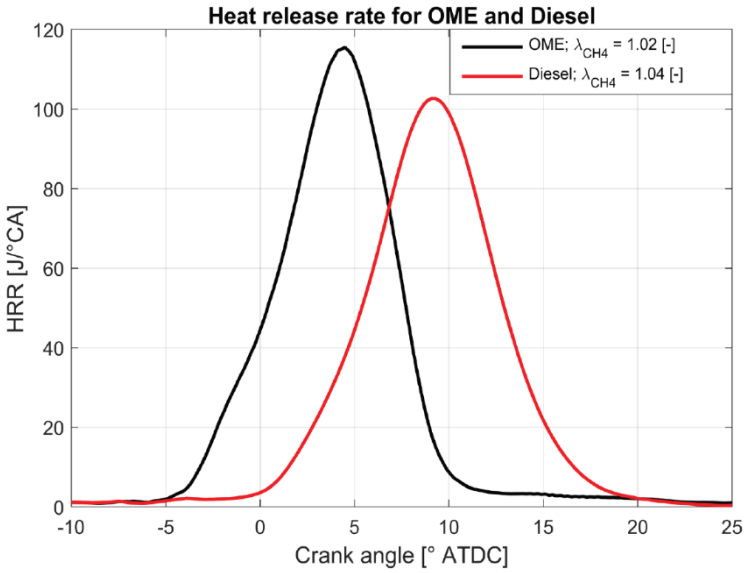

Figure 90: Heat release rates of natural gas combustion, ignited with OME (black) and Diesel (red) with similar injection settings.

1.15. Particulate Matter and Particulate Number Emissions

In the lower load operating condition, the share of pilot fuel can be up to 50%. The large amount of pilot fuel causes two major effects. The mixture of natural gas needs to be very lean (slow flame speed) and the core of the auto-ignition zone is fuel rich. The latter one cause high PM emissions. Figure 91 shows a comparison between 4 different engine settings at 4 bar BMEP with high EGR ratios.

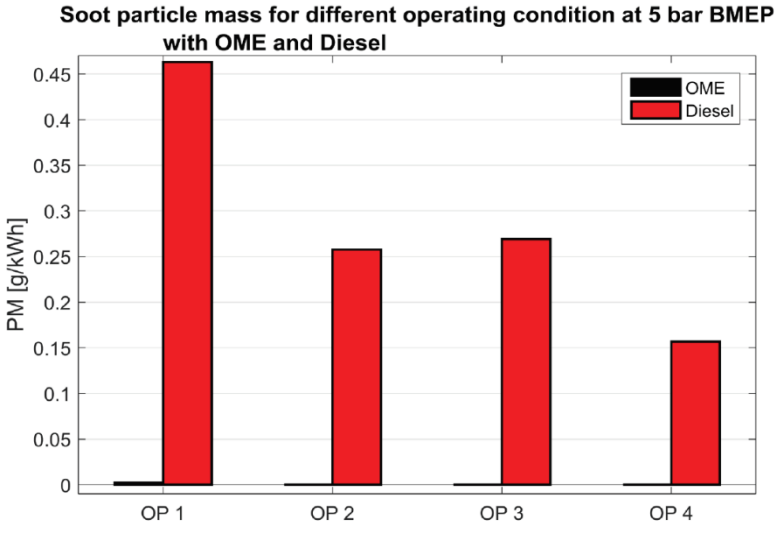

Figure 91: Comparison of PM emissions of OME (black) and Diesel (red)

It was shown that measures like swirl addition or reduction of the pilot injection duration help to reduce PM emissions, but the level remains high. Furthermore, the Figure 91 and Figure 92 show that, both, PM and PN are orders of magnitudes lower using OME instead of Diesel as a pilot fuel. This is attributed to the oxygen content of OME, inhibiting soot formation. Using OME, only OP1 shows detectable PN level. However, the size range indicates that the recorded particles are most likely of volatile nature. OME shows a huge potential to reduce PM/ PN emissions during low load operation of

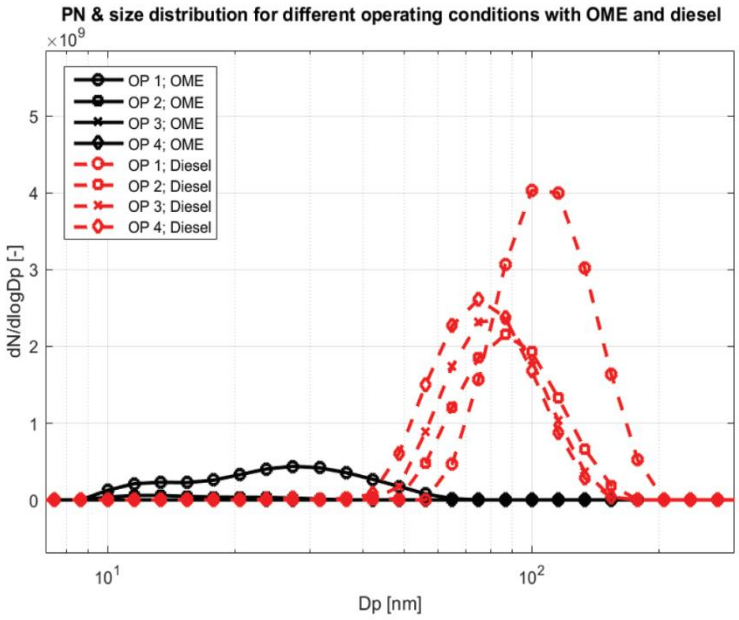

Figure 92: Comparison of spectral PN emissions of OME (black) and Diesel (red)

dual fuel engines.

National cooperation

NextICE

The three research groups from ETH Zurich and Empa are working together on the NextICE project. They actively supported each other with expertise on a wide range of topics. Some publications have been created together.

FlexFiDual

In this FlexFiDual project the LAV cooperates with the University of Applied Sciences North-West within the project FlexFiDual of CCEM.

International cooperation

GasOn

IDSC, LAV and Empa are cooperating with various European project partners in the Horizon2020 project GasOn. The aim of WP 5, which is headed by Volkswagen Group Research, is to research prechamber combustion processes for gas engines. The IDSC is carrying out reference measurements on the diesel-ignited natural gas engine as part of the GasOn project. In addition, the IDSC is developing the engine control system for the Empa's full-engine pre-chamber. The LAV conducts basic tests on optical test vehicles and detailed numerical simulations.

References

Barro, C., Parravicini, M., Boulouchos, K., and Liati, A., "Neat polyoxymethylene dimethyl ether in a diesel engine; part 2: Exhaust emission analysis." Fuel, 2018. 234: p. 1414-1421.

Hutter, R.; Ritzmann, J.; Elbert, P.; Onder, C. Low-load Limit in a Diesel-ignited Gas Engine, Energies, Volume 10; 2017

Hutter, R.; De Libero, L.; Elbert, P.; F.; Onder, C. Catalytic Methane Oxidation in the Exhaust Gas Aftertreatment of a Lean-burn Natural Gas Engine, Chemical Engineering Journal, Volume 349, 2018

Hutter, R.; Zurbriggen, F.; Onder, C. Diesel Minimal Combustion Control with Constraints in a Diesel-Ignited Gas Engine, FISITA automotive conference 2016, FISITA, 2016, 10

Iannuzzi, S. E.; Barro C.; Boulouchos K.; Burger, J. POMDME-Diesel Blends: Evaluation of Performance and Exhaust Emissions in a Single Cylinder Heavy-Duty Diesel Engine. Fuel, JFUE-D-16-01359 submitted 05. 2016, under review.

Schneider W, Soltic P, Omanovic A. Hydraulischer Antrieb zum Beschleunigen und Abbremsen dynamisch zu bewegender Bauteile. EP17172231, 2017.

Schneider W, Soltic P, Omanovic A. Hydraulischer Antrieb zum Beschleunigen und Abbremsen dynamisch zu bewegender Bauteile. EP18207848, 2018.

Zsiga N, Omanovic A, Soltic P, Schneider W. FlexWork – Lastregelung bei einem Motor mit elektrohydraulischem , vollvariablem Ventiltrieb. Ladungswechsel und Emiss. 11. MTZ-Fachtagung, 23. und 24. Oktober 2018, Stuttgart, 2018

Zurbriggen, F.; Hutter, R.; Onder, C. Diesel-Minimal Combustion Control of a Natural Gas-Diesel Engine. Energies 2016, 9(1), 58.

Posters

Barro, C.; Hutter, R.; Möri, F.; Boulouchos, K; Burger, J. Analysis of PM and PN in dual Fuel Engine, Fuelled with Natural Gas and OME, 20th ETH Conference on Combustion Generated Nanoparticles 2016, Zurich, Switzerland

Hutter, R.; Elbert, P.;, Onder, C., Poster NextICE, 2015, SCCER Mobility Annual Conference 2015, Zurich, Switzerland

Hutter, R.; Elbert, P.;, Onder, C., Poster NextICE, 2016, SCCER Mobility Annual Conference 2016, Zurich, Switzerland

Hutter, R.; Elbert, P.;, Onder, C., Poster NextICE, 2017, SCCER Mobility Annual Conference 2017, Zurich, Switzerland

To be published

Barro, C., Parravicini, M., and Boulouchos, K., "Neat Polyoxymethylene Dimethyl Ether in a Diesel Engine; Part 1: Detailed Combustion Analysis." Fuel, 2019. TBD(TBD)

Hutter, R.; Hänggi, S.; Albin, T.; Onder, C. Optimal Transition Control between Combustion Modes in a Diesel-ignited Gas Engine, not yet published